NATIONAL AERONAUTICS AND SPACE ADMINISTRATION

NASA MEMO 1-3-59A

for

UNITED STATES AIR FORCE

WIND-TUNNEL INVESTIGATION OF THE EFFECTS OF COMPONENT BUILD-UP ON THE INLET PERFORMANCE OF AN 0.05-SCALE AIR INDUCTION MODEL OF THE B-70 AIRPLANE AT MACH NUMBERS FROM 2.58 TO 2.96 (COORD. NO. AF-AM-163)*

By Robert U. Hofstetter, Kenneth C. Endicott, and Walter E. Isler

ABSTRACT

Experimental data are presented to show some effects of wing, fuselage, and canard on the inlet performance and external pressures in the vicinity of the inlet. The comparative effects of several wing configurations on inlet performance are included.

INDEX HEADINGS

Air Inlets 1.4.1

Airplanes - Components in Combination 1.7.1.1

NASA MEMO 1-3-59A

for

UNITED STATES AIR FORCE

WIND-TUNNEL INVESTIGATION OF THE EFFECTS OF COMPONENT BUILD-UP ON THE INLET PERFORMANCE OF AN 0.05-SCALE AIR INDUCTION MODEL OF THE B-70 AIRPLANE AT MACH NUMBERS FROM 2.58 TO 2.96 (COORD. NO. AF-AM-163)*

By Robert U. Hofstetter, Kenneth C. Endicott, and Walter E. Isler

SUMMARY

An experimental investigation was made to determine the effects of wing, fuselage, and canard on the inlet performance and external pressures of an 0.05-scale air induction model of the North American Aviation B-70 airplane.

Test observations showed that the addition of the canard increased the maximum inlet pressure recovery by 1.1 percent over that obtained in the presence of the fuselage forebody less canard. Lower surface wing pressures outboard of the 24-percent semispan location were unaffected by the addition of the canard.

No significant change in inlet performance was caused by the addition of both the fuselage forebody and canard.

Two of the wing configurations (North American Aviation Numbers 172 and 154) had a favorable effect on inlet performance, while the third (Number 145) wing affected performance adversely. The Number 172 wing generally exhibited more positive lower surface pressures than the Numbers 154 and 145 wing configurations.

INTRODUCTION

The North American B-70 airplane is an all-supersonic intercontinental bomber designed to cruise at a Mach number of 3.00. The successful

operation of the aircraft at this speed, over the range and with the loading set forth in reference 1, requires that specific values of engine performance be realized. To this end considerable developmental work has been done by the contractor on an air induction system which will satisfy stipulated engine requirements. The outgrowth of this development program has been a twin duct system utilizing two-dimensional-type inlets, and combining variable internal geometry with a boundary-layer bleed system.

At the request of the Air Research and Development Command of the United States Air Force an investigation was conducted in the 8- by 7-foot test section of the Ames Unitary Plan wind tunnel on an air induction model of the B-70 airplane incorporating the North American Number 172 inlet version. The purpose of the investigation was to evaluate the effects of wing, fuselage, and canard on the inlet performance and on pressures external to, but in the region of, the inlet. Evaluation of wing effect on inlet performance included a comparative investigation of several wing configurations to determine that which would produce a pressure field, behind the leading-edge shock wave, most favorable to the attainment of good inlet performance. The results of this investigation are reported herein.

SYMBOLS

A_c inlet capture area, 0.0933 sq ft

b wing span, ft

c wing chord, ft

M Mach number

m_c mass-flow rate based on free-stream conditions and inlet capture area, slugs/sec

m_o duct mass-flow rate at engine face station, slugs/sec

p static pressure, lb/sq ft

p_t total pressure, lb/sq ft

q dynamic pressure, lb/sq ft

$\frac{\Delta p}{q_\infty}$ pressure coefficient, $\frac{p - p_\infty}{q_\infty}$

α angle of attack of basic model reference axis, deg

[redacted]

β angle of sideslip of basic model reference axis, deg

X longitudinal body axis in the vertical plane of symmetry of the complete twin-duct system (denoted as the model reference axis in figure 1; positive rearward)

x distance measured along the X axis positive aft of model station 0.00, in.

Y lateral axis perpendicular to the vertical plane of symmetry of the complete twin-duct system, positive as shown in figure 1

y distance measured along the Y axis, in.

Z vertical axis in the vertical plane of symmetry of the complete twin-duct system, positive as shown in figure 1

z distance measured along the Z axis, in.

Subscripts

∞ free-stream conditions

2 duct station corresponding to the engine face location

MODEL

The basic model tested was an 0.05-scale model of the B-70 airplane air induction system furnished by North American Aviation, Incorporated. It consisted, as shown in figures 1 through 3, of an inlet-afterbody combination with a variable-geometry two-dimensional duct and true-scale contours on one side of the model center line. The opposite side of the model was unducted and designed so that the flow conditions occurring on the ducted side simulated those existing during twin-duct operation. Additionally, this offside portion of the model provided exits for the bleed flow originating at the porous ramp surfaces on the ducted side of the model. Mass-flow variation was accomplished by a remotely controlled plug as illustrated in figure 2. The model was sting-mounted from the wind-tunnel model support strut in an inverted attitude (see fig. 3).

The basic inlet used corresponded to the North American Aviation Number 172 version. Figures 2 through 7 show pertinent inlet geometry for this version, and indicate over-all areas available for the application of boundary-layer bleed control.

[redacted]

[redacted]

When wedge extensions were employed in conjunction with a supporting wing configuration (see fig. 8) modification to the external geometry of the Number 172 inlet version was possible. The extent of the alterations resulting from the use of the wedge extensions is indicated in figures 9 and 10. Interchangeable segments of the cowl side plate were also used to vary the cowl lip angle (see fig. 11).

The boundary-layer bleed capabilities of the Number 172 inlet version were determined by the porosity of the plates attached to the areas available for bleed control. Variation separately of the porosity of these plates, and the effective porous area, altered the bleed characteristics of the inlet. Four boundary-layer bleed configurations were used and are tabulated in table I. Since a comparison of the effects of porosity variation is desired rather than a detailed evaluation of bleed mass flow, the diminution of the net porous plate area caused by the webbing supporting the plates is not considered.

Provision was made for the addition to the basic model of a wing, a wing and forebody, and a wing, forebody, and canard. These components were also furnished by the contractor. Several wings were tested in conjunction with the basic model to establish which configuration resulted in a pressure field at the inlet conducive to the best inlet performance. The various wings are shown in figure 12, and a photograph of one version is presented in figure 13.

Figures 14 and 15 show the configuration consisting of the addition to the basic model of a wing plus forebody. Figures 16 and 17 show the configuration composed of the basic model and a wing plus forebody and canard.

A summary of all configurations tested is given in table II.

MODEL COMPONENT DESIGNATION

The model component identifying symbols and version number designations established by North American Aviation, Inc., have been retained, except where noted, and are defined as follows:

B_T Number 172 fuselage version, including a forebody and the afterbody portion of the basic model (fig. 15)

C cowl side plate with an 11° cowl lip angle
(Subscripts 1, 2, 3, and 4 designate the boundary-layer bleed configuration (see table I) used on the side plate.)

[redacted]

[redacted]

C' cowl side plate with an 8° cowl lip angle[1]
(Subscripts 1, 2, 3, and 4 designate the boundary-layer bleed configuration (see table I) used on the side plate.)

C_T Number 172 canard version (fig. 16)

I Number 172 inlet version (schematically shown in fig. 4)
(The first ramp extends from model station -8.60 to -5.80, and the bleed gutter height between the inlet and wing is 0.100 in.)

I_2 Number 145 inlet version
(This is a modification of the Number 172 inlet version obtained by extending the first ramp forward to model station -17.455 by means of wedge extension number 1 (fig. 10), used in conjunction with the Number 145 wing version (figs. 8 and 9).)

I_4 same as I_2 above except the bleed gutter height between wing and inlet is increased to 0.165 inch

I_5 same as I_2 above except wedge extension number 2 (fig. 10) is used

I_6 same as I_2 above except wedge extension number 3 (fig. 10) is used

R movable ramp system of the inlet
(Subscripts 1, 2, 3, and 4 designate the boundary-layer bleed configuration (see table I) used on the ramp system.)

S upper and lower cowl plates
(Subscripts 1, 2, 3, and 4 designate the boundary-layer bleed configuration (see table I) used on the plates.)

W_T Number 172 wing version (fig. 12)

W_{T_2} Number 154 wing version (fig. 12)

W_{T_3} Number 145 wing version (fig. 12)

TEST PROCEDURE

The test was conducted in the 8- by 7-foot test section of the Ames Unitary Plan wind tunnel. Pitch runs were made through an angle-of-attack range from 0.2° to 4.2° at 0° angle of sideslip. Yaw runs were made at angles of sideslip of -2.2° to +2.1° at 0° angle of attack, and at 1.0° angle of sideslip at 2.2° angle of attack. All data were taken at a nominal total pressure of 2808 pounds per square foot absolute.

[1]The symbol used by the contractor for this side-plate configuration is C_4.

[redacted]

[redacted]

Since the inlet was located behind the wing leading edge, the Mach number just ahead of the inlet was less than the free-stream value because of the influence of the wing leading-edge shock wave. To provide inlet performance comparison between configurations involving no component additions ahead of the inlet with those which included a wing, the Mach number schedule listed below was used.

Free-stream Mach number used for basic model with no components ahead of the inlet	Free-stream Mach number used for basic model with a wing version added
2.880	2.955
2.700	2.799
2.498	2.578

Pressures existing in the model duct and over the external model surfaces were indicated on multiple tube manometers, and photographically recorded. Figures 18 through 21 show static-pressure orifice locations on all model components.

The total pressure existing at the engine face was obtained by averaging 26 total-pressure tubes located at the engine face station.

The duct mass-flow rate existing at the engine face was determined by use of an ISA flow nozzle located downstream of the engine face station. The flow nozzle was calibrated against a standard ASME orifice plate to obtain a correction factor to be applied to the nozzle mass-flow measurements.

Precision of Data

The uncertainties estimated to exist in the test data are listed below:

Parameter	Uncertainty
α	$\pm 0.20^{\circ}$
β	$\pm 0.20^{\circ}$
p_{t_∞}	± 3.5 lb/sq ft
M_∞	± 0.005
p_{t_2}/p_{t_∞}	± 0.002
p/p_{t_∞}	± 0.002
$\Delta p/q_\infty$	± 0.008
m_o/m_c	± 0.003

[redacted]

RESULTS

Results of the present investigation are shown in the form of graphs and tables. Plots of inlet performance showing effects of alteration of the basic model, as well as the effects of free-stream conditions, model attitude, and wing addition, are presented in figures 22 through 29. No inlet performance data are given for configurations including the forebody, wedge extension numbers 2 and 3, alteration of basic bleed gutter height between wing and inlet, and the cowl configuration employing no boundary-layer bleed control. This omission is the result of failure of model instrumentation affecting the mass-flow rate measurements obtained during tests of the aforementioned configurations. Qualitative analysis of inlet performance, based on pressure recovery alone, is possible however, and is discussed in the following section.

Pressure coefficient data are presented graphically and in tabular form (see figs. 30 through 35) showing representative effects of Mach number variation, and component variation on the pressures over the lower wing surfaces. Table III is an index to figures 22 through 35.

External cowl surface pressure ratios are included (tables V and VI) to show the variations resulting from the addition of a wing and forebody to the basic model. These data were obtained during runs in which solid plates were faired over the cowl bleed areas preventing outflow through the cowl surface.

Pressure ratios obtained within the duct are also presented in tables VII through XV. The data selected for presentation in this report have been chosen to illustrate the effects on the internal flow of variation of free-stream conditions, model attitude, and component variation. Table IV is an index to tables V through XV.

The geometry of the subsonic portion of the duct was suitable for use in assessing only incremental changes of inlet performance since it was known to provide nonuniform flow to the engine. Presentation of engine face flow distortion values would, therefore, not be meaningful and are not included as part of the results.

DISCUSSION

The following discussion does not include an analysis of all the data contained herein, but merely summarizes the significant findings of the investigation relating to the over-all effects of component addition on inlet performance.

[redacted]

The four inlet bleed configurations tested are compared in figure 22. Bleed configuration 4 was used in subsequent evaluations of the incremental effects of component addition or alteration. (The scope of the investigation did not include developmental refinements of the bleed system, and bleed configuration 4 is not to be construed as necessarily optimum.)

Variation of inlet performance caused by the addition of the various wing versions to the basic model is shown in figure 26. For the model attitude and stream conditions noted in the figure, the W_T and W_{T_2} wings had nearly the same effect on performance - favorable, except near optimum operating conditions where a loss of 2.7 percent in pressure recovery occurred. The addition of the W_{T_3} wing to the basic model affected the inlet adversely.

No significant difference in optimum inlet performance for the basic model with the W_T wing as compared to the basic model plus the W_{T_2} wing was noted for variations in Mach number and angle of attack (see figs. 27 and 28).

Presentation of inlet performance data showing the effect of the canard and the forebody was precluded by model instrumentation failure affecting mass flow measurements. Qualitatively, however, these effects were indicated by pressure recovery data observed during the test. In comparative runs, where the only variable was the canard, it was found that maximum inlet pressure recovery for the canard-on configuration was 1.1 percent higher than in the case of the canard-off configuration. Comparative runs between configurations with and without the forebody-canard combination showed no significant change in peak inlet pressure recovery.

For the stream conditions and model attitudes shown in figures 30, 31, and 32, the W_T wing had generally more positive lower surface pressures outboard of the 19-percent b/2 spanwise station than the W_{T_2} and W_{T_3} wings.

The addition of forebody and canard to the $W_T IR_4C_4S_4$ configuration (fig. 35) increased the lower surface wing pressures slightly at the 50-percent b/2 and 40-percent b/2 spanwise locations. No effect was apparent at the 30-percent b/2, 24-percent b/2, or 19-percent b/2 locations. The addition of the canard (fig. 34) had no effect on pressures outboard of the 24-percent b/2 location.

Ames Research Center
National Aeronautics and Space Administration
Moffett Field, Calif., Nov. 3, 1958

[redacted]

REFERENCE

1. Anon.: Weapon System 110-A, AF33(600)-31801. Rep. No. NA-57-394-1, North American Aviation, Inc.

[redacted]

TABLE I.- BLEED CONFIGURATIONS

Configuration 1			
Bleed plate location	Bleed plate porosity, percent	Net porous area, sq in.	Bleed plate geometry, dimensions in inches
Third ramp	8	13.48	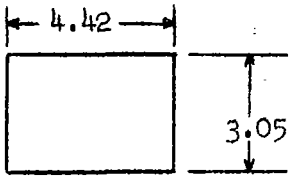
Fourth ramp	8	8.54	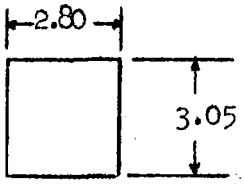
Fifth ramp	8	16.28	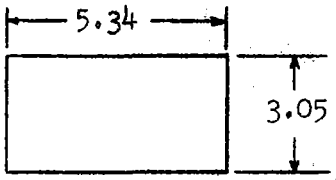
Cowl side plate	$3\frac{1}{2}$	24.21	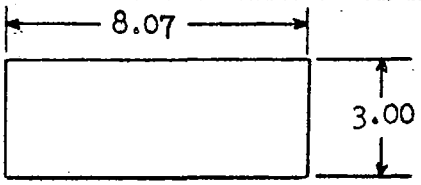
Cowl top and bottom plates	8	26.17	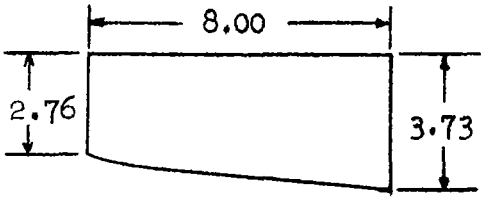

Note: Unshaded areas indicate portions of bleed plates through which bleed flow may occur.

[redacted]

TABL[redacted]

Configuration 2			
Bleed plate location	Bleed plate porosity, percent	Net porous area, sq in.	Bleed plate geometry, dimensions in inches
Third ramp	8	6.93	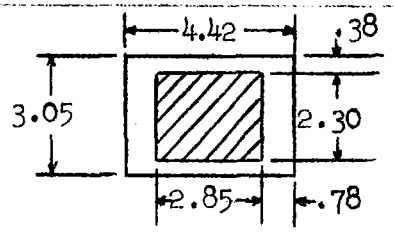
Fourth ramp	8	3.50	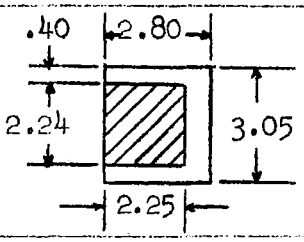
Fifth ramp	8	8.35	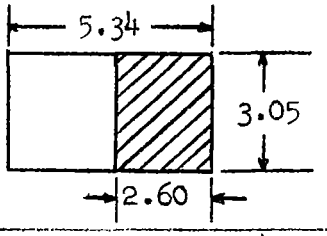
Cowl side plate	$3\frac{1}{2}$	13.80	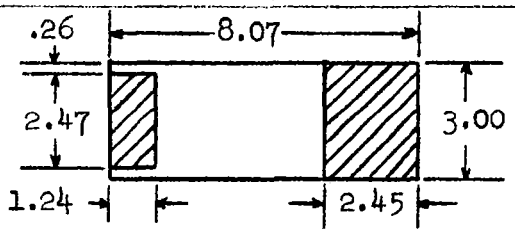
Cowl top and bottom plates	8	21.12	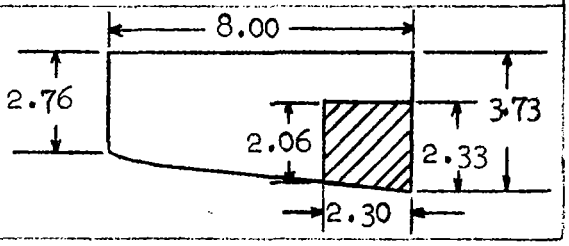

Note: Unshaded areas indicate portions of bleed plates through which bleed flow may occur.

[redacted]

TABLE I.- BLEED CONFIGURATIONS - Continued

Configuration 3			
Bleed plate location	Bleed plate porosity, percent	Net porous area, sq in.	Bleed plate geometry, dimensions in inches
Third ramp	8	9.03	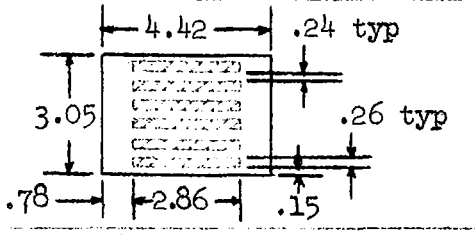
Fourth ramp	8	5.16	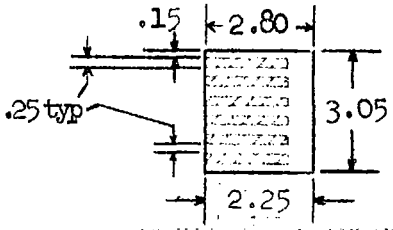
Fifth ramp	8	12.38	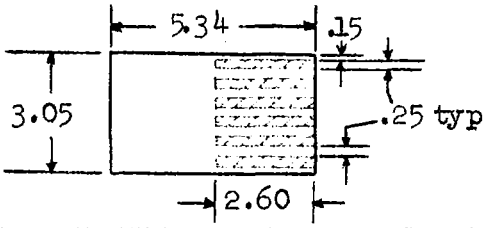
Cowl side plate	$3\frac{1}{2}$	20.52	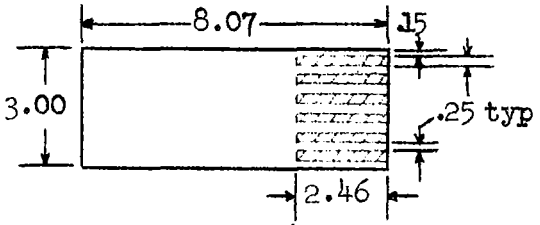
Cowl top and bottom plates	8	23.69	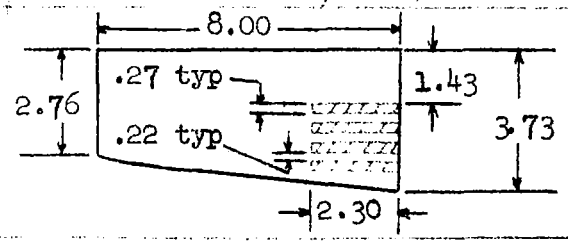

Note: Unshaded areas indicate portions of bleed plates through which bleed flow may occur.

TABLE I.- BLEED CONFIGURATIONS- Concluded

Configuration 4			
Bleed plate location	Bleed plate porosity, percent	Net porous area, sq in.	Bleed plate geometry, dimensions in inches
Third ramp	$3\frac{1}{2}$	13.48	Same as Configuration 1
Fourth ramp	$3\frac{1}{2}$	8.54	Same as Configuration 1
Fifth ramp	$3\frac{1}{2}$	16.28	Same as Configuration 1
Cowl side plate	$3\frac{1}{2}$	24.62	Same as Configuration 1
Cowl top and bottom plates	$3\frac{1}{2}$	26.17	Same as Configuration 1

TABLE II.- SUMMARY LISTING OF CONFIGURATIONS TESTED

Configuration designation	Basic model inlet details					Wing version	Forebody version	Canard version
	Inlet version	Cowl lip angle, deg	Bleed config.	Wing-inlet bleed gutter, ht., in.	Wedge ext. config.			
IRCS	172	11	No bleed	0.100				
$IR_1C_1S_1$	172	11	1	.100				
$IR_2C_2S_2$	172	11	2	.100				
$IR_3C_3S_3$	172	11	3	.100				
$IR_4C_4S_4$	172	11	4	.100				
$IR_4C'_4S_4$	172	8	4	.100				
$W_TIR_4C_4S_4$	172	11	4	.100		172		
$W_{T_2}IR_4C_4S_4$	172	11	4	.100		154		
$W_{T_3}I_2R_4C_4S_4$	145	11	4	.100	1	145		
W_TB_TIRCS	172	11	No bleed	.100		172	172	
$W_TB_TIR_4C'_4S_4$	172	8	4	.100		172	172	
$W_TB_TC_TIR_4C_4S_4$	172	11	4	.100		172	172	172
$W_TB_TC_TIR_4C'_4S_4$	172	8	4	.100		172	172	172
$W_{T_2}I_4R_4C_4S_4$	172	11	4	.165		154		
$W_{T_3}I_5R_4C_4S_4$	145	11	4	.100	2	145		
$W_{T_3}I_6R_4C_4S_4$	145	11	4	.100	3	145		

TABLE III.- INDEX TO GRAPHICAL DATA

Subject	Configuration	Figure
Pressure recovery, bleed effect	$IR_1C_1S_1$, $IR_2C_2S_2$ $IR_3C_3S_3$, $IR_4C_4S_4$	22
Pressure recovery, Mach number effect	$IR_4C_4S_4$	23
Pressure recovery, cowl lip angle effect	$IR_4C_4S_4$ $IR_4C'_4S_4$	24
Pressure recovery, attitude effect	$IR_4C_4S_4$	25
Pressure recovery, wing effect	$IR_4C_4S_4$ $W_TIR_4C_4S_4$ $W_{T_2}IR_4C_4S_4$ $W_{T_3}IR_4C_4S_4$	26
Pressure recovery, angle-of-attack effect at three Mach numbers	$W_TIR_4C_4S_4$	27
Pressure recovery, angle-of-attack effect at three Mach numbers	$W_{T_2}IR_4C_4S_4$	28
Pressure recovery, angle-of-attack effect	$W_{T_3}I_2R_4C_4S_4$	29
Wing pressure coefficients, comparison of wing types for various angles of attack	$W_TIR_4C_4S_4$ $W_{T_2}IR_4C_4S_4$ $W_{T_3}IR_4C_4S_4$	30, 31, 32
Wing pressure coefficients, Mach number effect	$W_TIR_4C_4S_4$	33
Wing pressure coefficients, canard effect	$W_TB_TC_TIR_4C'_4S_4$ $W_TB_TIR_4C'_4S_4$	34
Wing pressure coefficients, forebody and canard effect	$W_TIR_4C_4S_4$ $W_TB_TC_TIR_4C_4S_4$	35

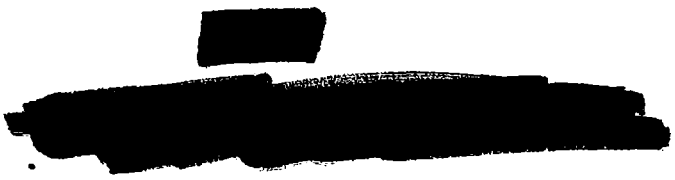

TABLE IV.- INDEX TO TABULATED DATA

Subject	Configuration	Table
Bleed configurations	All	I
List of configurations tested	All	II
External cowl pressure ratios	IRCS	V
External cowl pressure ratios	W_TB_TIRCS	VI
Internal duct pressure ratios, showing effect of bleed configuration	$IR_1C_1S_1$ $IR_2C_2S_2$ $IR_3C_3S_3$ $IR_4C_4S_4$	VII
Internal duct pressure ratios, showing effect of Mach number	$IR_4C_4S_4$	VIII
Internal duct pressure ratios, showing effect of wing additions	$IR_4C_4S_4$ $W_TIR_4C_4S_4$ $W_{T_2}IR_4C_4S_4$ $W_{T_3}IR_4C_4S_4$	IX
Internal duct pressure ratios, showing effect of variation of cowl lip angle	$IR_4C_4S_4$ $IR_4C'_4S_4$	X
Internal duct pressure ratios, showing effect of variations of model attitude	$IR_4C_4S_4$	XI
Internal duct pressure ratios, showing effect of wing, forebody, and canard	$IR_4C_4S_4$	XII
Internal duct pressure ratios, showing effect of the canard	$W_TB_TC_TIR_4C'_4S_4$ $W_TB_TIR_4C'_4S_4$	XIII
Internal duct pressure ratios, showing effect of variation in bleed gutter height	$W_{T_2}IR_4C_4S_4$ $W_{T_2}I_4R_4C_4S_4$	XIV
Internal duct pressure ratios, showing effect of the wedge extensions	$W_{T_3}I_2R_4C_4S_4$ $W_{T_3}I_5R_4C_4S_4$ $W_{T_3}I_6R_4C_4S_4$	XV

[redacted]

TABLE V.- EXTERNAL SURFACE-PRESSURE RATIOS FOR THE IRCS CONFIGURATION AT OPTIMUM INLET PRESSURE RECOVERY

	(a) $M_\infty = 2.955$, $\beta = 0^\circ$			(b) $M_\infty = 2.799$, $\beta = 0^\circ$		(c) $M_\infty = 2.578$, $\beta = 0^\circ$		
	p/p_{t_∞}			p/p_{t_∞}		p/p_{t_∞}		
Orifice number	$\alpha=0.2^\circ$	$\alpha=2.2^\circ$	$\alpha=4.2^\circ$	$\alpha=2.2^\circ$	$\alpha=4.2^\circ$	$\alpha=0.2^\circ$	$\alpha=2.2^\circ$	$\alpha=4.2^\circ$
36	0.094	0.092	0.116	0.108	0.138	0.148	0.128	0.132
36A	.074	.072	.095	.085	.097	.104	.096	.093
36B	.053	.036	.058	.064	.055	.080	.078	.060
36C	.040	.038	.033	.039	.031	.050	.047	.035
37	.038	.037	.035	.041	.038	.058	.052	.048
38	.040	.034	.030	.039	.037	.057	.056	.053
39	.039	.040	.040	.045	.046	.064	.062	.063
40	.026	.028	.032	.037	.040	.052	.052	.055
41	.022	.022	.021	.025	.026	.038	.037	.037
42	.096	.100	.055	.097	.074	.113	.116	.095
42A	.070	.072	.050	.066	.060	.088	.081	.077
42B	.045	.046	.041	.052	.054	.075	.067	.065
42C	.040	.042	.043	.049	.052	.067	.063	.066
43	.039	.041	.042	.046	.049	.059	.058	.060
44	.034	.034	.035	.039	.041	.056	.054	.055
45	.038	.041	.040	.047	.047	.066	.066	.067
46	.030	.034	.037	.042	.045	.058	.057	.062
47	.018	.021	.023	.026	.029	.039	.038	.042
48	.022	.029	.034	.037	.042	.052	.053	.058
49	.022	.027	.030	.034	.038	.048	.048	.053
50	.028	.030	.033	.039	.040	.055	.055	.057
51	.028	.030	.032	.037	.039	.052	.051	.054
52	.027	.029	.033	.036	.039	.050	.050	.055
53	.045	.049	.045	.048	.047	.067	.056	.063
54	.032	.035	.040	.045	.048	.061	.061	.066
55	.031	.035	---	.043	.045	.060	.060	.065
56	.031	.033	---	.041	.044	.051	.055	.059
57	.028	.030	---	.037	.040	.052	.052	.055
58	.029	.032	---	.037	.040	.050	.050	.053
59	.030	.035	---	.041	.052	.058	.060	.069
60	.030	.033	---	.041	.046	.057	.058	.063
61	.032	.035	---	.043	.047	.062	.063	.065
62	.029	.033	---	.041	.044	.055	.055	.060
63	.028	.030	---	.036	.041	.025	.050	.053
64	.028	.030	---	.036	.037	.049	.048	.050

[redacted]

[redacted]

TABLE VI.- EXTERNAL SURFACE-PRESSURE RATIOS FOR THE W_TB_TIRCS CONFIGURATION AT OPTIMUM INLET PRESSURE RECOVERY

	(a) $M_\infty = 2.955$, $\beta = 0^\circ$		(b) $M_\infty = 2.578$, $\beta = 0^\circ$	
	p/p_{t_∞}		p/p_{t_∞}	
Orifice number	$\alpha = 2.2^\circ$	$\alpha = 4.2^\circ$	$\alpha = 2.2^\circ$	$\alpha = 4.2^\circ$
36	0.107	0.110	0.157	0.161
36A	.072	.084	.109	.129
36B	.067	.065	.117	.125
36C	.044	.050	.075	.082
37	.051	.054	.075	.079
38	.040	.045	.061	.068
39	.048	.038	.060	.067
40	.032	.035	.060	.063
41	.070	.057	.045	.050
42	.085	.103	.133	.120
42A	.073	.076	.097	.096
42B	.060	.052	.083	.089
42C	.048	.050	.065	.072
43	.043	.052	.067	.077
44	.040	.044	.063	.063
45	.035	.039	.060	.069
46	.031	.035	.055	.061
47	.023	.027	.041	.046
48	.029	.034	.050	.057
49	.029	.032	.048	.054
50	.033	.037	.055	.063
51	.029	.033	.050	.055
52	.030	.034	.050	.056
53	.046	.053	.065	.079
54	.037	.040	.065	.070
55	.035	.040	.067	.073
56	.035	.038	.056	.063
57	.030	.033	.052	.057
58	.030	.033	.049	.055
59	.033	.036	.057	.064
60	.032	.035	.057	.062
61	.037	.039	.069	.075
62	.034	.038	.057	.062
63	.030	.033	.051	.056
64	.029	.031	.048	.053

[redacted]

TABLE VII.- INTERNAL DUCT SURFACE-PRESSURE RATIOS AT OPTIMUM INLET PRESSURE RECOVERY FOR THE BASIC MODEL EMPLOYING FOUR DIFFERENT BOUNDARY-LAYER BLEED CONFIGURATIONS; $M_\infty = 2.88$, $\alpha = 0.2^\circ$, $\beta = 0^\circ$

Orifice number	p/p_{t_∞}				Orifice number	p/p_{t_∞}			
	$IR_1C_1S_1$	$IR_2C_2S_2$	$IR_3C_3S_3$	$IR_4C_4S_4$		$IR_1C_1S_1$	$IR_2C_2S_2$	$IR_3C_3S_3$	$IR_4C_4S_4$
65	0.056	0.057	0.055	0.057	91	0.210	0.216	0.223	0.229
66	.071	.071	.069	.071	92	.676	.378	.306	.420
67	.093	.095	.091	.077	93	.364	.362	.369	.476
68	.096	.098	.094	.097	94	.363	.509	.360	.488
69	.052	.053	.052	.053	95	.366	.595	.535	.602
70	.053	.055	.052	.055	96	.628	.614	.750	.729
71	.052	.054	.052	.054	97	.615	.606	.600	.663
72	.068	.068	.067	.069	98	.616	.591	.600	.653
73	.069	.070	.069	.070	99	.648	.603	.612	.670
74	.095	.091	.095	.088	100	.680	.625	.643	.717
75	.121	.123	.135	.132	101	.646	.573	.612	.651
76	.267	.222	.243	.273	102	.834	.731	.795	.820
77	.221	.173	.239	.346	103	.856	.744	.822	.845
78	.308	.293	.322	.269	104	.864	.731	.830	.854
79	.280	.425	.321	.421	105	.869	.729	.834	.858
80	.500	.533	.543	.496	106	.870	.728	.835	.859
81	.625	.570	.595	.582	107	.244	.303	.253	.167
82	.653	.579	.632	.619	108	.121	.168	.123	.220
83	.795	.663	.747	.771	109	.112	.235	.123	.188
84	.831	.728	.792	.693	110	.074	.211	.073	.085
85	.853	.761	.820	.844	111	.873	.784	.837	.863
86	.864	.773	.830	.854	112	.287	.300	.295	.073
87	.869	.777	.833	.857	113	.044	.108	.042	.046
88	.873	.784	.837	.864	114	.097	.255	.081	.082
89	.137	.135	.134	.133	115	.203	.449	.169	.126
90	.167	.165	.166	.163	116	.871	.780	.835	.860

TABLE VIII.- INTERNAL DUCT SURFACE-PRESSURE RATIOS AT OPTIMUM INLET PRESSURE RECOVERY FOR THE BASIC MODEL AT FOUR DIFFERENT MACH NUMBERS; $\alpha = 0.2^{\circ}$, $\beta = 0^{\circ}$

$IR_4C_4S_4$ configuration									
Orifice number	p/p_{t_∞}				Orifice number	p/p_{t_∞}			
	$M_\infty = 2.498$	$M_\infty = 2.700$	$M_\infty = 2.880$	$M_\infty = 2.955$		$M_\infty = 2.498$	$M_\infty = 2.700$	$M_\infty = 2.880$	$M_\infty = 2.955$
65	0.103	0.074	0.057	0.050	91	0.271	0.223	0.229	0.213
66	.116	.088	.071	.063	92	.330	.341	.420	.411
67	.126	.108	.077	.085	93	.258	.287	.476	.389
68	.125	.109	.097	.089	94	.276	.373	.488	.422
69	.091	.068	.053	.048	95	.278	.512	.602	.391
70	.092	.069	.055	.048	96	.639	.661	.729	.501
71	.091	.068	.054	.048	97	.672	.634	.663	.486
72	.113	.086	.069	.061	98	.683	.642	.653	.415
73	.118	.088	.070	.063	99	.701	.662	.670	.394
74	.113	.098	.088	.081	100	.739	.710	.717	.636
75	.076	.061	.132	.045	101	.681	.650	.651	.613
76	.086	.158	.273	.254	102	.815	.815	.820	.796
77	.136	.174	.346	.076	103	.835	.838	.845	.824
78	.318	.304	.269	.252	104	.846	.849	.854	.832
79	.335	.286	.421	.376	105	.855	.856	.858	.837
80	.269	.430	.496	.364	106	.859	.860	.859	.839
81	.617	.584	.582	.371	107	.265	.251	.167	.139
82	.662	.630	.619	.573	108	.325	.336	.220	.151
83	.772	.768	.771	.739	109	.533	.521	.188	.118
84	.810	.810	.693	.791	110	.620	.589	.085	.061
85	.827	.835	.844	.824	111	.862	.863	.863	.842
86	.845	.850	.854	.833	112	.277	.314	.073	.043
87	.856	.856	.857	.836	113	.308	.362	.046	.038
88	.865	.863	.864	.842	114	.550	.507	.082	.038
89	.134	.133	.133	.129	115	.606	.595	.126	.055
90	.166	.174	.163	.155	116	.859	.860	.860	.839

TABLE IX.- INTERNAL DUCT SURFACE-PRESSURE RATIOS AT OPTIMUM INLET PRESSURE RECOVERY FOR THE BASIC MODEL AT $M_\infty = 2.88$, AND THE BASIC MODEL PLUS WING ADDITIONS AT $M_\infty = 2.955$; $\alpha = 0.2^\circ$, $\beta = 0^\circ$

Orifice number	p/p_{t_∞}				Orifice number	p/p_{t_∞}			
	$IR_4C_4S_4$	$W_TIR_4C_4S_4$	$W_{T_2}IR_4C_4S_4$	$W_{T_3}IR_4C_4S_4$		$IR_4C_4S_4$	$W_TIR_4C_4S_4$	$W_{T_2}IR_4C_4S_4$	$W_{T_3}IR_4C_4S_4$
65	0.057	0.049	0.051	0.056	91	0.229	0.194	0.195	0.222
66	.071	.062	.063	.066	92	.420	.416	.023	.407
67	.077	.084	.088	.089	93	.476	.396	.389	.392
68	.097	.772	.414	.435	94	.488	.412	.421	.420
69	.053	.044	.048	.064	95	.602	.539	.436	.533
70	.055	.046	.050	.064	96	.729	.707	.694	.711
71	.054	.046	.049	.064	97	.663	.705	.657	.603
72	.069	.060	.063	.064	98	.653	.614	.640	.587
73	.070	.062	.065	.064	99	.670	.637	.660	.610
74	.088	.770	.083	.076	100	.717	.680	.707	.621
75	.132	.782	.048	.064	101	.651	.627	.645	.595
76	.273	.263	.259	.279	102	.820	.798	.696	.790
77	.346	.308	.220	.308	103	.845	.836	.835	.815
78	.269	.236	.256	.244	104	.854	.837	.843	.823
79	.421	.377	.246	.379	105	.858	.843	.848	.826
80	.496	.474	.501	.469	106	.859	.849	.851	.831
81	.582	.556	.601	.533	107	.167	.146	.134	.089
82	.619	.609	.630	.578	108	.220	.731	.156	.114
83	.771	.750	.763	.739	109	.188	.782	.126	.024
84	.693	.794	.807	.668	110	.085	.066	.078	.068
85	.844	.822	.833	.816	111	.863	.849	.853	.834
86	.854	.838	.845	.823	112	.073	.038	.158	.143
87	.857	.845	.848	.825	113	.046	.038	.045	.039
88	.864	.851	.853	.833	114	.082	.037	.150	.122
89	.133	.148	.138	.126	115	.126	.053	.156	.122
90	.163	.165	.161	.144	116	.860	.846	.850	.831

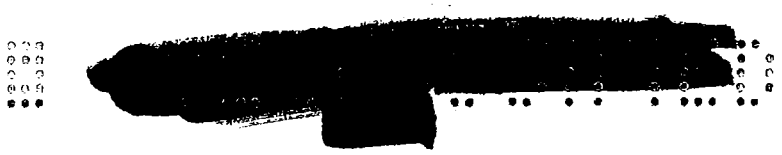

TABLE X.- INTERNAL DUCT SURFACE-PRESSURE RATIOS AT OPTIMUM INLET PRESSURE RECOVERY FOR THE BASIC MODEL EMPLOYING CONSTANT INTERNAL DUCT GEOMETRY AND VARYING COWL LIP ANGLES; $M_\infty = 2.880$, $\alpha = 0.2^\circ$, $\beta = 0^\circ$

Orifice number	p/p_{t_∞}		Orifice number	p/p_{t_∞}	
	$IR_4C_4S_4$	$IR_4C'_4S_4$		$IR_4C_4S_4$	$IR_4C'_4S_4$
65	0.057	0.055	91	0.229	0.289
66	.071	.070	92	.420	.330
67	.077	.092	93	.476	.174
68	.097	.095	94	.488	.415
69	.053	.052	95	.602	.443
70	.055	.103	96	.729	.575
71	.054	.103	97	.663	.623
72	.069	.067	98	.653	.654
73	.070	.070	99	.670	.674
74	.088	.087	100	.717	.689
75	.132	.049	101	.651	.711
76	.273	.313	102	.820	.817
77	.346	.175	103	.845	.844
78	.269	.232	104	.854	.857
79	.421	.330	105	.858	.857
80	.496	.504	106	.859	.860
81	.582	.590	107	.167	.168
82	.619	.634	108	.220	.226
83	.771	.769	109	.188	.208
84	.693	.814	110	.085	.100
85	.844	.842	111	.863	.862
86	.854	.853	112	.073	.056
87	.857	.857	113	.046	.044
88	.864	.863	114	.082	.039
89	.133	.164	115	.126	.115
90	.163	.140	116	.860	.860

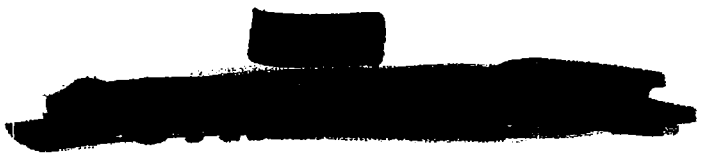

[redacted]

TABLE XI.- INTERNAL DUCT SURFACE-PRESSURE RATIOS AT OPTIMUM INLET PRESSURE RECOVERY FOR THE BASIC MODEL AT THREE ATTITUDES; M_∞=2.880

$IR_4C_4S_4$ configuration							
Orifice number	p/p_{t_∞}			Orifice number	p/p_{t_∞}		
	$\alpha = 0.2^\circ$ $\beta = 0^\circ$	$\alpha = 2.2^\circ$ $\beta = 0^\circ$	$\alpha = 0.2^\circ$ $\beta = 2.2^\circ$		$\alpha = 0.2^\circ$ $\beta = 0^\circ$	$\alpha = 2.2^\circ$ $\beta = 0^\circ$	$\alpha = 0.2^\circ$ $\beta = 2.2^\circ$
65	0.057	0.050	0.066	91	0.229	0.212	0.211
66	.071	.064	.080	92	.420	.430	.337
67	.077	.089	.101	93	.476	.396	.318
68	.097	.097	.105	94	.488	.452	.439
69	.053	.052	.062	95	.602	.570	.428
70	.055	.053	.063	96	.729	.700	.451
71	.054	.049	.062	97	.663	.622	.509
72	.069	.065	.078	98	.653	.623	.632
73	.070	.066	.080	99	.670	.642	.631
74	.088	.088	.091	100	.717	.692	.693
75	.132	.049	.048	101	.651	.620	.646
76	.273	.276	.243	102	.820	.800	.804
77	.346	.336	.192	103	.845	.830	.831
78	.269	.252	.286	104	.854	.843	.842
79	.421	.404	.256	105	.858	.850	.849
80	.496	.470	.273	106	.859	.856	.657
81	.582	.543	.579	107	.167	.193	.310
82	.619	.599	.609	108	.220	.209	.304
83	.771	.745	.756	109	.188	.175	.361
84	.693	.796	.800	110	.085	.078	.267
85	.844	.825	.826	111	.863	.858	.854
86	.854	.843	.842	112	.073	.093	.330
87	.857	.851	.849	113	.046	.048	.252
88	.864	.858	.856	114	.082	.102	.444
89	.133	.137	.133	115	.126	.141	.532
90	.163	.164	.173	116	.860	.855	.852

[redacted]

[redacted]

TABLE XII.- INTERNAL DUCT SURFACE-PRESSURE RATIOS AT OPTIMUM INLET PRESSURE RECOVERY FOR THE BASIC MODEL AT $M_\infty = 2.880$, AND THE BASIC MODEL PLUS A WING, FOREBODY, AND CANARD AT $M_\infty = 2.955$; $\alpha = 2.2^\circ$, $\beta = 0^\circ$

Orifice number	p/p_{t_∞}		Orifice number	p/p_{t_∞}	
	$IR_4C_4S_4$	$W_TB_TC_TIR_4C_4S_4$		$IR_4C_4S_4$	$W_TB_TC_TIR_4C_4S_4$
65	0.050	0.055	91	0.212	0.209
66	.064	.072	92	.430	.560
67	.089	.093	93	.396	.527
68	.097	.099	94	.452	.528
69	.052	.054	95	.570	.528
70	.053	.056	96	.700	.585
71	.049	.059	97	.622	.508
72	.065	.072	98	.623	.459
73	.066	.076	99	.642	.439
74	.088	.091	100	.692	.426
75	.049	.046	101	.620	.333
76	.276	.295	102	.800	.768
77	.336	.317	103	.830	.798
78	.252	.463	104	.843	.809
79	.404	.445	105	.850	.816
80	.470	.375	106	.856	.821
81	.543	.407	107	.193	.174
82	.599	.338	108	.209	.117
83	.745	.704	109	.175	.099
84	.796	.739	110	.078	.044
85	.825	.792	111	.858	.823
86	.843	.813	112	.093	.043
87	.851	.819	113	.048	.043
88	.858	.823	114	.102	.043
89	.137	.149	115	.141	.054
90	.164	.196	116	.855	.818

[redacted]

[redacted]

TABLE XIII.- INTERNAL DUCT SURFACE-PRESSURE RATIOS AT OPTIMUM INLET PRESSURE RECOVERY FOR THE BASIC MODEL WITH A WING, FOREBODY, AND CANARD, AND WITH A WING AND FOREBODY; $M_\infty = 2.955$, $\alpha = 2.2^\circ$, $\beta = 0^\circ$

Orifice number	p/p_{t_∞}		Orifice number	p/p_{t_∞}	
	$W_TB_TC_TIR_4C'_4S_4$	$W_TB_TIR_4C'_4S_4$		$W_TB_TC_TIR_4C'_4S_4$	$W_TB_TIR_4C'_4S_4$
65	0.057	0.023	91	0.259	0.253
66	.072	.059	92	.320	.319
67	.092	.082	93	.370	.326
68	.098	.093	94	.389	.353
69	.055	.050	95	.416	.426
70	.057	.051	96	.471	.571
71	.060	.050	97	.584	.595
72	.072	.062	98	.627	.630
73	.170	.203	99	.646	.649
74	.090	.083	100	.661	.662
75	.048	.051	101	.556	.536
76	.308	.297	102	.799	.796
77	.273	.165	103	.824	.820
78	.293	.205	104	.832	.805
79	.313	.312	105	.841	.837
80	.419	.495	106	.739	.698
81	.566	.577	107	.668	.667
82	.616	.619	108	.155	.164
83	.752	.749	109	.806	.173
84	.774	.745	110	.078	.084
85	.816	.702	111	.848	.843
86	.820	.840	112	.043	.041
87	.841	.837	113	.047	.047
88	.849	.812	114	.051	.061
89	.173	.163	115	.102	.096
90	.153	.139	116	.844	.842

[redacted]

[redacted]

TABLE XIV.- INTERNAL DUCT SURFACE-PRESSURE RATIOS AT OPTIMUM INLET PRESSURE RECOVERY FOR THE BASIC MODEL PLUS A WING CONFIGURATION, USING TWO BLEED GUTTER HEIGHTS BETWEEN THE WING AND INLET; $M_\infty = 2.955$, $\alpha = 0.2^\circ$, $\beta = 0^\circ$

Orifice number	p/p_{t_∞}		Orifice number	p/p_{t_∞}	
	$W_{T_2}IR_4C_4S_4$	$W_{T_2}I_4R_4C_4S_4$		$W_{T_2}IR_4C_4S_4$	$W_{T_2}I_4R_4C_4S_4$
65	0.053	0.051	91	0.261	0.195
66	.065	.063	92	.360	.023
67	.088	.088	93	.351	.389
68	.093	.414	94	.516	.421
69	.048	.048	95	.588	.436
70	.050	.050	96	.532	.694
71	.049	.049	97	.601	.657
72	.063	.063	98	.621	.640
73	.065	.065	99	.651	.660
74	.081	.083	100	.687	.707
75	.138	.048	101	.557	.645
76	.268	.259	102	.700	.696
77	.320	.220	103	.673	.835
78	.259	.256	104	.663	.843
79	.426	.246	105	.658	.848
80	.507	.501	106	.673	.851
81	.584	.601	107	.160	.134
82	.611	.630	108	.200	.156
83	.754	.763	109	.099	.126
84	.781	.807	110	.150	.078
85	.829	.833	111	.850	.853
86	.842	.845	112	.130	.158
87	.660	.848	113	.042	.045
88	.850	.853	114	.121	.150
89	.139	.138	115	.139	.156
90	.142	.161	116	.847	.850

[redacted]

TABLE XV.- INTERNAL DUCT SURFACE-PRESSURE RATIOS AT OPTIMUM INLET PRESSURE RECOVERY FOR THE BASIC MODEL-PLUS-WING CONFIGURATION EMPLOYING CONSTANT INTERNAL DUCT GEOMETRY AND THREE WEDGE EXTENSION SHAPES; $M_\infty = 2.955$, $\alpha = 0.2^\circ$, $\beta = 0^\circ$

Orifice number	p/p_{t_∞}			Orifice number	p/p_{t_∞}		
	$W_{T_3}I_2R_4C_4S_4$	$W_{T_3}I_5R_4C_4S_4$	$W_{T_3}I_6R_4C_4S_4$		$W_{T_3}I_2R_4C_4S_4$	$W_{T_3}I_5R_4C_4S_4$	$W_{T_3}I_6R_4C_4S_4$
65	0.056	0.056	0.056	91	0.222	0.249	0.275
66	.066	.068	.067	92	.407	.455	.454
67	.089	.092	.091	93	.392	.378	.441
68	.435	.091	.088	94	.420	.459	.491
69	.064	.066	.066	95	.533	.437	.458
70	.064	.067	.066	96	.711	.382	.456
71	.064	.066	.066	97	.603	.454	.447
72	.064	.066	.066	98	.587	.427	.418
73	.064	.066	.066	99	.610	.550	.531
74	.076	.083	.080	100	.621	.630	.627
75	.064	.127	.136	101	.595	.518	.496
76	.279	.293	.289	102	.790	.732	.772
77	.308	.307	.339	103	.815	.801	.802
78	.244	.249	.294	104	.823	.815	.813
79	.379	.362	.380	105	.826	.822	.821
80	.469	.355	.369	106	.831	.793	.657
81	.533	.410	.413	107	.089	.137	.145
82	.578	.552	.545	108	.114	.155	.172
83	.739	.708	.709	109	.024	.093	.104
84	.668	.747	.747	110	.068	.123	.128
85	.816	.801	.801	111	.834	.829	.828
86	.823	.815	.800	112	.143	.069	.064
87	.825	.821	.818	113	.039	.037	.038
88	.833	.828	.828	114	.122	.041	.038
89	.126	.144	.131	115	.122	.057	.082
90	.144	.166	.153	116	.831	.824	.823

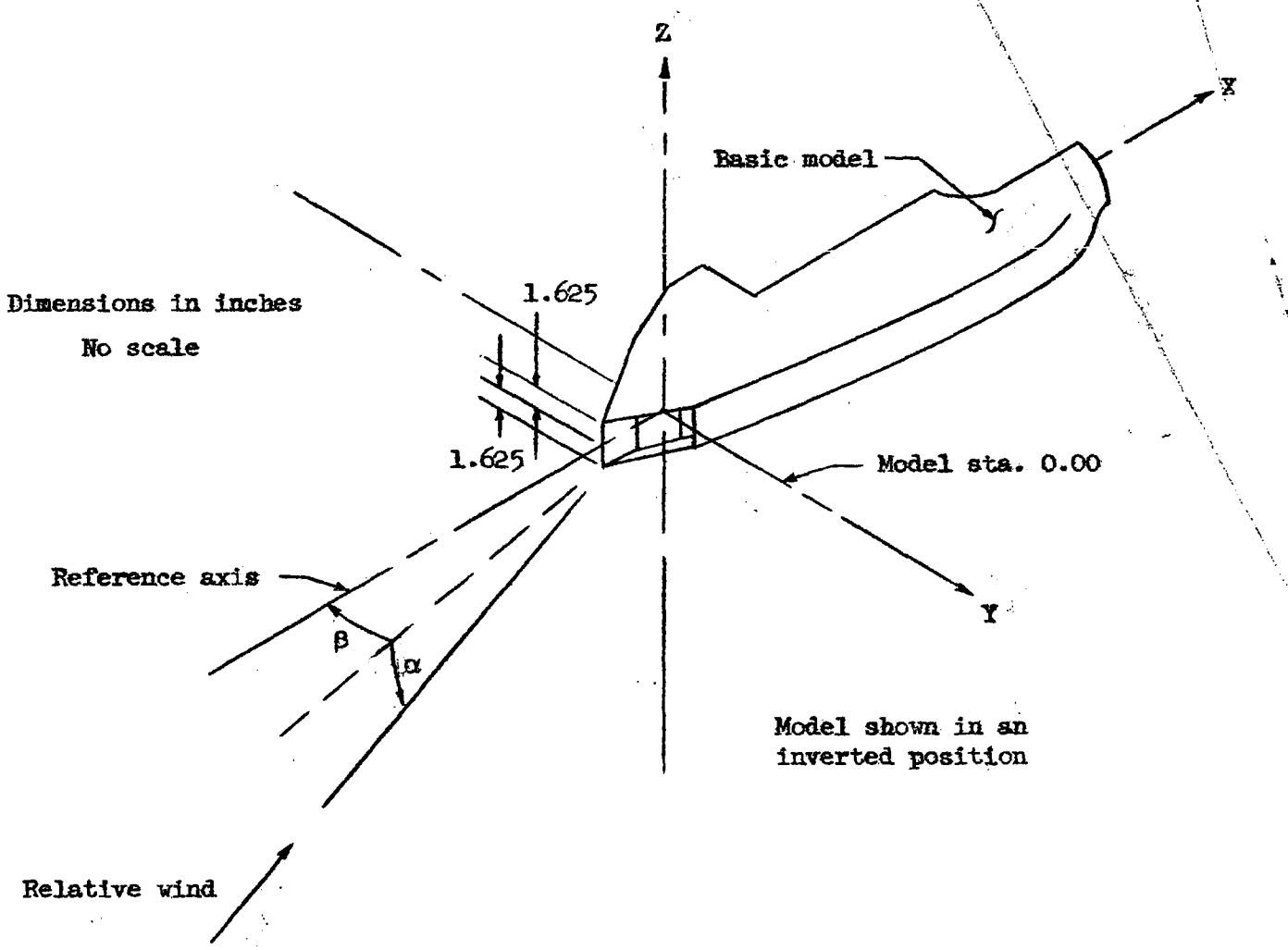

Figure 1.- System of axes and positive direction of angles.

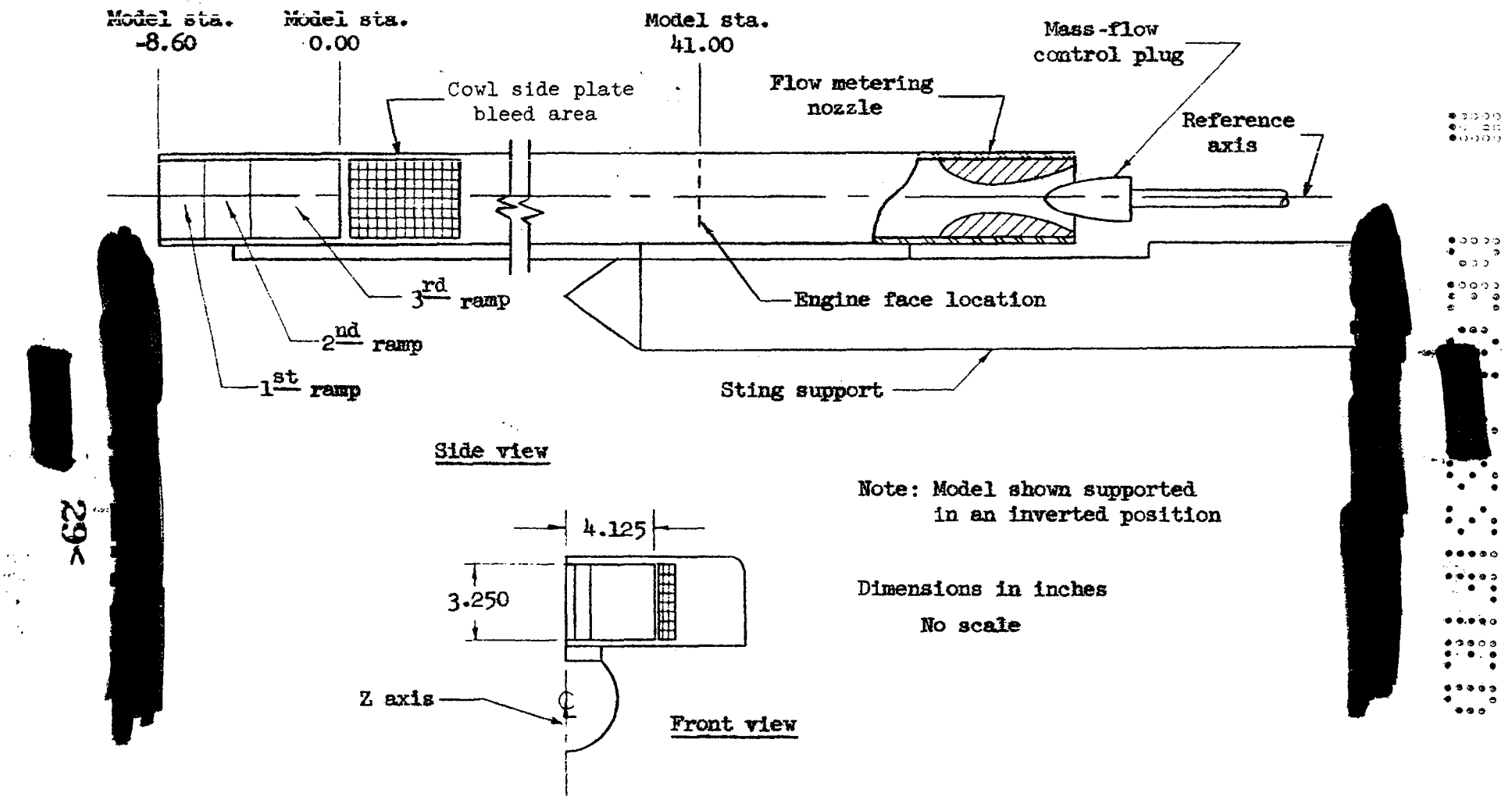

Figure 2.- Side view of the basic model incorporating the Number 172 inlet version.

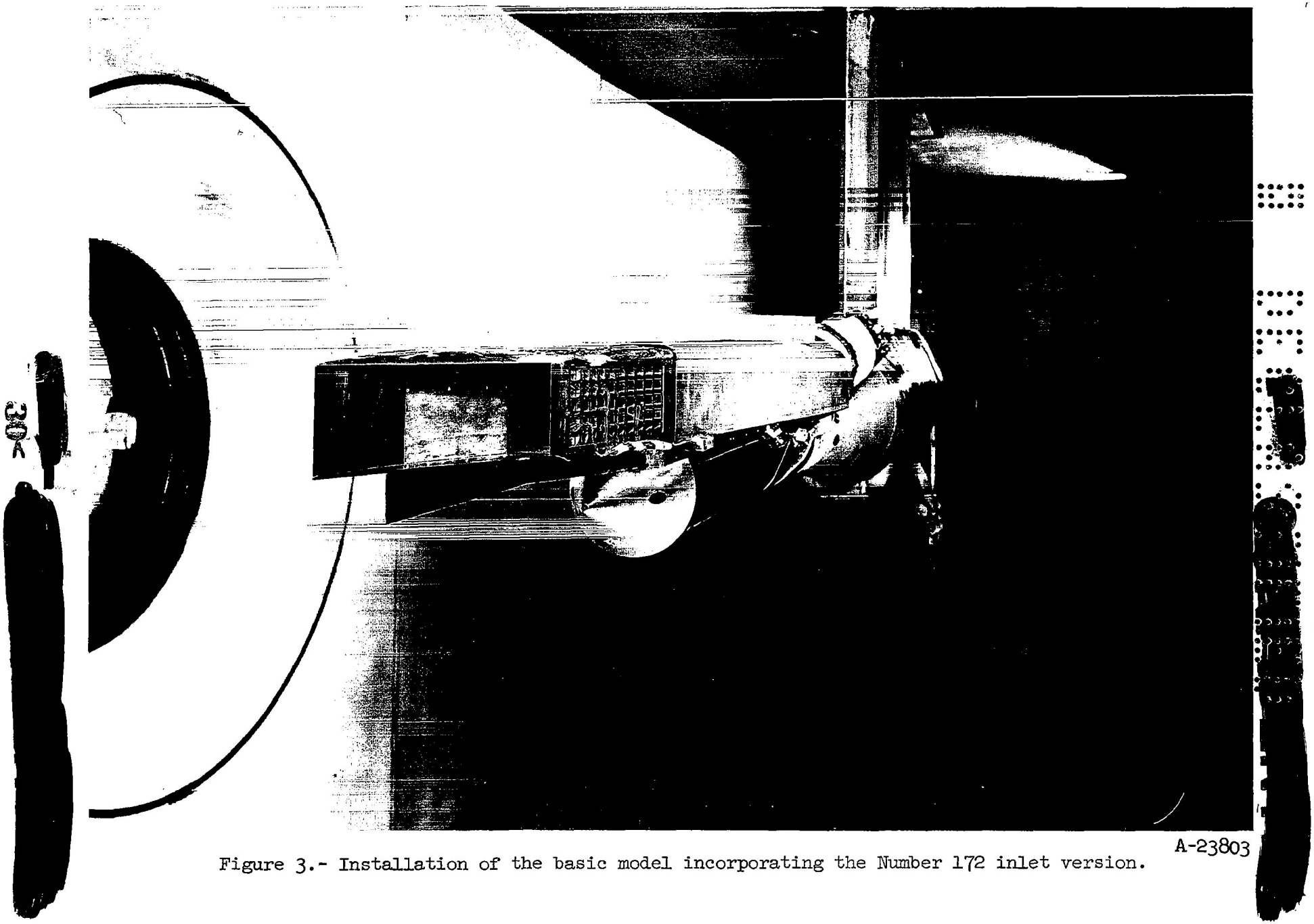

A-23803

Figure 3.- Installation of the basic model incorporating the Number 172 inlet version.

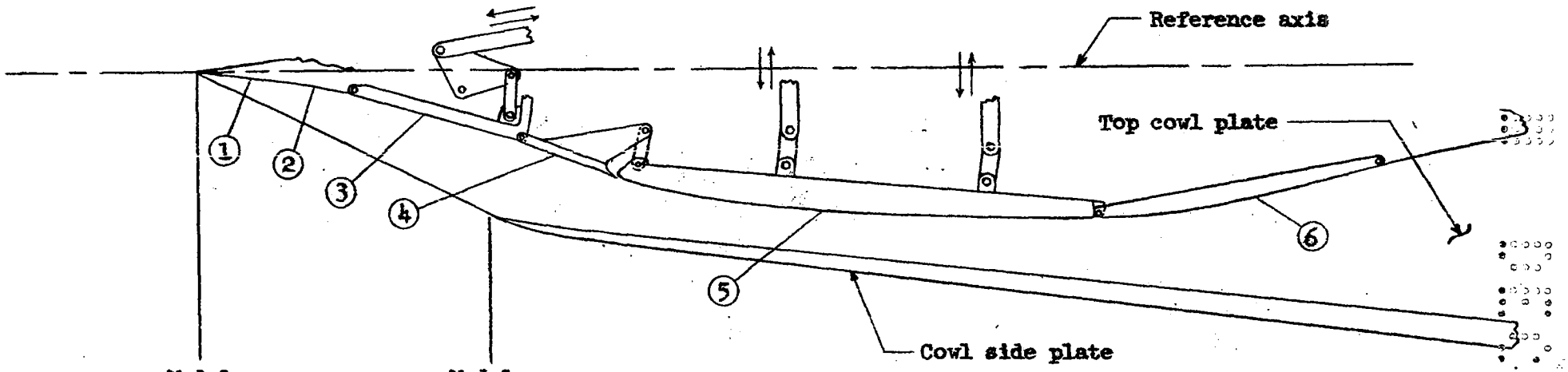

Notes - Numbers on figure indicate ramp designation

The angle between the first and second ramp surfaces and the reference axis are fixed at 7° and 11°, respectively.

Model is shown in inverted position.

No scale

Ramp Dimensional Data

Ramp number	Ramp length, in.	Ramp height, in.	Total ramp area, sq in.	Ramp area available for bleed control, sq in.
1	2.821	3.250	9.168	0.000
2	1.681	3.250	5.463	0.000
3	4.952	3.250	16.094	10.917
4	2.850	3.250	9.262	5.168
5	13.750*	varies	13.455*	13.455
6	8.130*	varies	20.065*	0.000

*Nominal values

Figure 4.- Schematic drawing of the number 172 inlet version, with bottom cowl plate removed showing the variable ramp system.

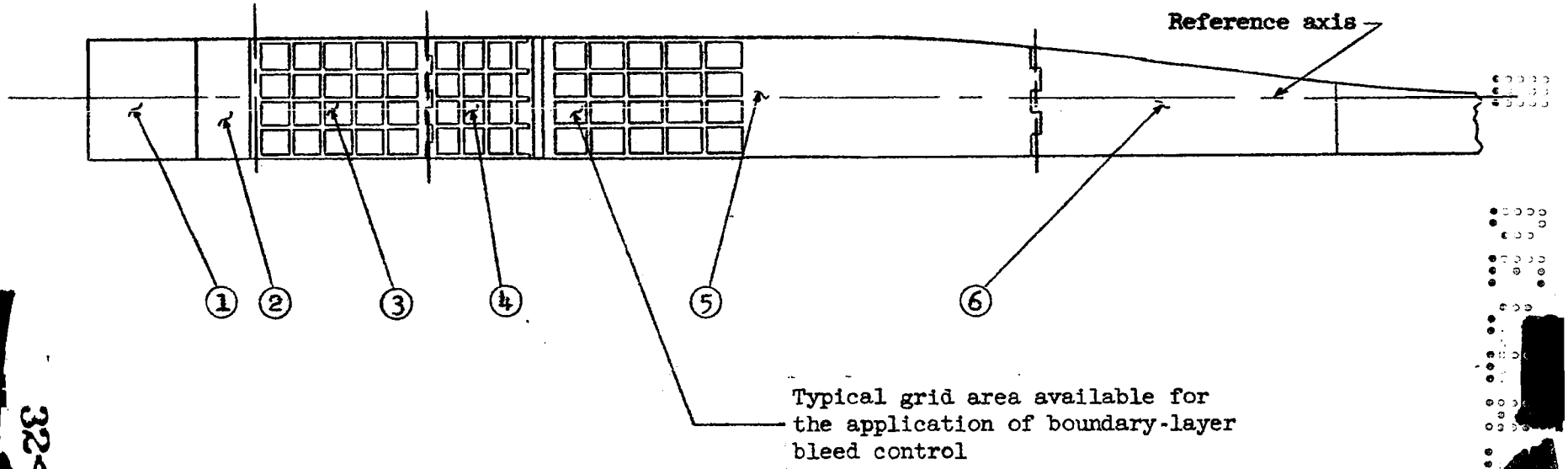

Note- Numbers on figure indicate ramp designation

Model is shown in inverted position

No scale

Figure 5.- Schematic side view of the variable ramp system shown in figure 3 showing relative locations of ramp areas available for boundary-layer bleed control.

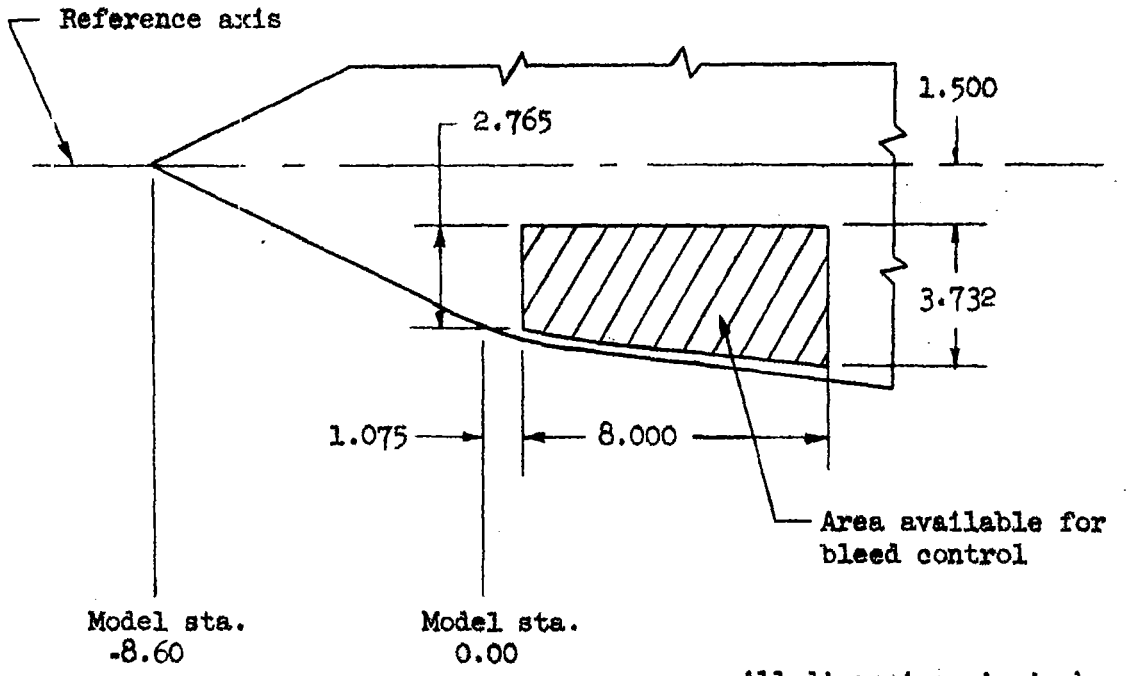

Note: Top cowl plate shown
Bottom cowl plate identical

Figure 6.- Schematic plan-view detail of top and bottom cowl plates of the Number 172 inlet version.

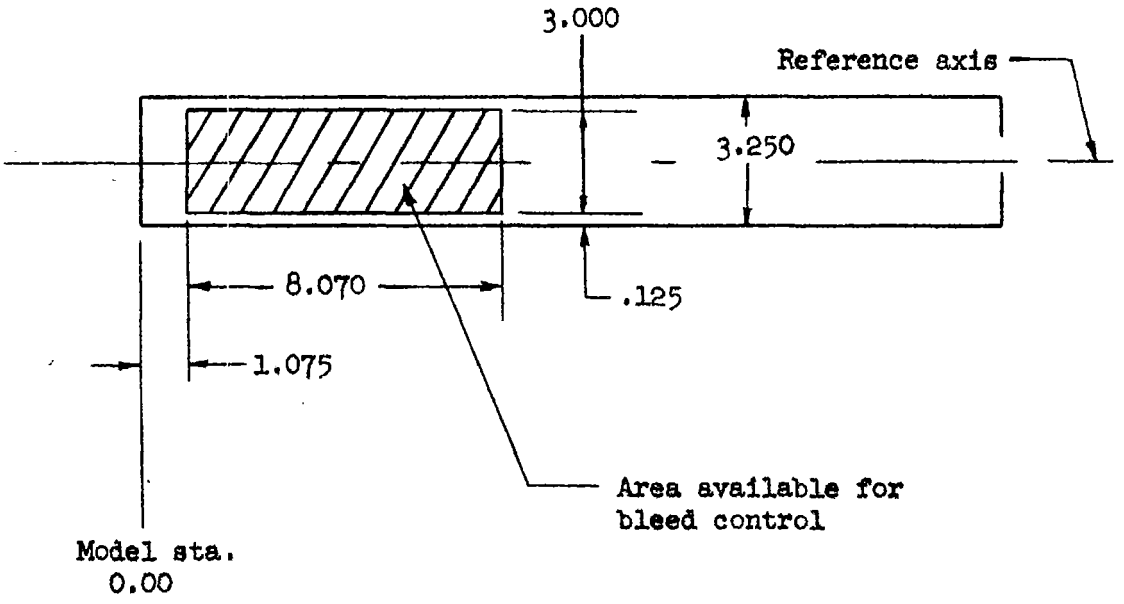

All dimensions in inches

No scale

Figure 7.- Schematic side-view detail of cowl side plate.

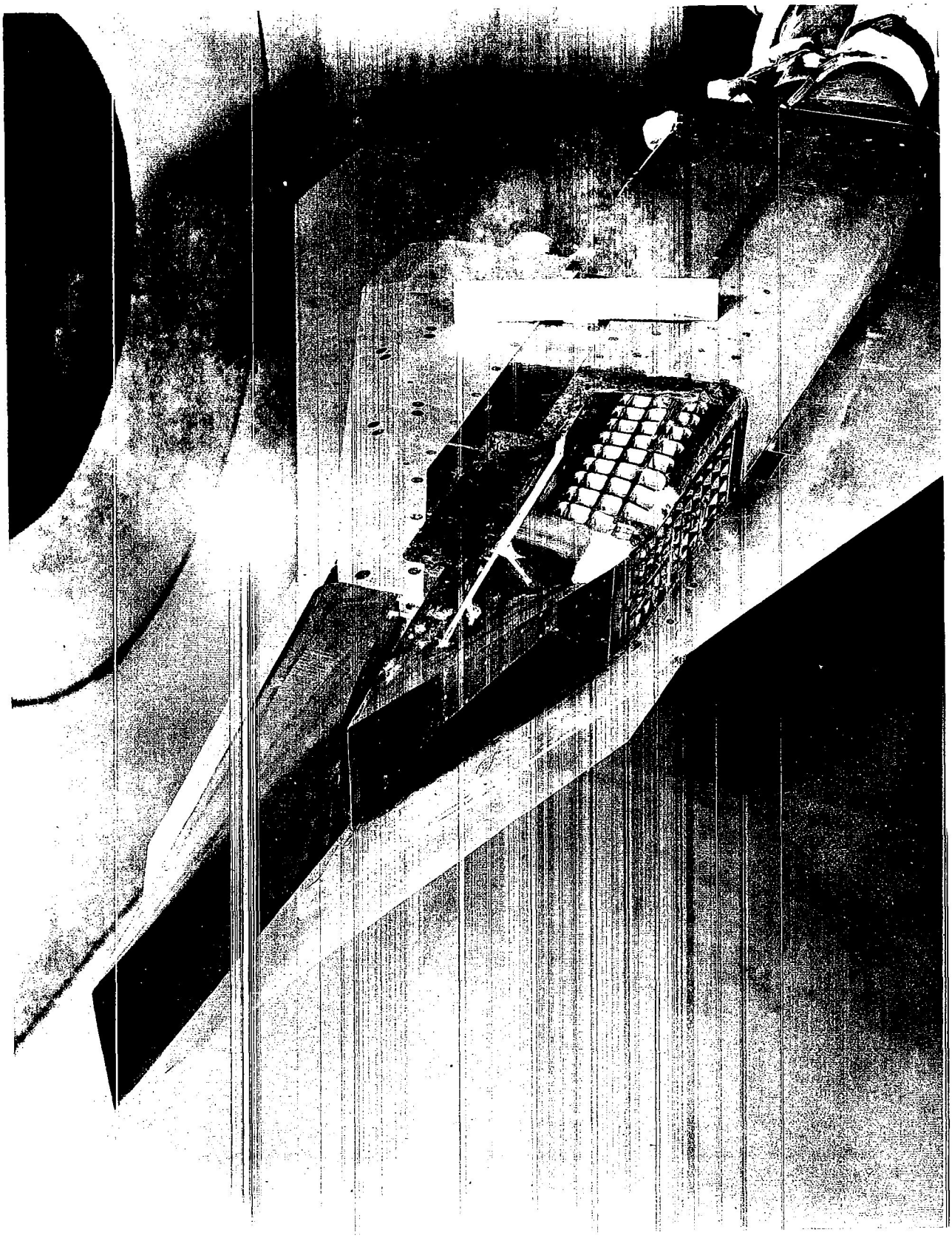

A-23851

Figure 8.- Modification of the inlet from the Number 172 version to the Number 145 version by use of wedge extension 1 and the W_T wing version.

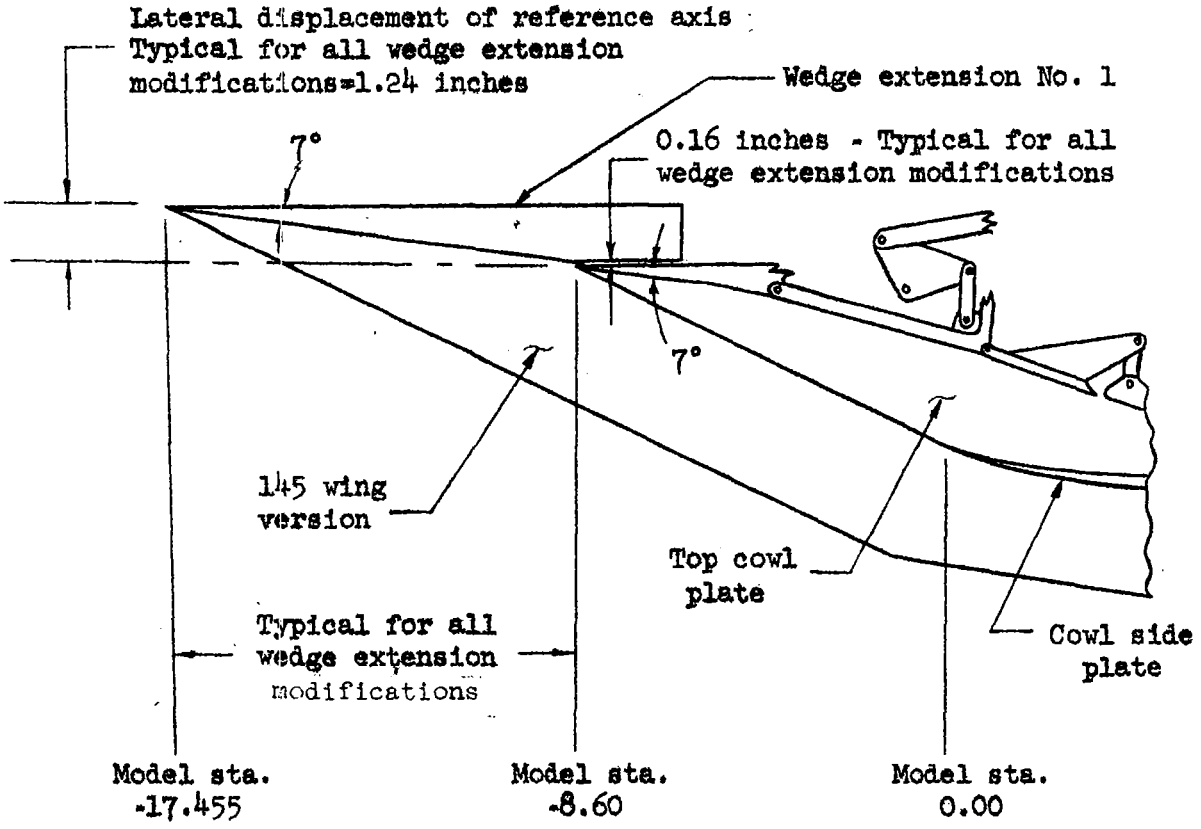

Figure 9.- Drawing of the Number 172 inlet version modified by the use of a typical wedge extension to the Number 145 version.

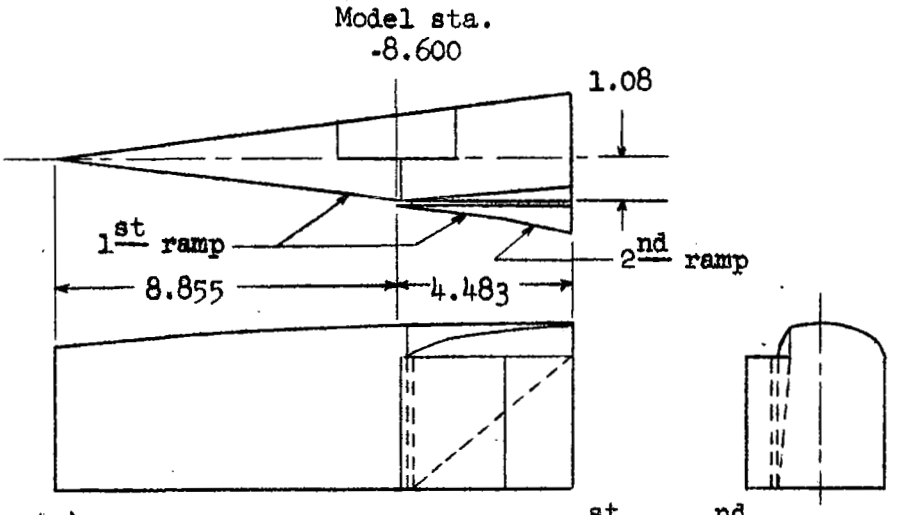

(a) Wedge extension Number 1 with 1st and 2nd ramps

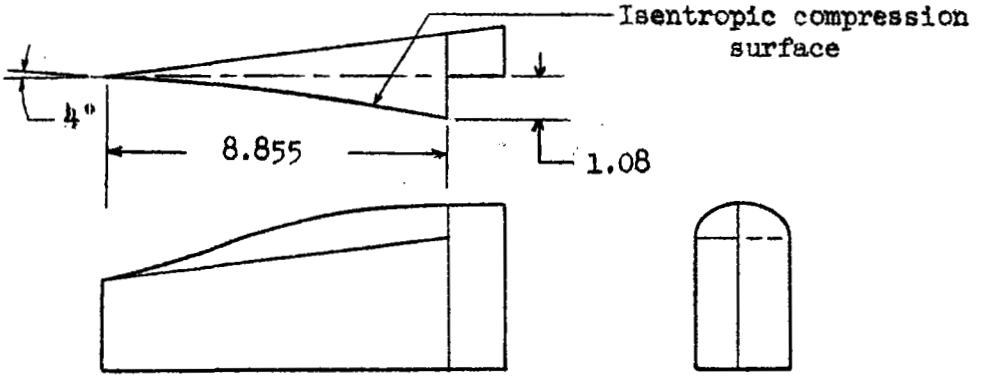

(b) Wedge extension Number 2

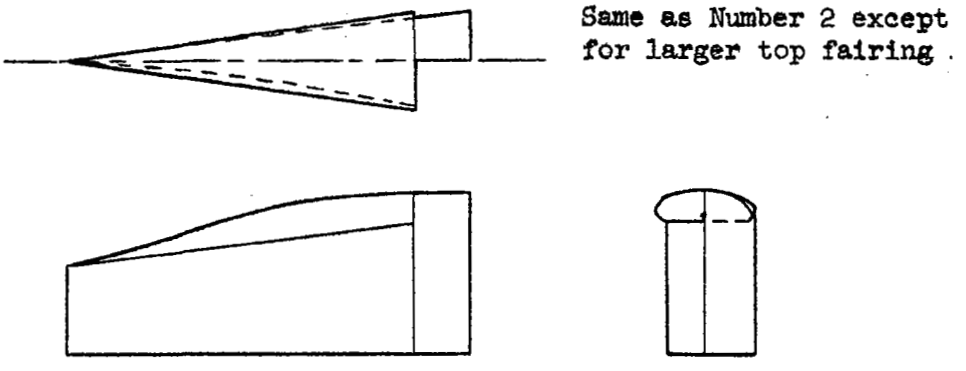

(c) Wedge extension Number 3

Figure 10.- Details of wedge extensions investigated.

[redacted]

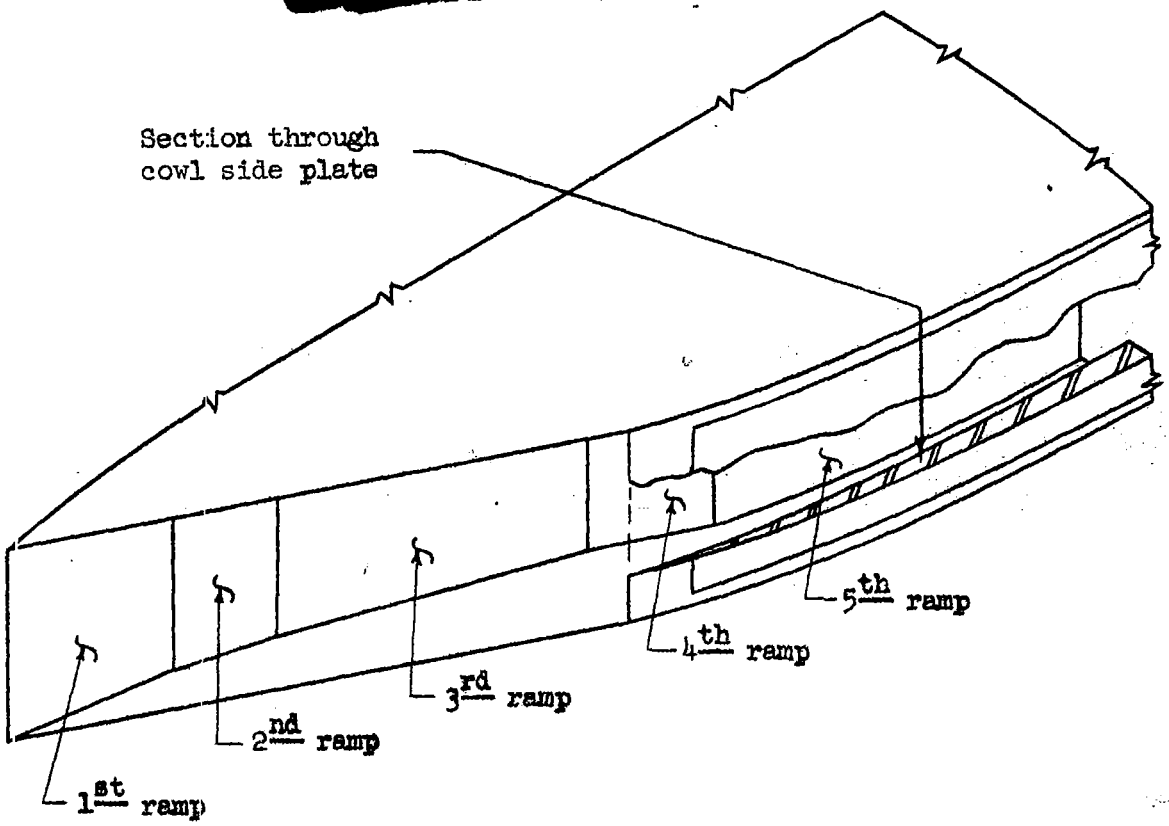

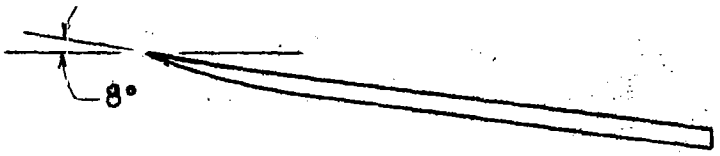

(a) Cowl side plate with lip angle of 8° with model ℄.

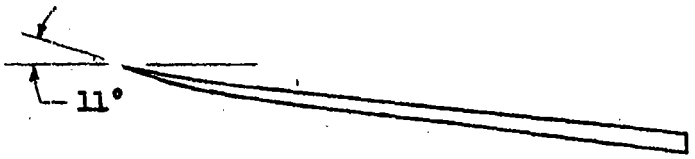

(b) Cowl side plate with lip angle of 11° with model ℄.

Figure 11.- Details of the cowl side plate showing the 8° and 11° lip angle.

[redacted]

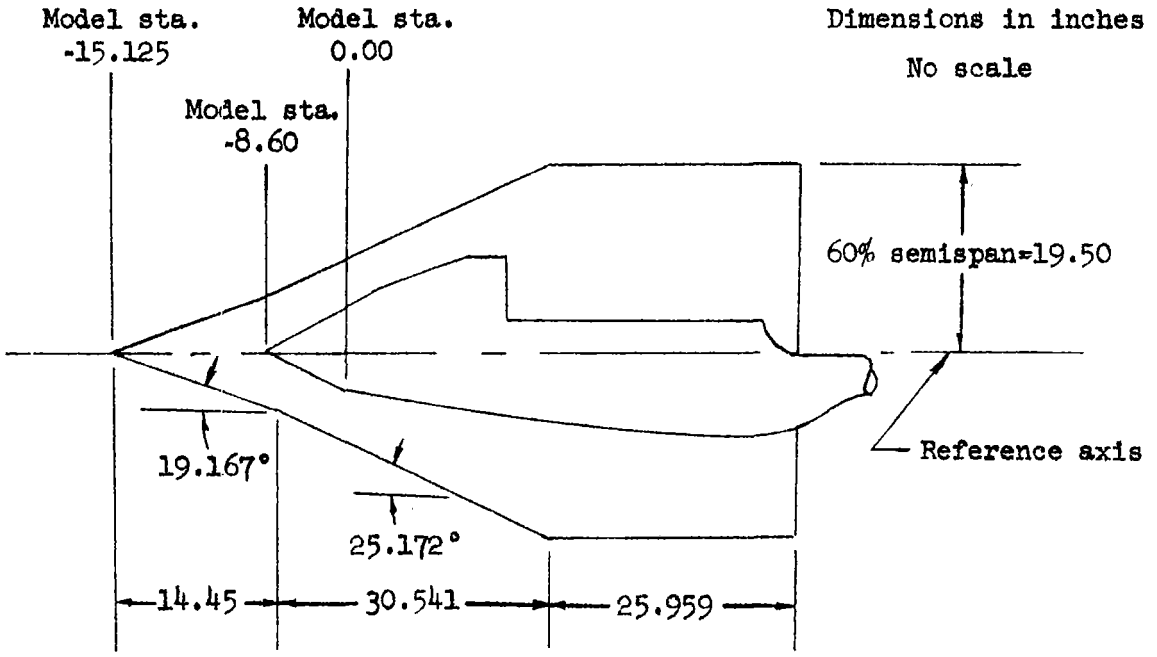

Wing data

Airfoil section forward of the 45% element - NACA 66A002.5
Airfoil section aft of the 45% element - 45% to 70% hexagonal, 2.5% thick

Aspect ratio - 1.880
Taper ratio - 0

Bleed gutter height between wing and inlet - 0.100 inches

(a) Basic model with Number 172 inlet version and the W_T wing

Figure 12.- Schematic drawing of basic model-plus-wing configurations tested.

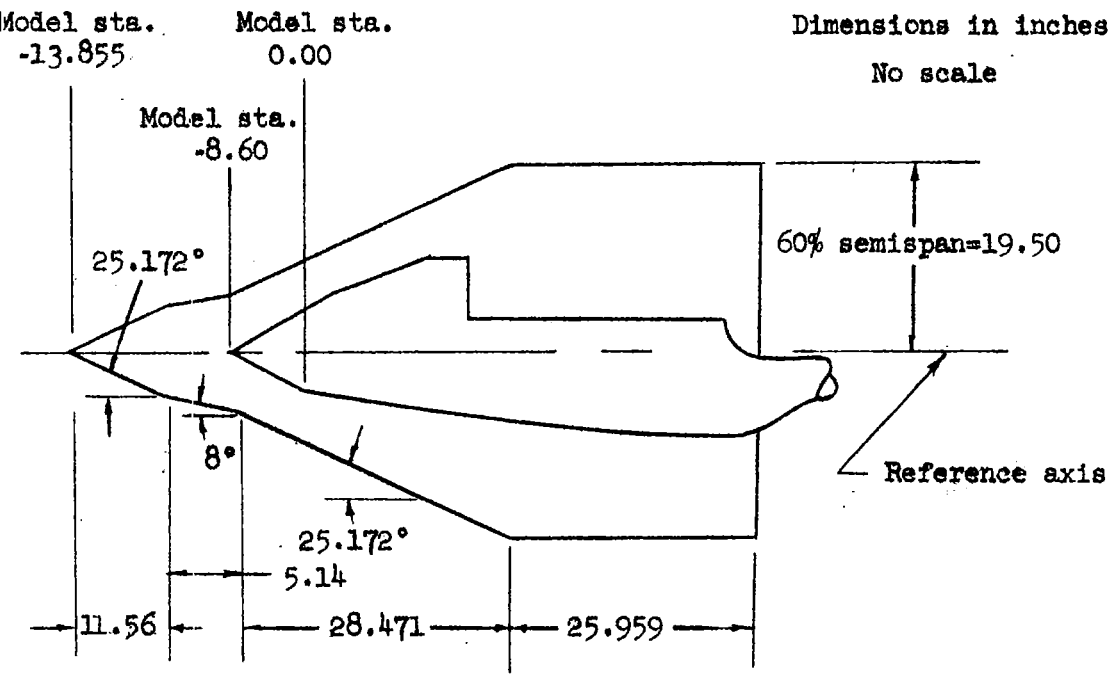

Wing data

Airfoil section forward of the 45% element - NACA 66A002.5
Airfoil section aft of the 45% element - 45% to 70% hexagonal, 2.5% thick

Aspect ratio - 1.880
Taper ratio - 0

Bleed gutter height between wing and inlet - 0.100 inches

(b) Basic model with the Number 172 inlet version and the W_{T_2} wing

Figure 12.- Continued.

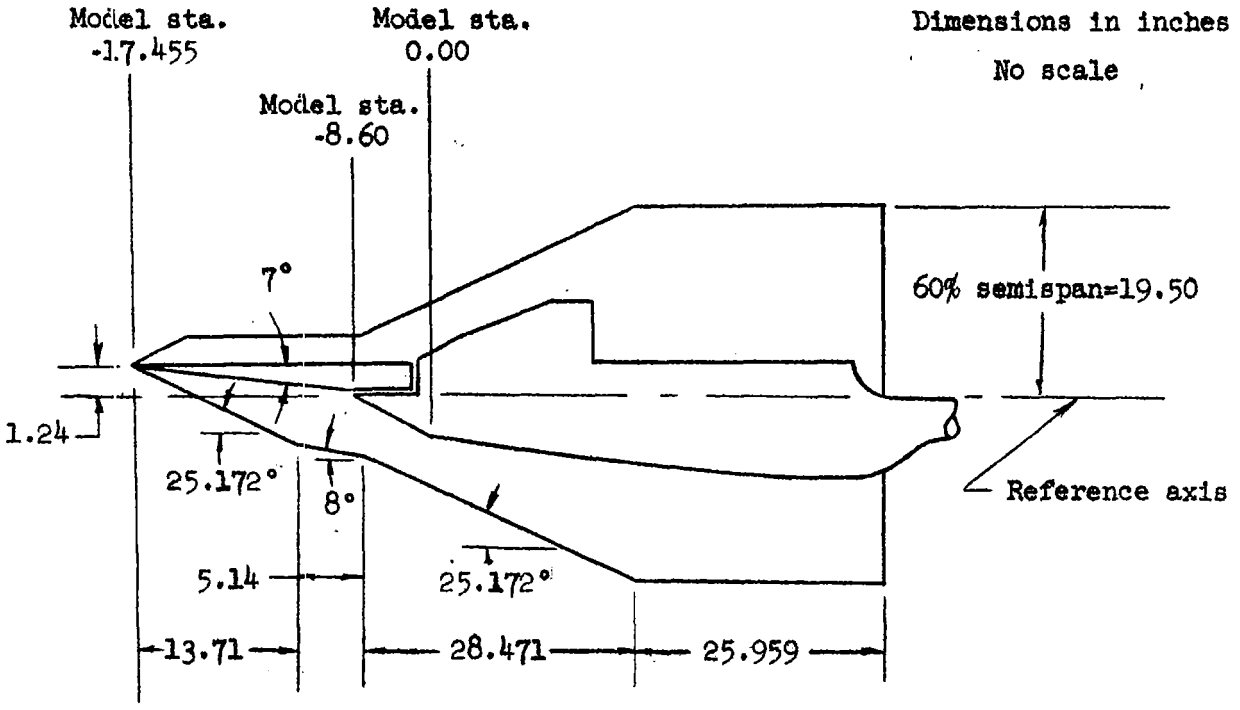

. Wing data

Airfoil section forward of the 45% element - NACA 66A002.5
Airfoil section aft of the 45% element - 45% to 70% hexagonal, 2.5% thick

Aspect ratio - 1.880
Taper ratio - 0

Bleed gutter height between wing and inlet - 0.100 inches

(c) Basic model with the Number 145 inlet version and the W_{T_3} wing

Figure 12.- Concluded.

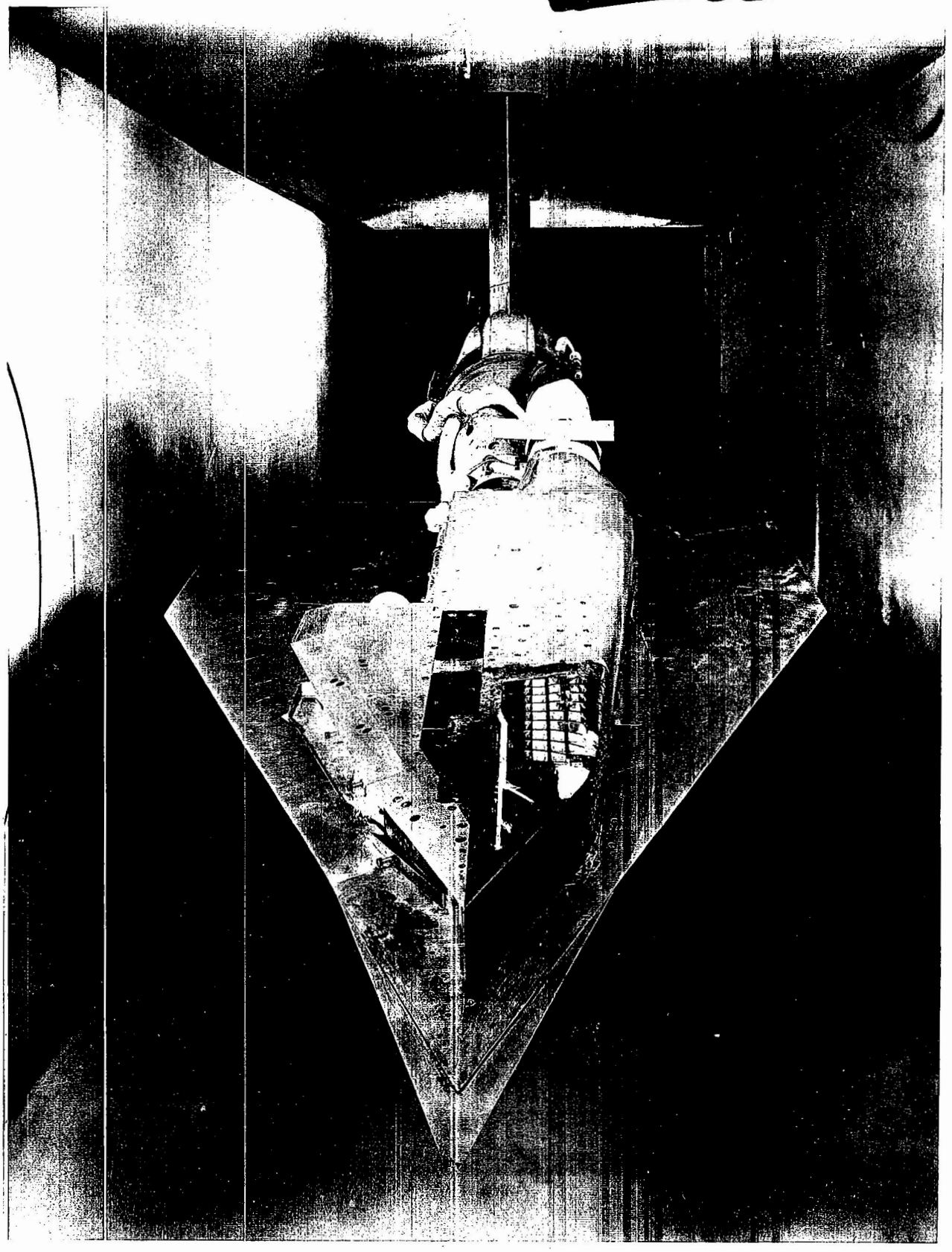

A-23843

Figure 13.- Installation photograph of the $W_T IR_4 C_4 S_4$ model configuration.

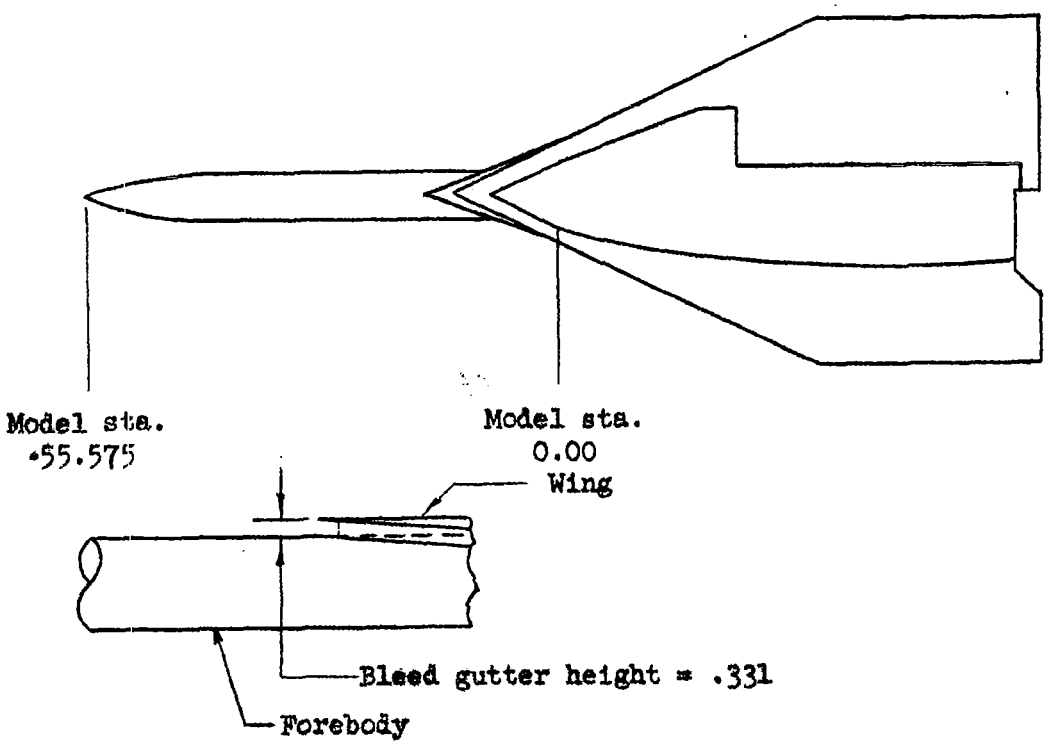

Detail of bleed gutter between forebody and wing

Note: Dimensions in inches
No scale

Figure 14.- Typical model configuration including the forebody.

A-23861

Figure 15.- Installation photograph of the $W_T B_T I R_4 C'_4 S_4$ model configuration.

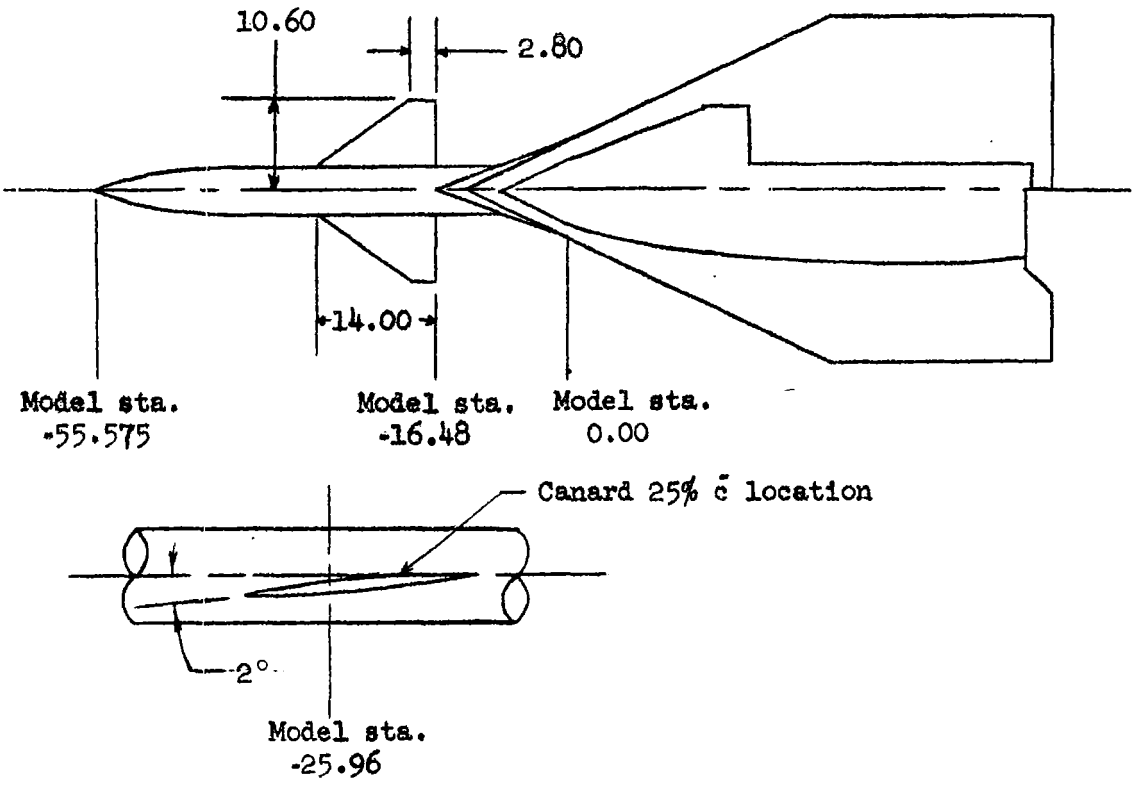

Detail showing angular incidence of canard

Canard data

Sweep of 25% element	- 47°
Airfoil section	- NACA 66A003
Aspect ratio	- 2.078
Taper ratio	- .1591

Figure 16.- Typical model configuration including the forebody and canard.

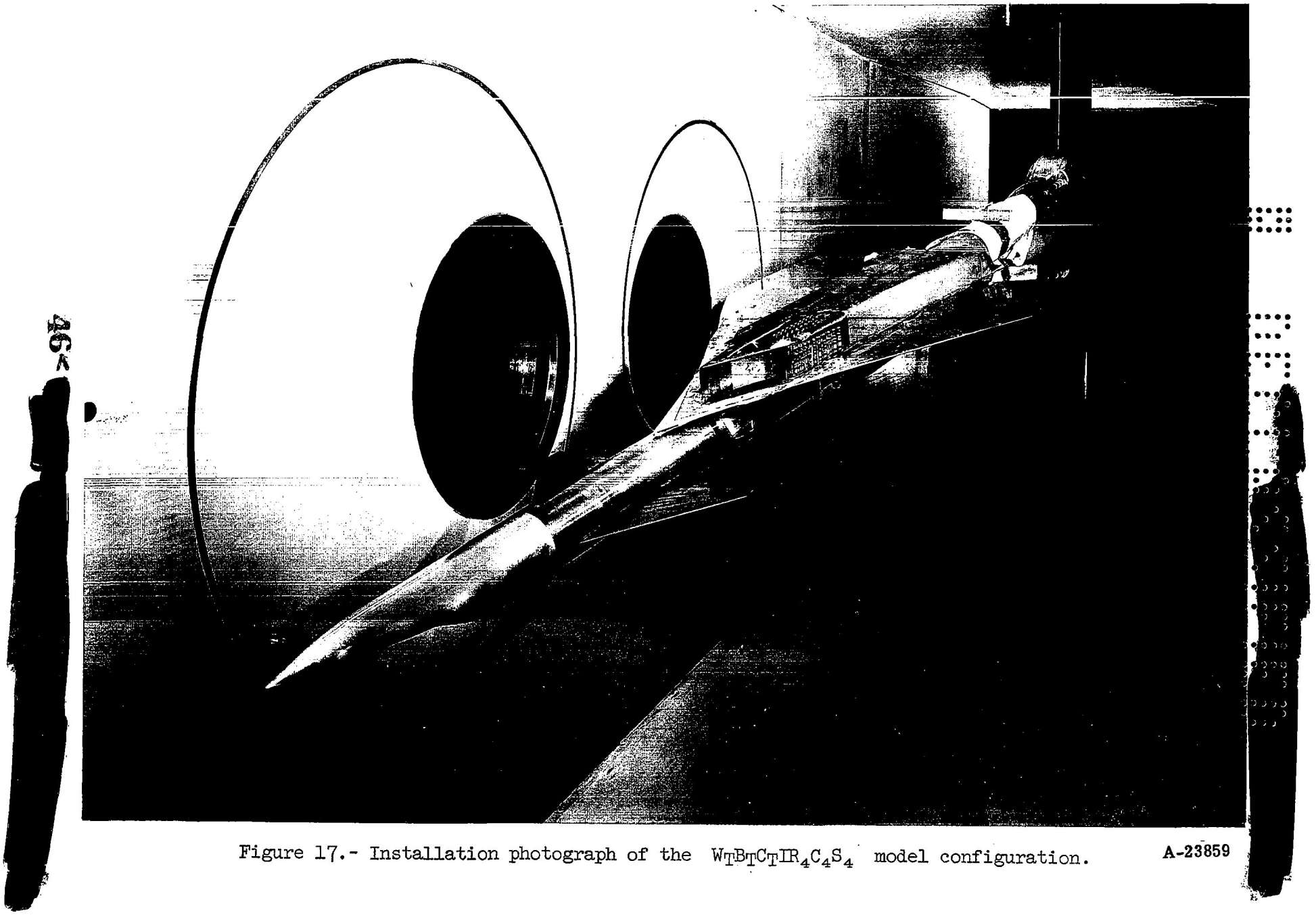

Figure 17.- Installation photograph of the $W_T B_T C_T IR_4 C_4 S_4$ model configuration. A-23859

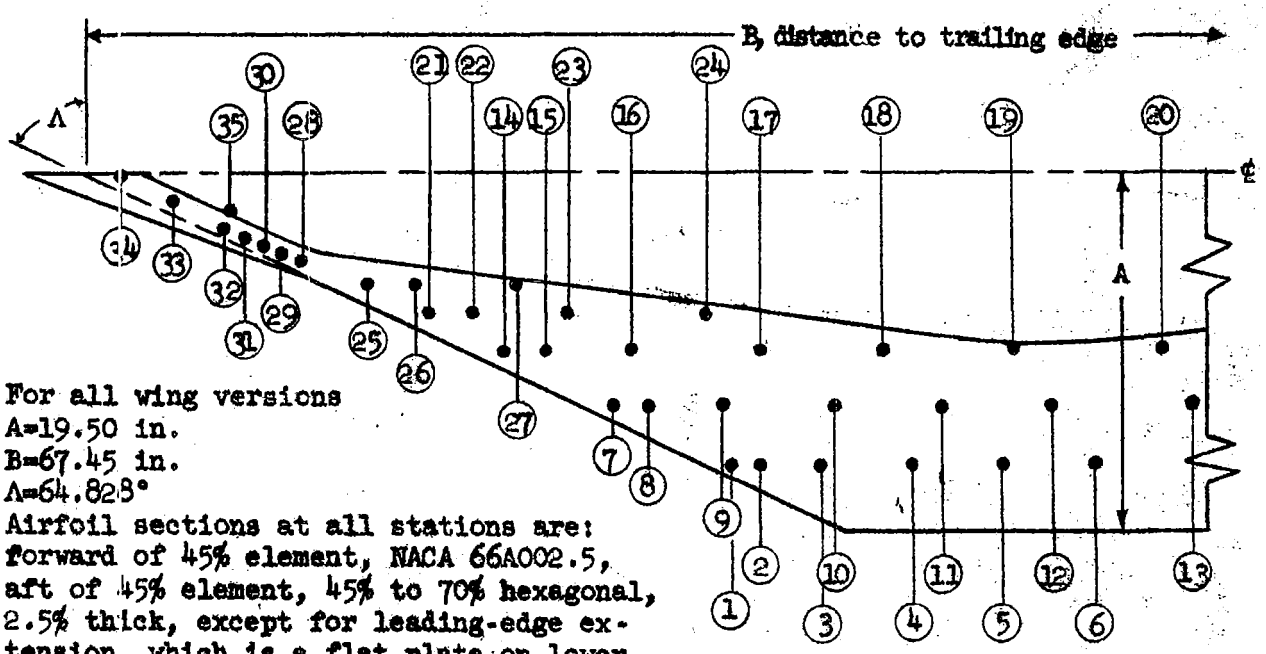
B, distance to trailing edge
Λ
A
¢
For all wing versions
A=19.50 in.
B=67.45 in.
Λ=64.828°
Airfoil sections at all stations are: forward of 45% element, NACA 66A002.5, aft of 45% element, 45% to 70% hexagonal, 2.5% thick, except for leading-edge extension, which is a flat plate on lower surface.
No scale
Numbers on figure are orifice numbers

Orifice No.	Location	
	% b/2	% c
1	50	5
2	50	10
3	50	20
4	50	35
5	50	50
6	50	65
7	40	5
8	40	10
9	40	20
10	40	35
11	40	50
12	40	65

Orifice No.	Location	
	% b/2	% c
13	40	85
14	30	5
15	30	10
16	30	20
17	30	35
18	30	50
19	30	65
20	30	85
21	24	5
22	24	10
23	24	20
24	24	35

Orifice No.	Location	
	% b/2	% c
25	19	5
26	19	10
27	19	20
28	14.70	3.54
29	13.40	3.28
30	12.12	2.96
31	10.83	2.65
32	9.54	2.36
33	4.60	2.84
34	0.00	3.13
35	7.00	5.06

Figure 18.- Location of pressure orifices on the lower surface of all wing versions.

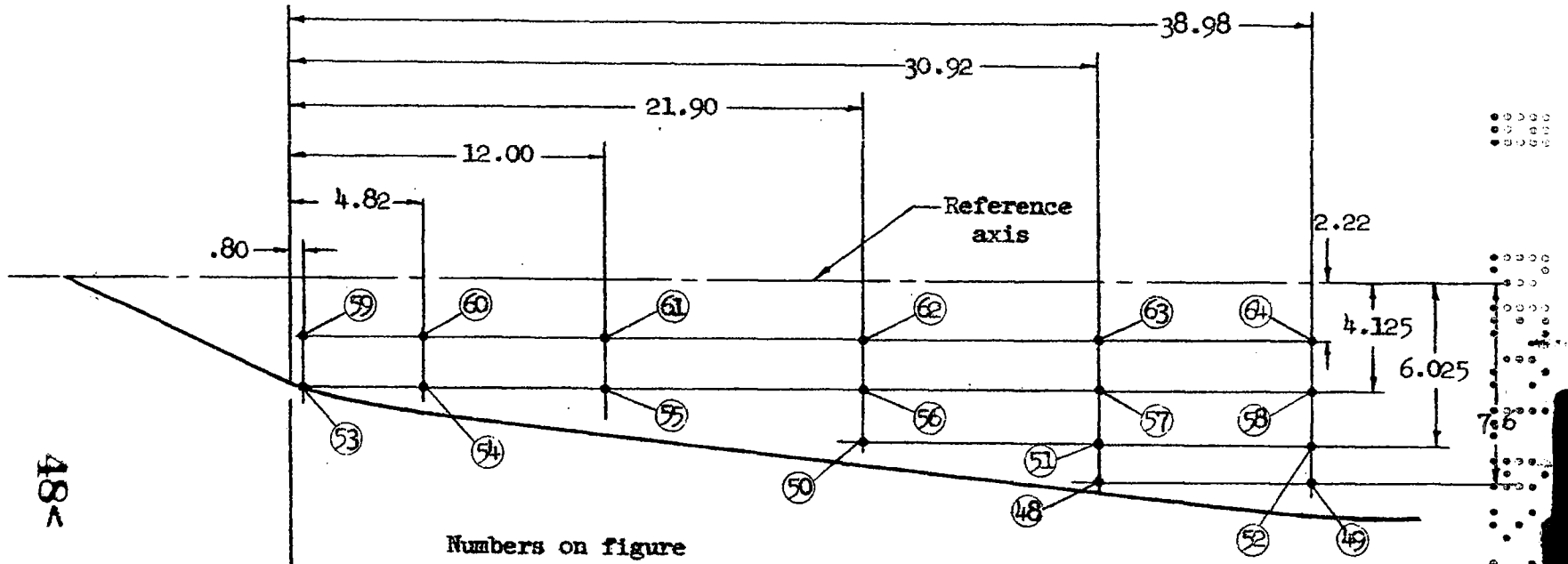

Figure 19.- Location of external pressure orifices on bottom cowl plate.

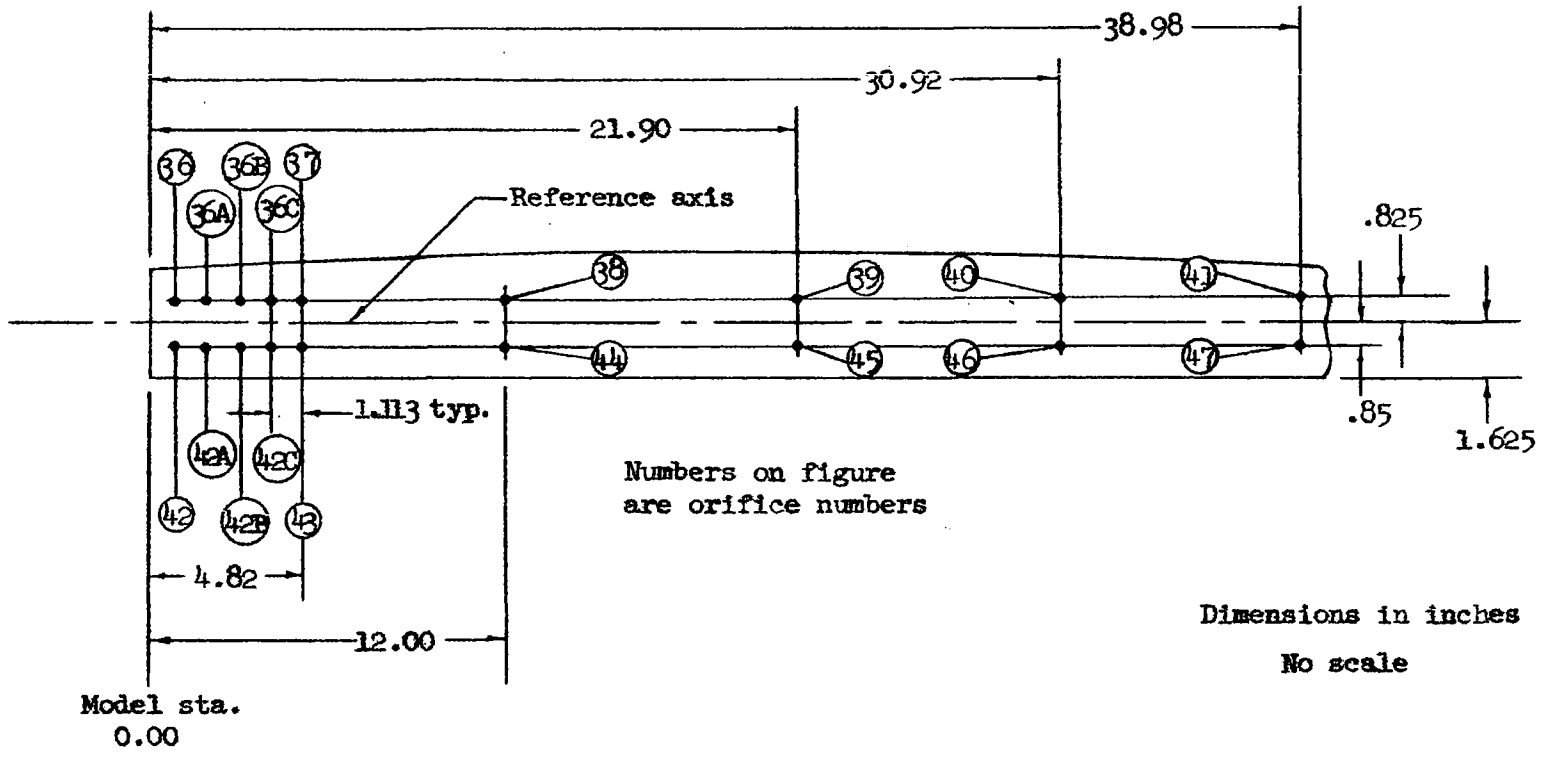

Figure 20.- Location of external pressure orifices on cowl side plate.

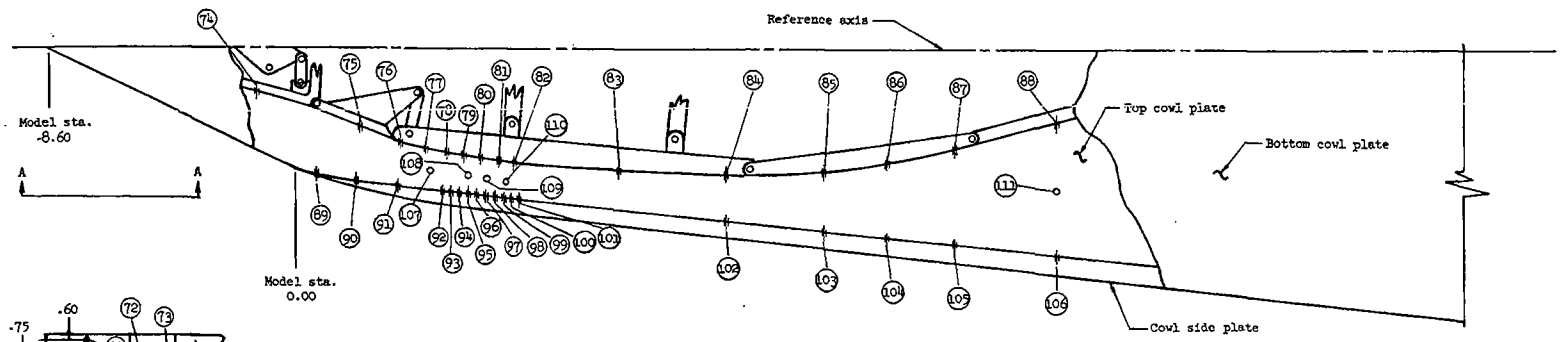

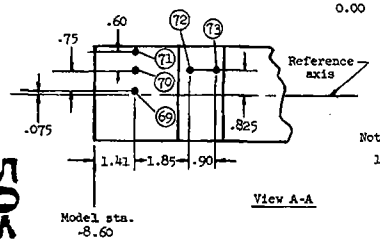

Dimensions in inches

No scale

Notes:

1. X-dimensions for ramp surface orifices are based on ramps positioned such that angles between the ramp surfaces and the reference axis are:

   7° for first ramp
   11° for second ramp
   16° for third ramp
   21° for fourth ramp

2. Orifices number 112, 113, 114, 115, and 116 are not shown, but lie on the bottom cowl plate directly opposite orifices 107, 108, 109, 110, and 111.

3. Model is shown in an inverted position.

Orifice no.	Orifice location	
	x,in.	z,in.
74	-1.5	0
75	2.3	0
76	3.5	0
77	4.3	0
78	5.3	0
79	5.8	0
80	6.4	0
81	6.9	0
82	7.5	0
83	11.3	0
84	15.6	-.08

Orifice no.	Orifice location	
	x,in.	z,in.
85	18.8	-.19
86	21.1	-.34
87	23.4	-.53
88	26.9	-.725
89	0.8	0
90	2.0	0
91	3.5	0
92	5.0	0
93	5.3	0
94	5.6	0
9595	5.9	0

Orifice no.	Orifice location	
	x,in.	z,in.
96	6.2	0
97	6.5	0
98	6.8	0
99	7.1	0
100	7.4	0
101	7.7	0
102	15.6	-.08
103	18.8	-.19
104	21.1	-.34
105	23.4	-.53
106	26.9	-.725

Orifice no.	Orifice location	
	x,in.	z,in.
107	4.6	4.08
108	5.9	4.27
109	6.6	4.35
110	7.3	4.45
111	26.9	4.75
112	4.6	4.08
113	5.9	4.27
114	6.6	4.35
115	7.3	4.45
116	26.9	4.75

Figure 21.- Schematic drawing showing locations of the duct internal static-pressure orifices.

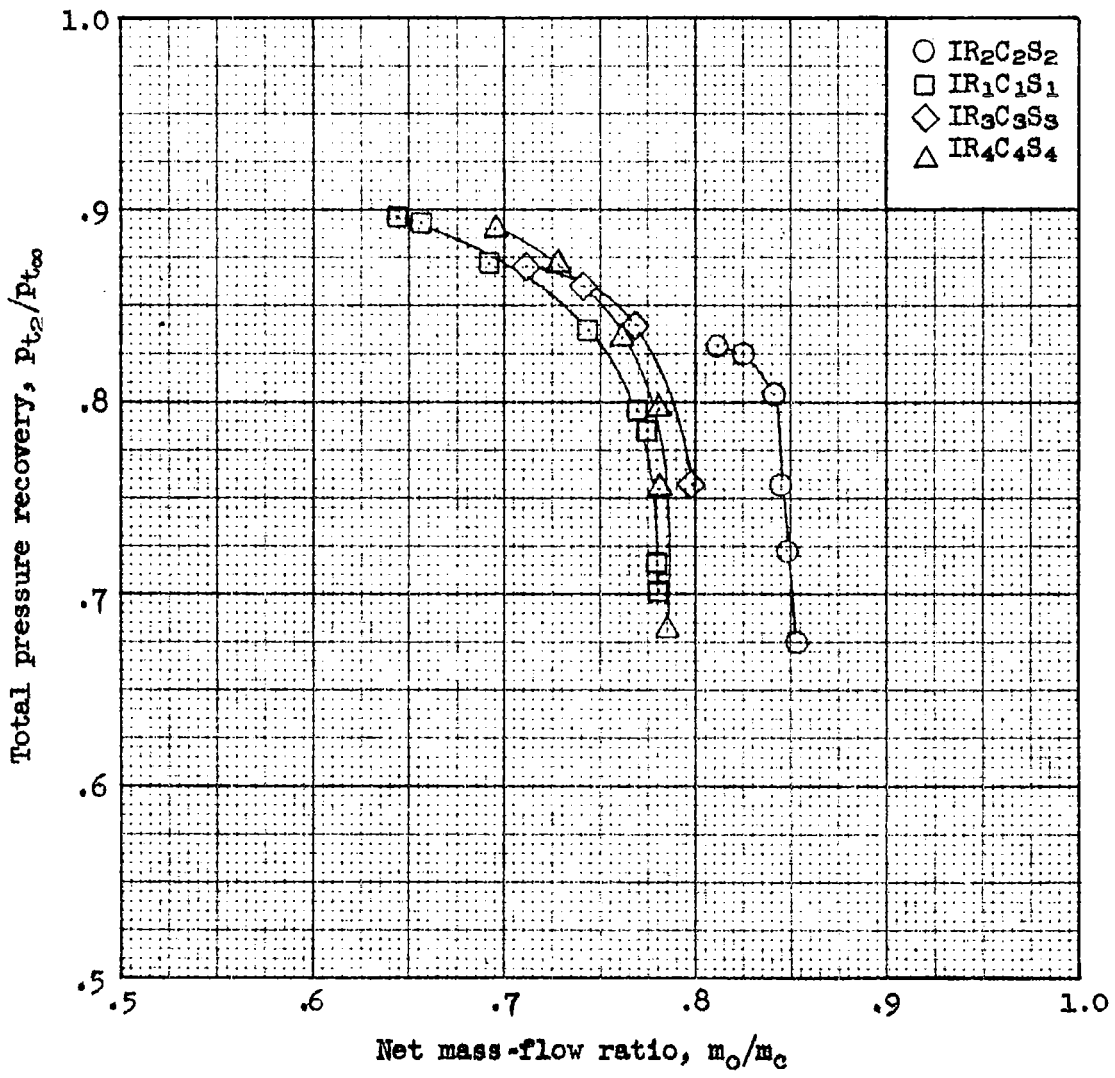

Figure 22.- Effect of boundary-layer bleed on the optimum performance of the Number 172 inlet version, with an 11° cowl lip, at M_∞=2.880, α=0.2°, β=0°.

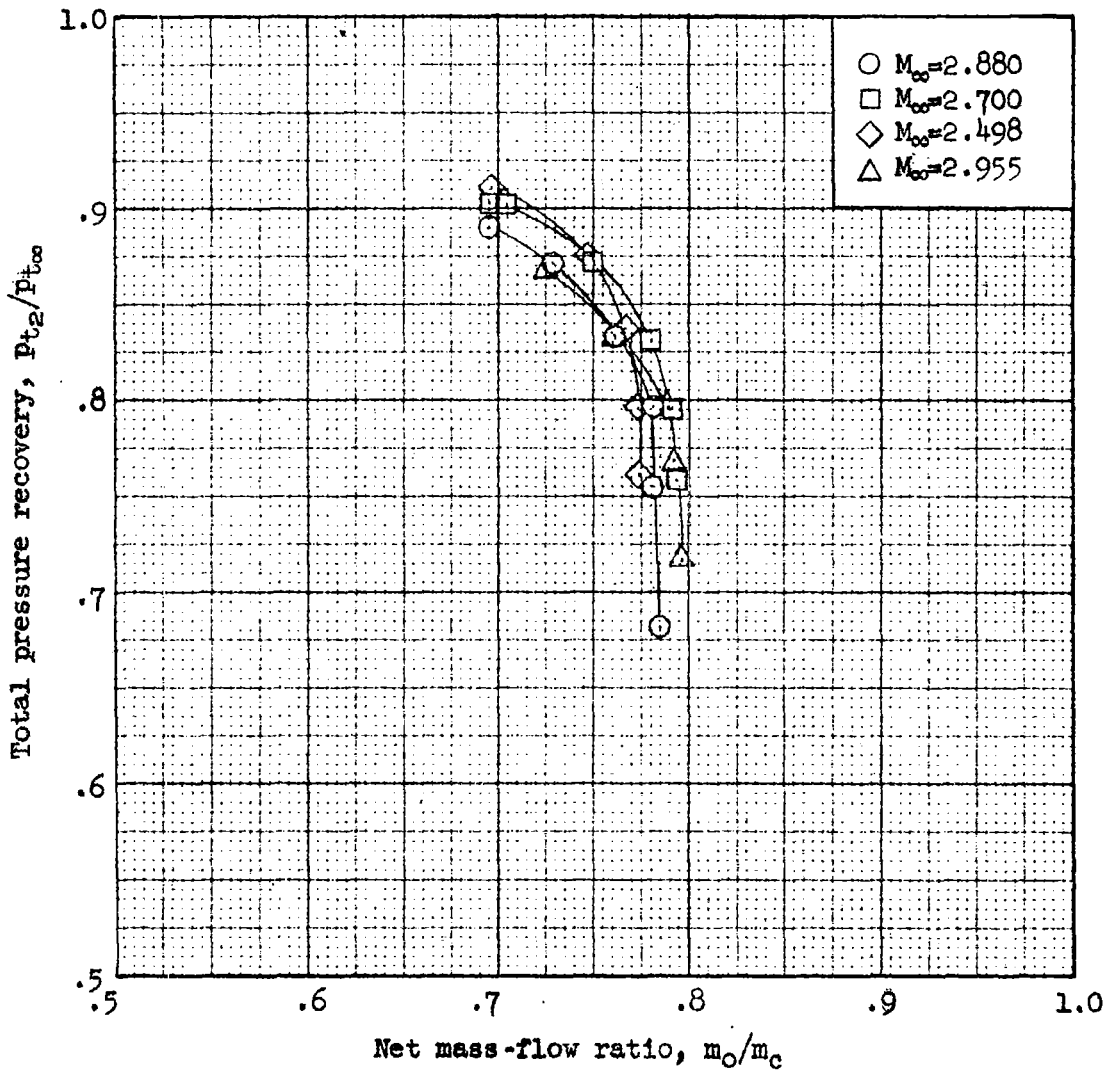

Figure 23.- Effect of Mach number variation on the optimum performance of the $IR_4C_4S_4$ inlet configuration at α=0.2°, β=0°.

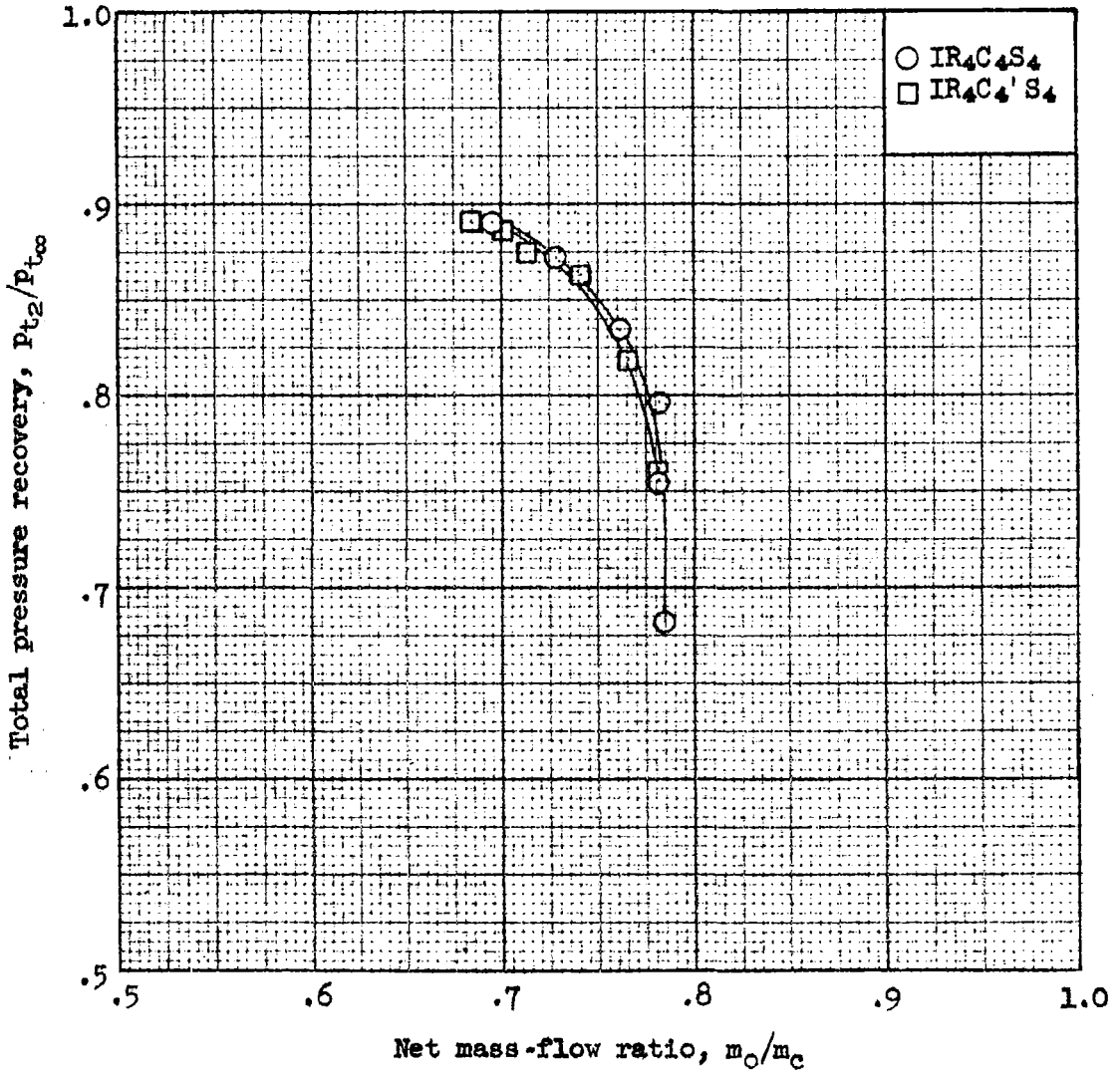

Figure 24.- Effect of variation of cowl lip angle on optimum inlet performance at M_∞=2.880, α=0.2°, β=0°.

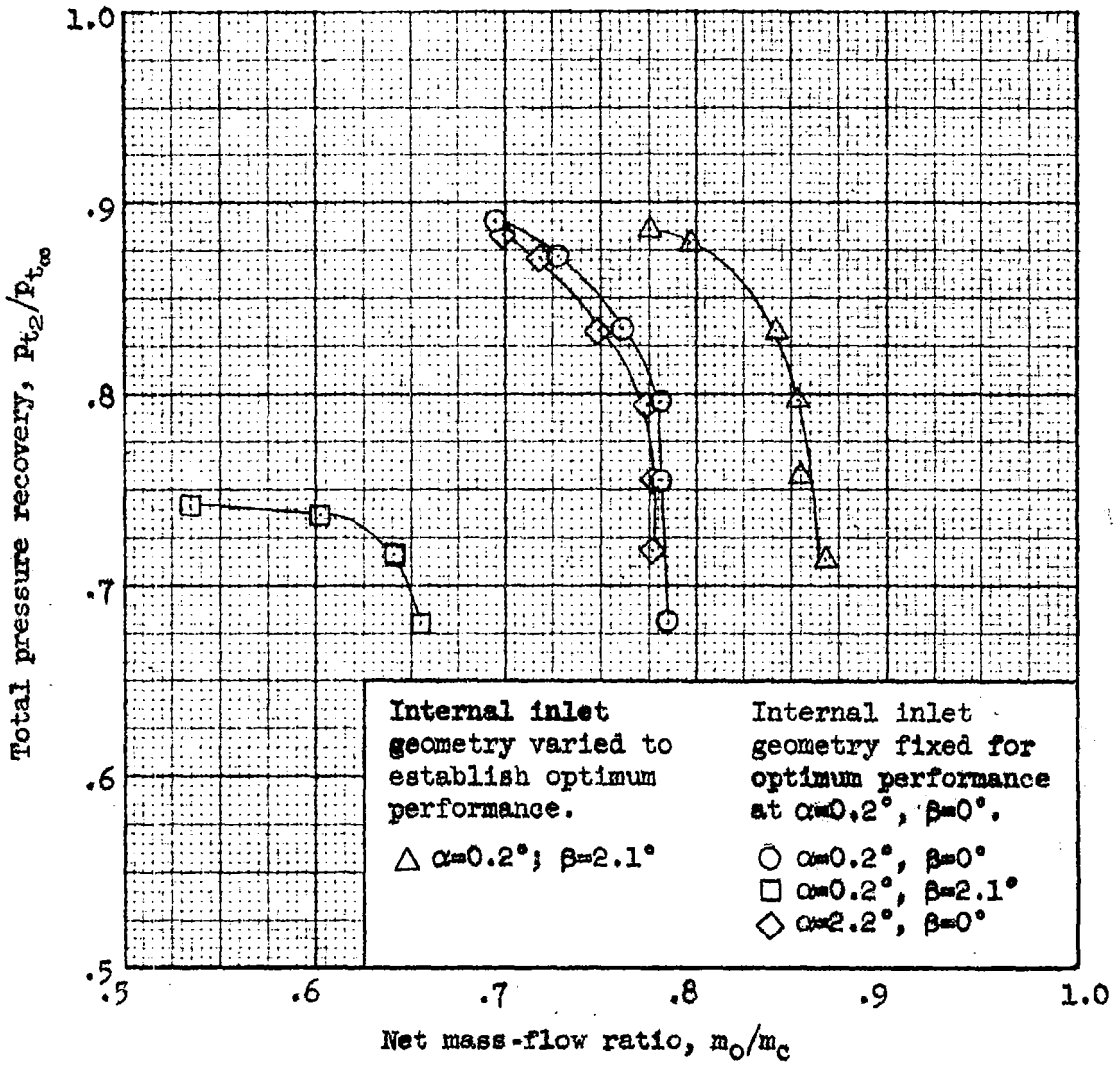

Figure 25.- Effect of variation of model attitude on the performance of the $IR_4C_4S_4$ inlet configuration at M_∞=2.880.

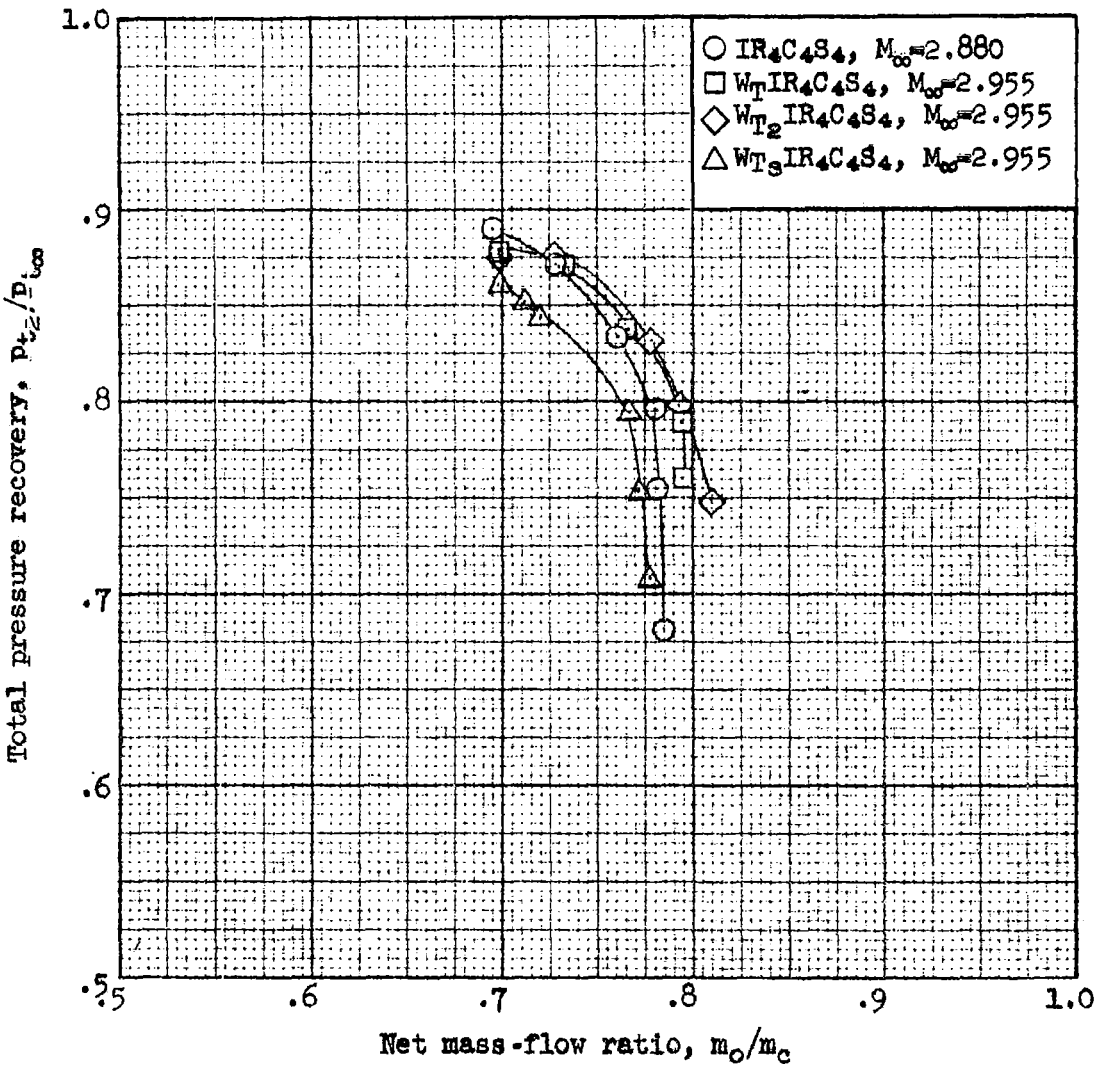

Figure 26.- Effect of wing addition to the basic model on optimum inlet performance at $\alpha=0.2°$, $\beta=0°$.

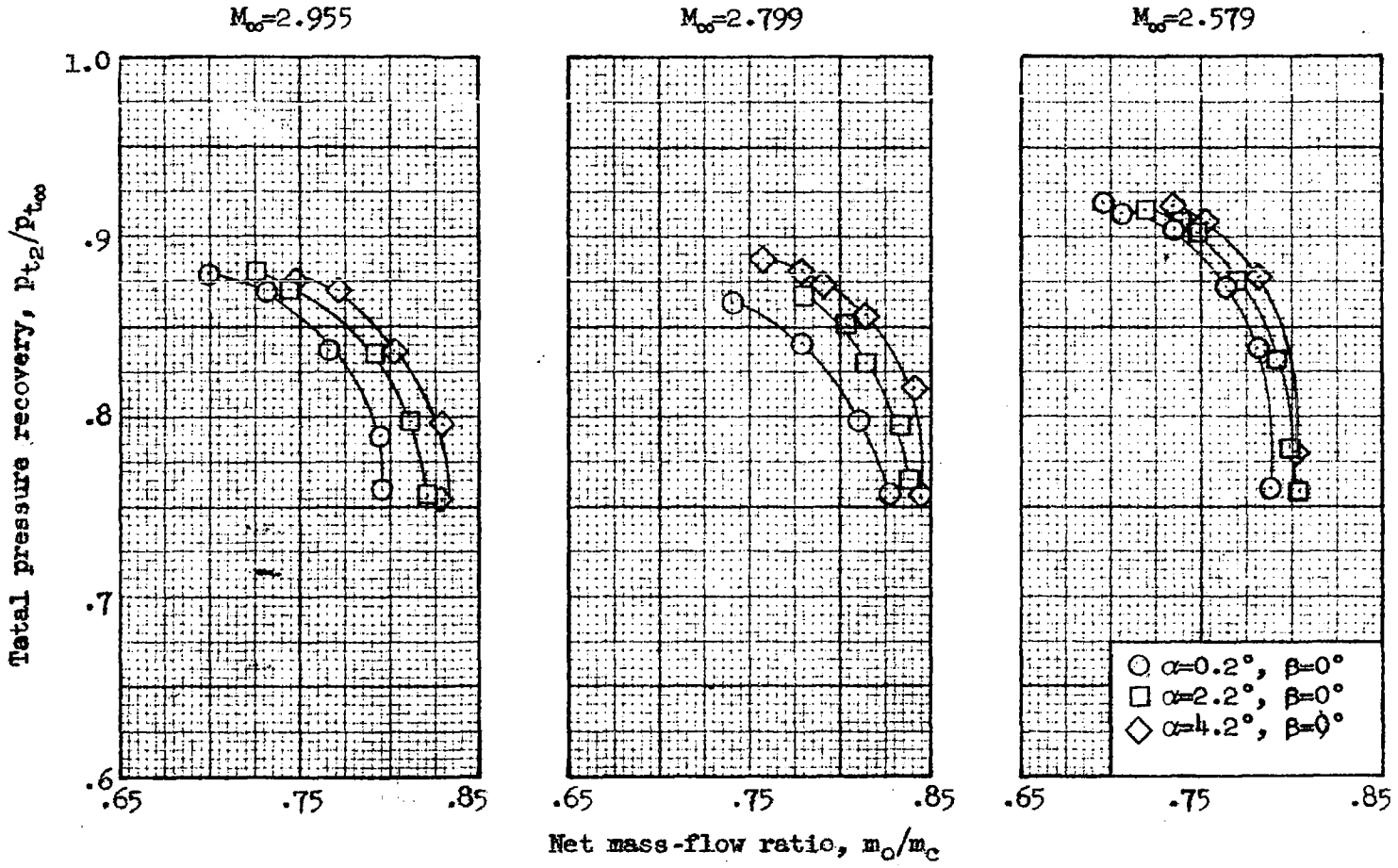

Figure 27.- Optimum inlet performance characteristics of the $W_T IR_4 C_4 S_4$ configuration at varying angle of attack for several Mach numbers.

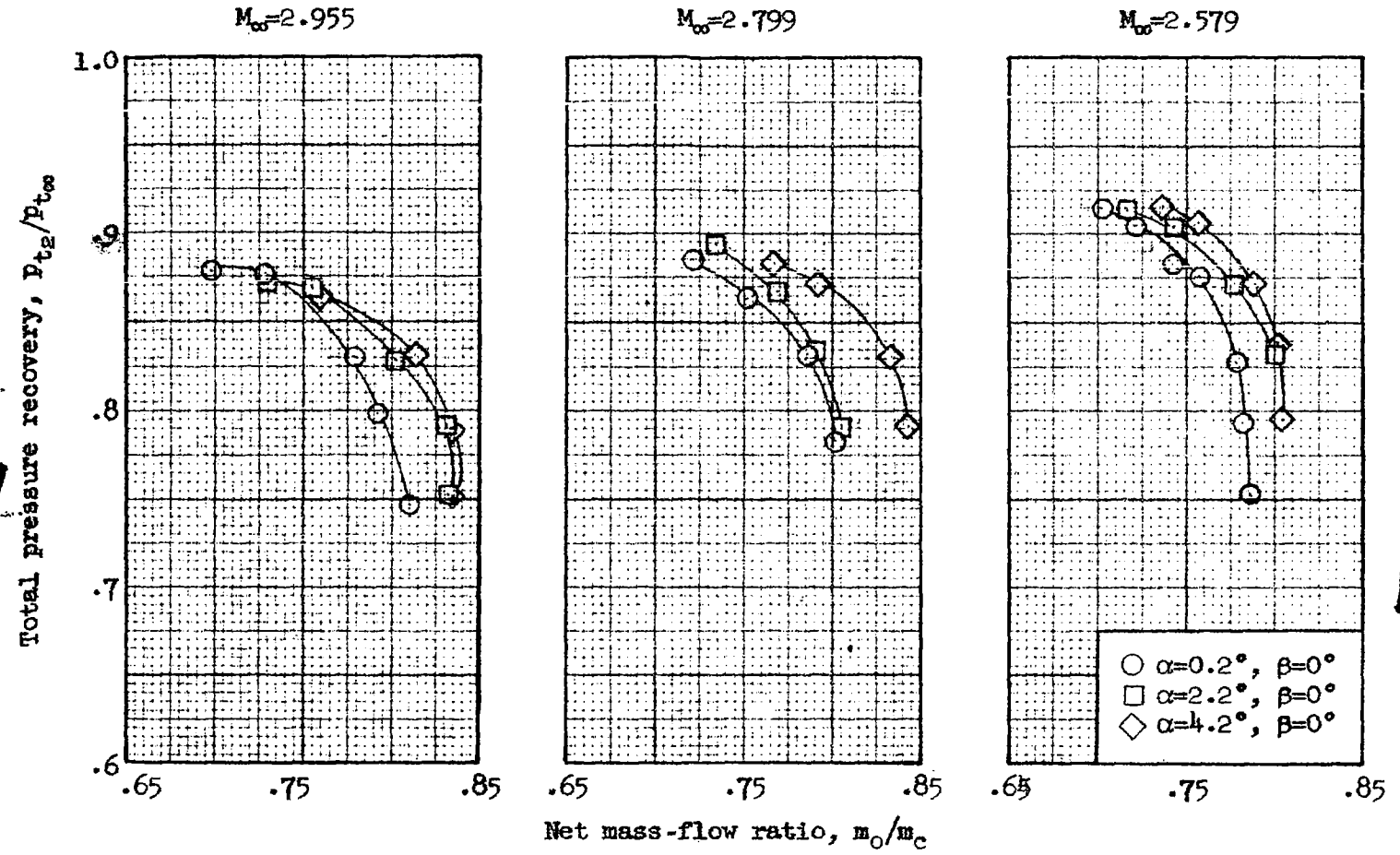

Figure 28.- Optimum inlet performance characteristics of the $W_{T_2}IR_4C_4S_4$ configuration at varying angle of attack for several Mach numbers.

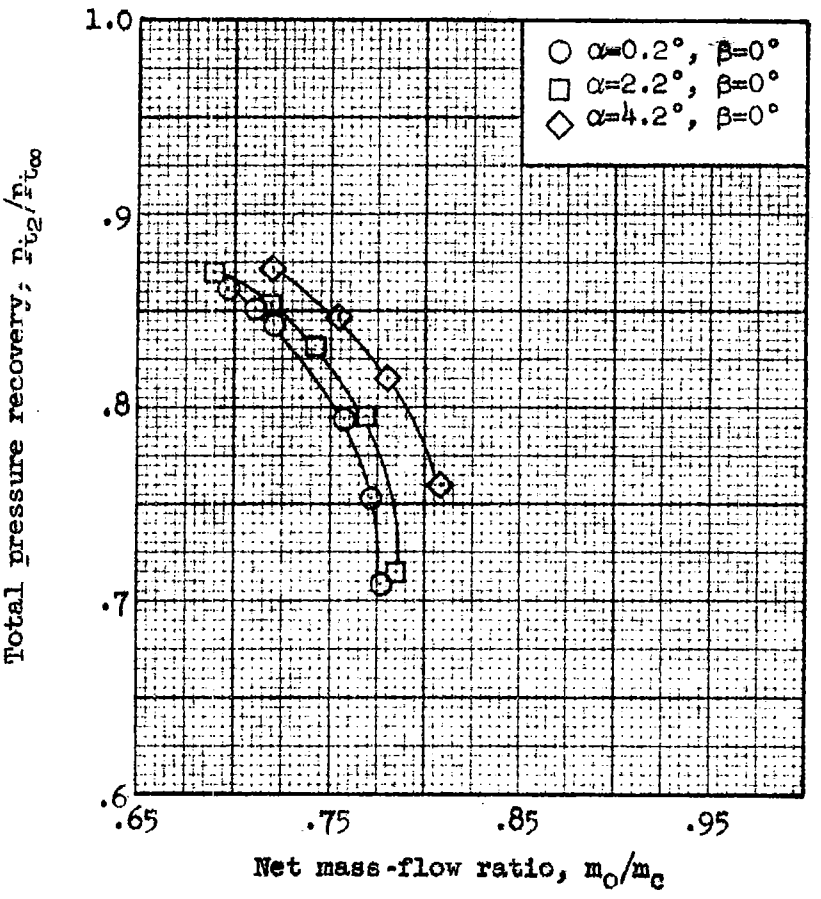

Figure 29.- Optimum inlet performance characteristics of the $W_{T_2}I_2R_4C_4S_4$ configuration at varying angle of attack for M_∞=2.955.

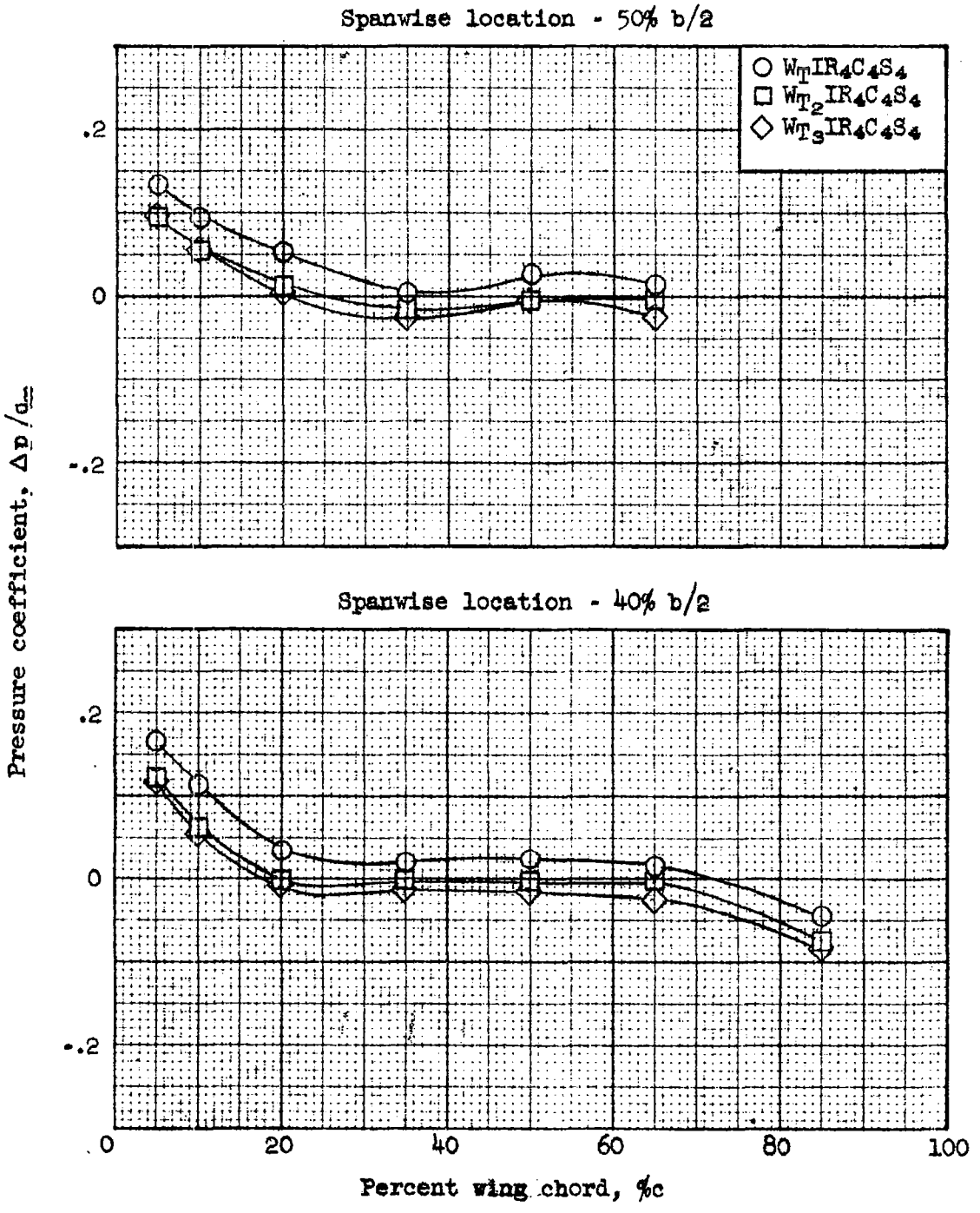

(a)

Figure 30.- Comparison of pressure coefficients on the lower surface of the Number 172, 154, and 145 wing versions for optimum inlet pressure recovery at M_∞=2.955, α=0.2°, β=0°.

[redacted]

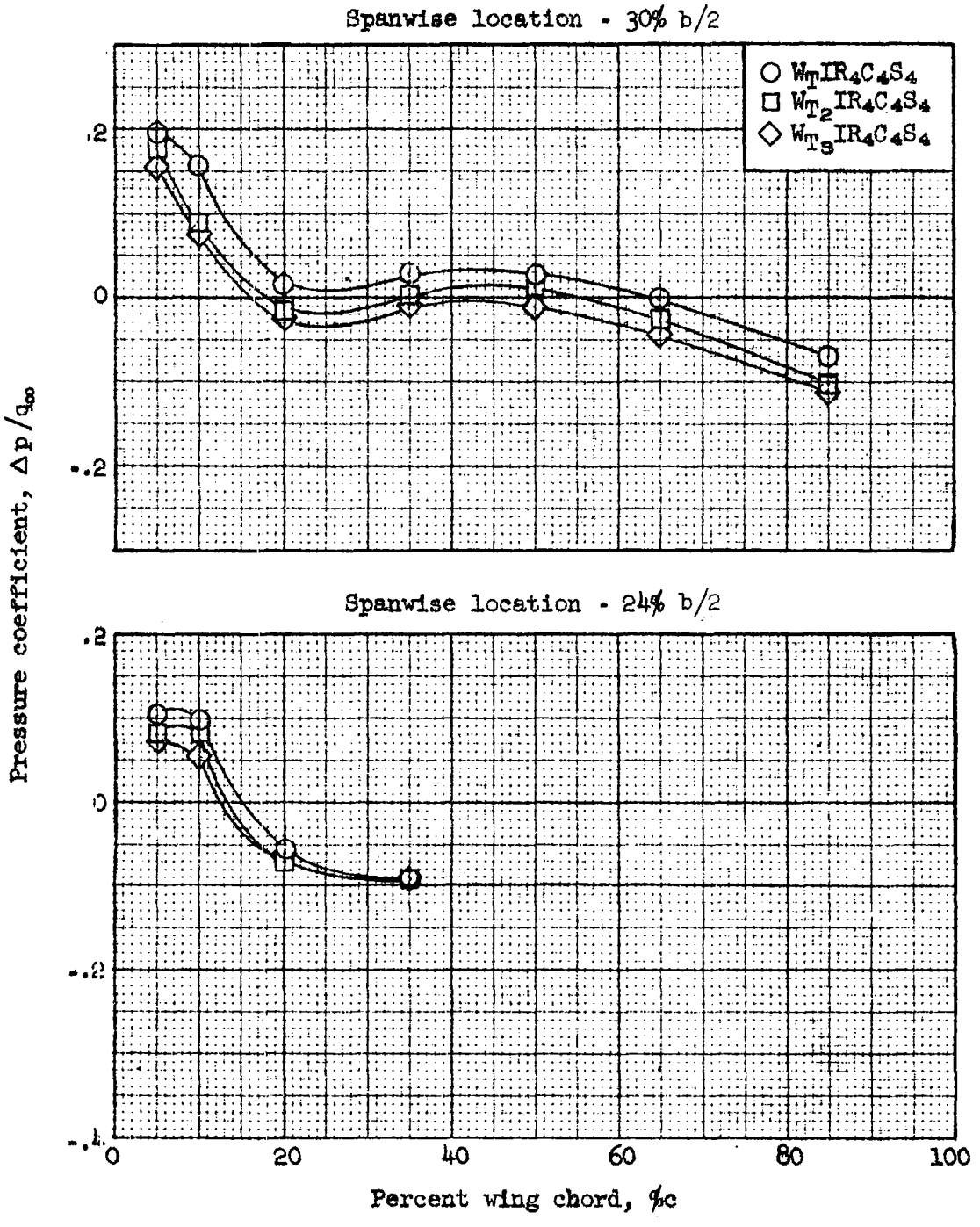

(b)

Figure 30.- Continued.

[redacted] 60<

[redacted]

[redacted]

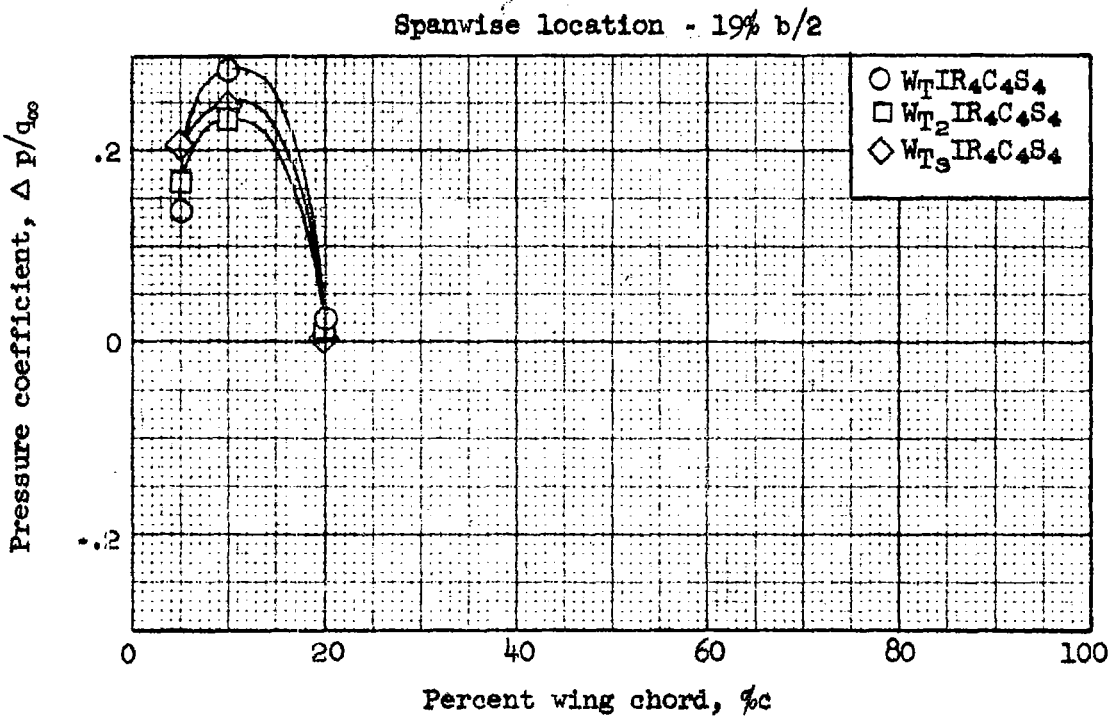

% b/2	%c	Δ p/q∞		
		$W_TIR_4C_4S_4$	$W_{T_2}IR_4C_4S_4$	$W_{T_3}IR_4C_4S_4$
14.70	3.54	.024	.435	.480
13.40	3.28	.024	.069	.192
12.12	2.96	.030	.031	.142
10.83	2.65	.024	.003	.094
9.54	2.36	.024	-.001	.092
7.00	5.06	.042	.041	.156
4.60	2.84	.024	-.001	.011
0.00	3.13	.016	-.007	.098

(c)

Figure 30.- Concluded.

[redacted]

[redacted]

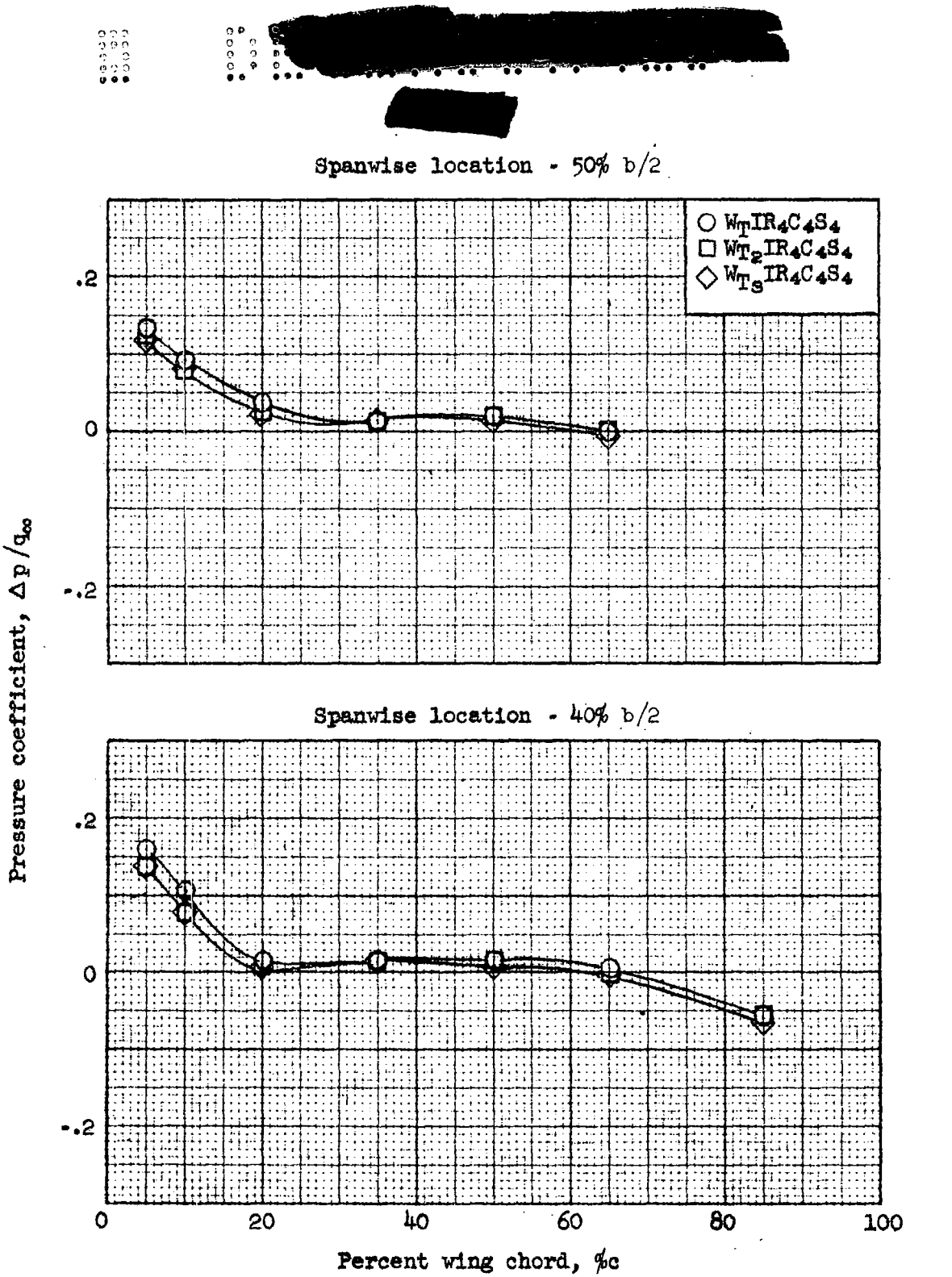

(a)

Figure 31.- Comparison of pressure coefficients on the lower surface of the Number 172, 154, and 145 wing versions for optimum inlet pressure recovery at M_∞=2.955, α=2.2°, β=0°.

[redacted]

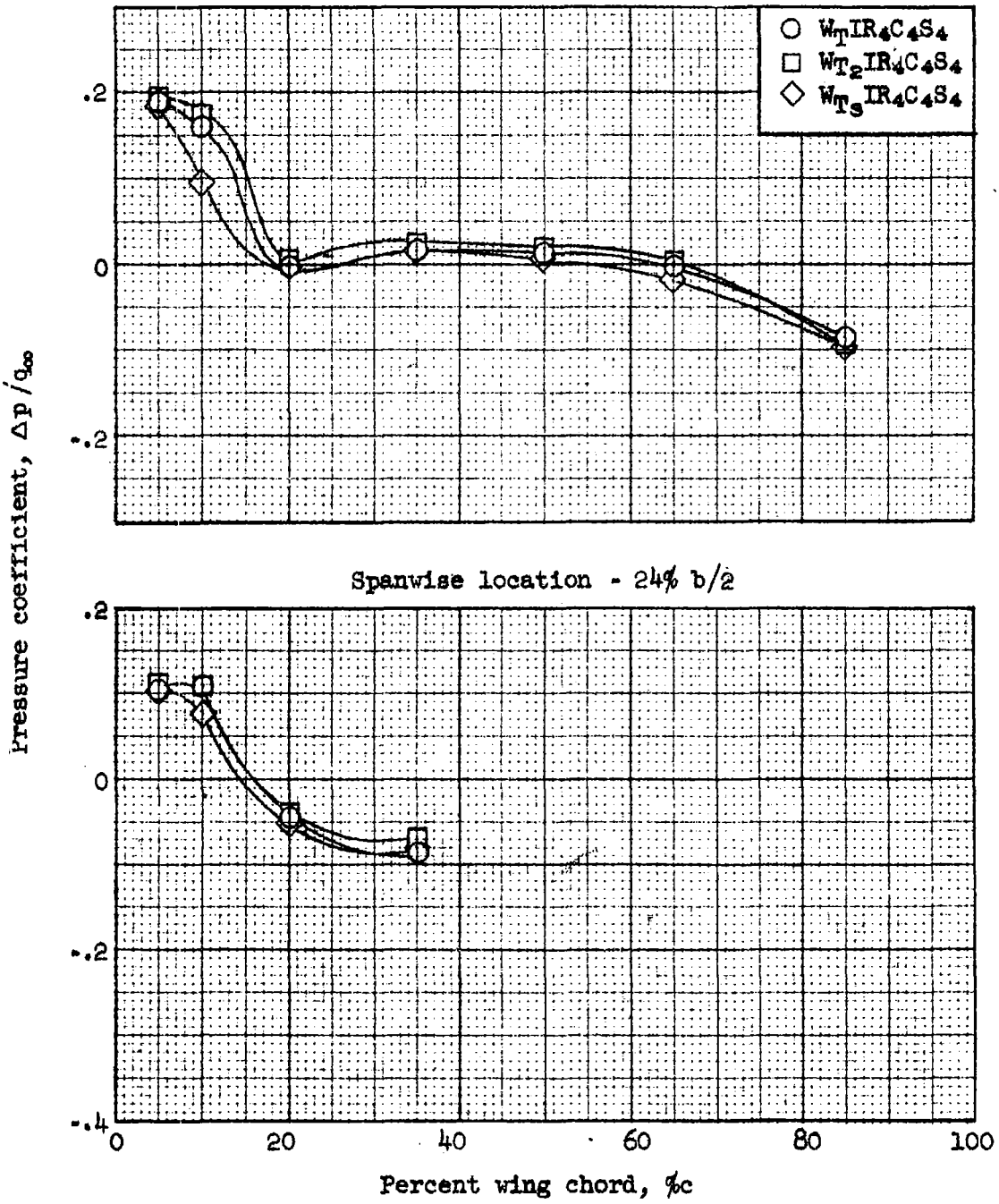

(b)

Figure 31.- Continued.

[redacted]

[redacted]

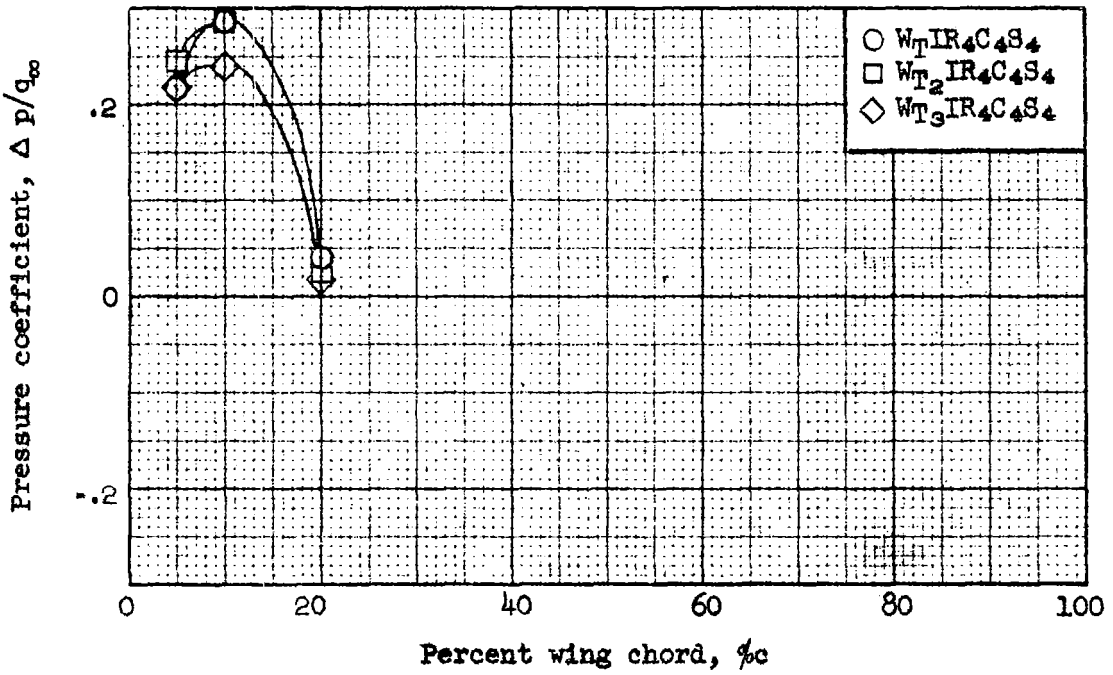

% b/2	%c	Δ p/q∞		
		$W_TIR_4C_4S_4$	$W_{T_2}IR_4C_4S_4$	$W_{T_3}IR_4C_4S_4$
14.70	3.54	.034	.486	.430
13.40	3.28	.034	.132	.202
12.12	2.96	.034	.070	.146
10.83	2.65	.014	.026	.108
9.54	2.36	.012	.018	.108
7.00	5.06	.026	.106	.146
4.60	2.84	.010	.026	.122
0.00	3.13	.006	.004	.122

(c)

Figure 31.- Concluded.

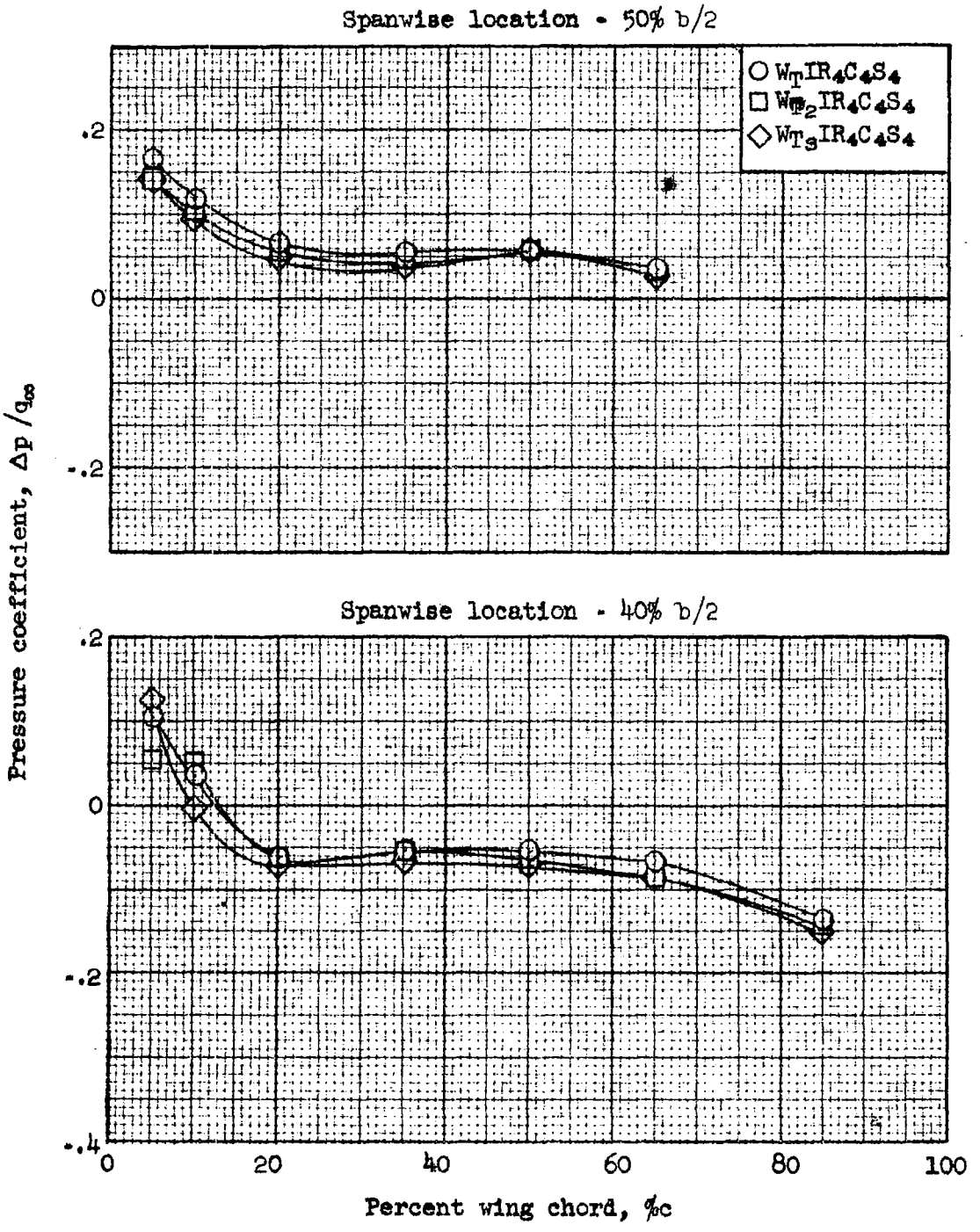

(a)

Figure 32.- Comparison of pressure coefficients on the lower surface of the Number 172, 154, and 145 wing versions for optimum inlet pressure recovery at M_∞=2.955, α=4.2°, β=0°.

[redacted]

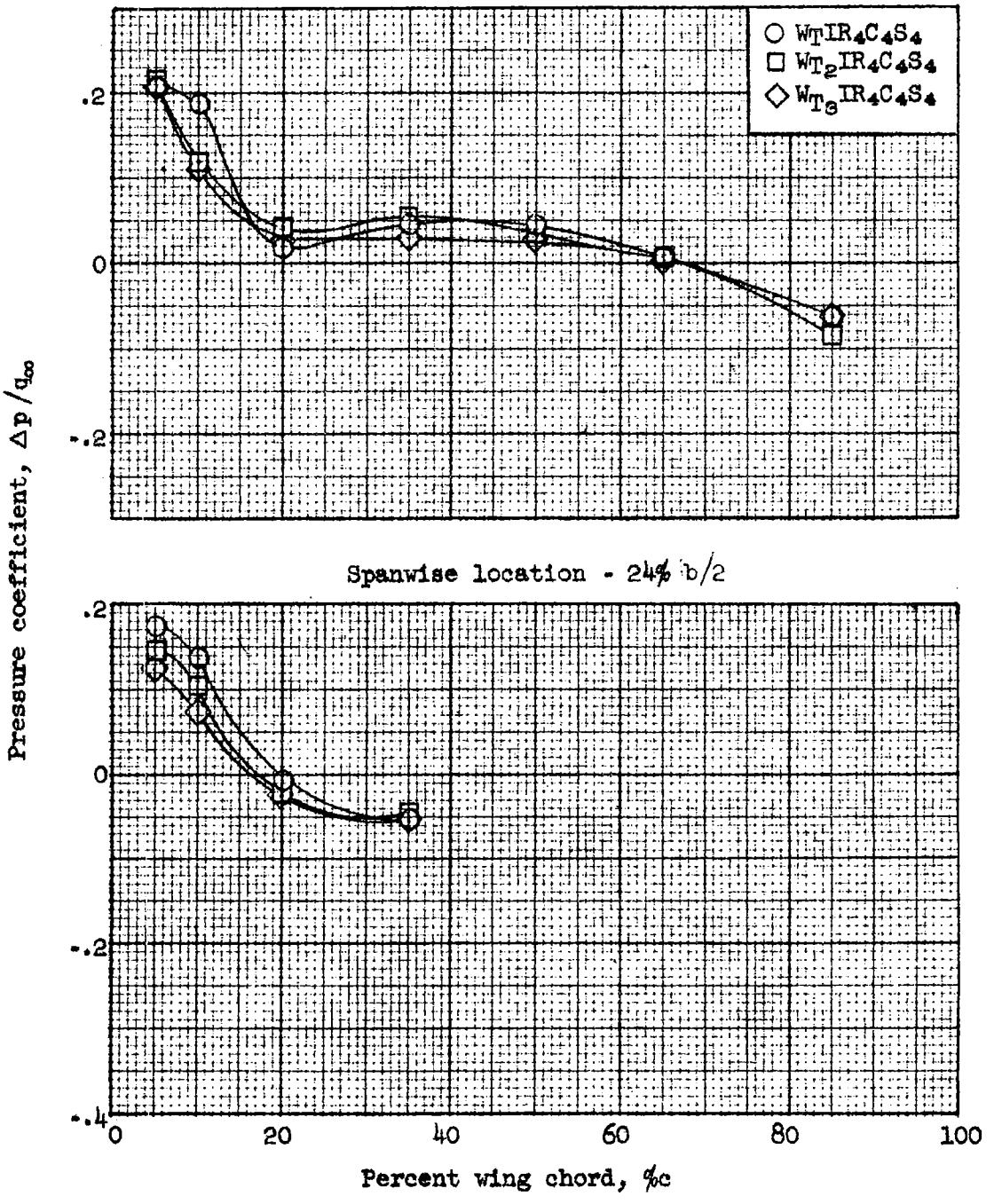

(b)

Figure 32.- Continued.

[redacted]

[redacted]

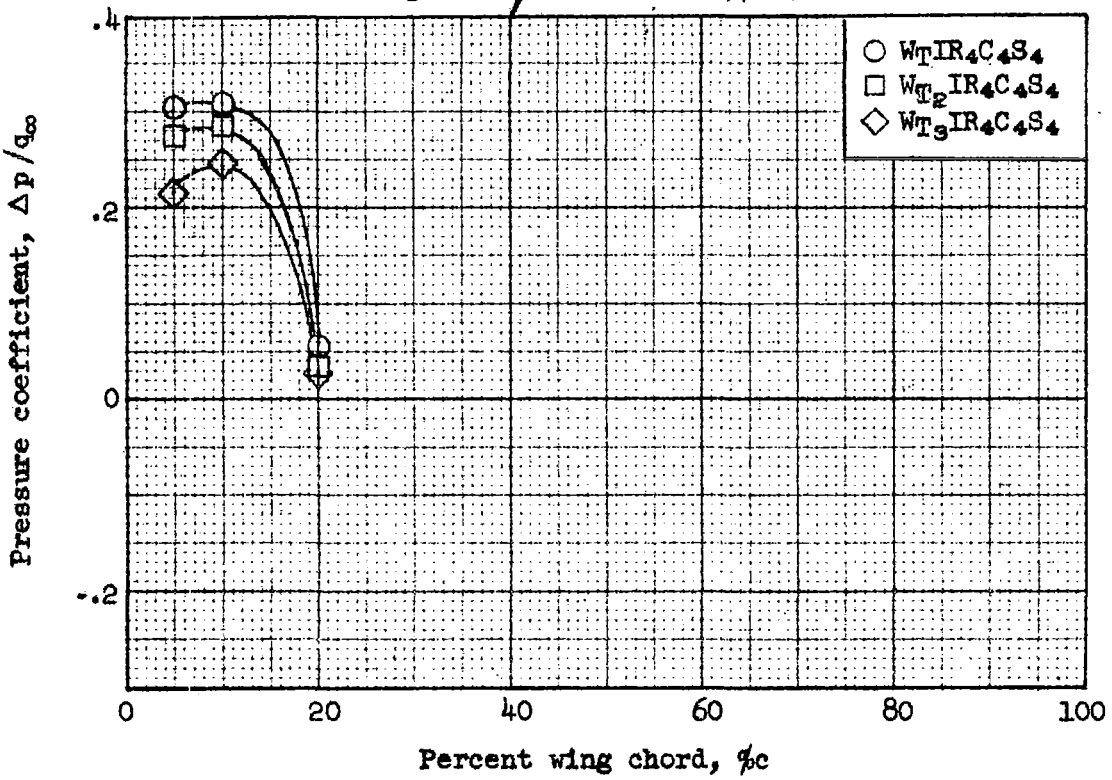

% b/2	%c	$\Delta p/q_\infty$		
		$W_T IR_4C_4S_4$	$W_{T_2} IR_4C_4S_4$	$W_{T_3} IR_4C_4S_4$
14.70	3.54	.061	.554	.442
13.40	3.28	.061	.238	.244
12.12	2.96	.149	.160	.304
10.83	2.65	.055	.080	.126
9.54	2.36	.051	.042	.126
7.00	5.06	.013	.136	.156
4.60	2.84	.047	.037	.142
0.00	3.13	.033	.028	.142

(c)

Figure 32.- Concluded.

[redacted]

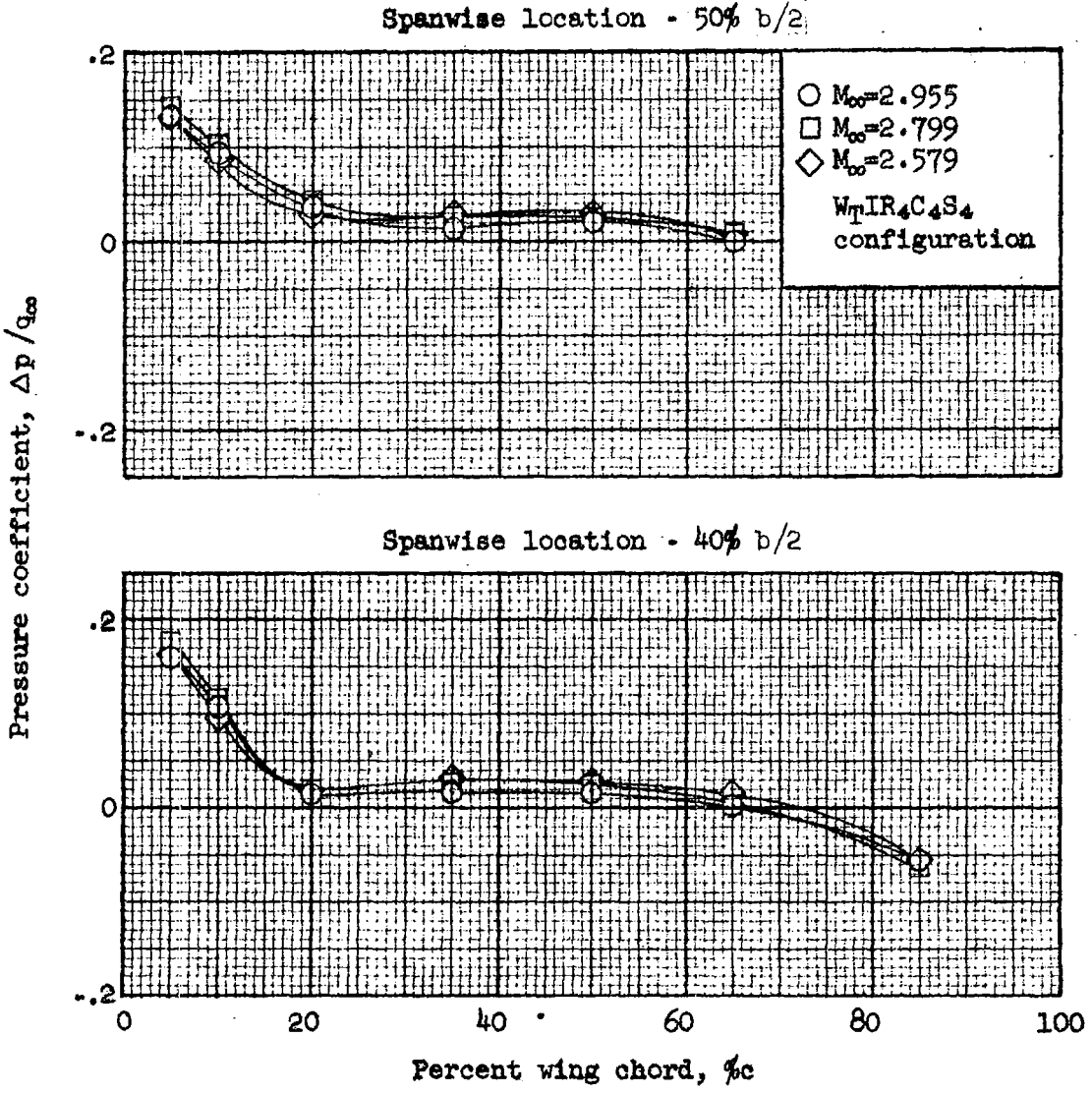

(a)

Figure 33.- Effect of Mach number variation on the lower surface pressure coefficients of the Number 172 wing version for optimum inlet pressure recovery at α=2.2°, β=0°.

[redacted]

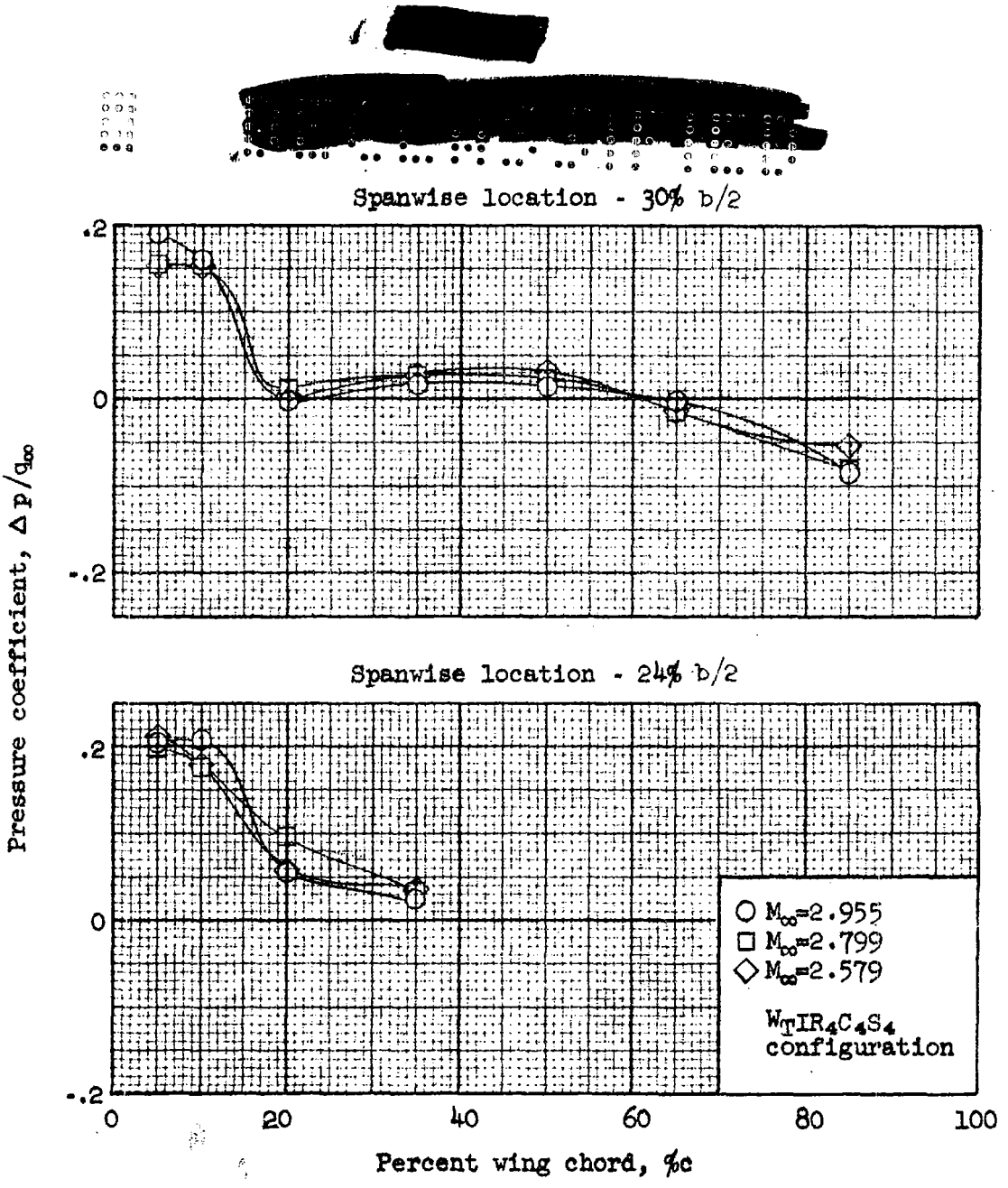

(b)

Figure 33.- Continued.

[redacted]

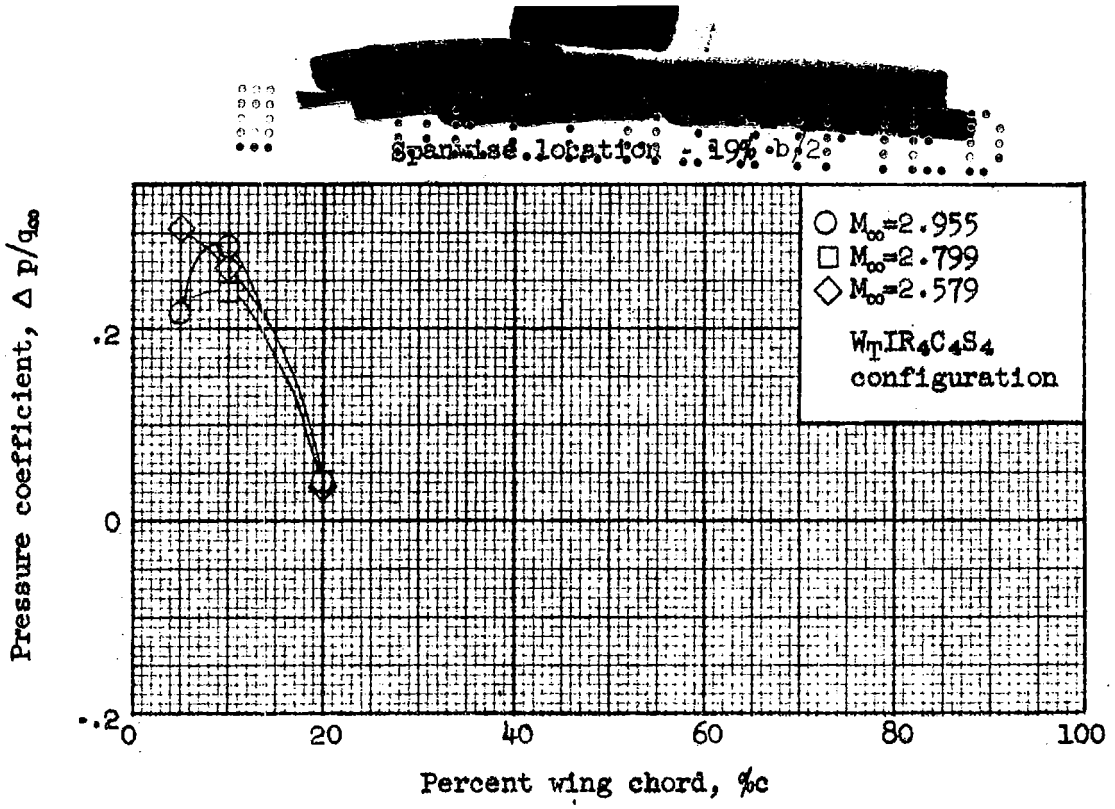

% b/2	%c	M_∞=2.955	M_∞=2.799	M_∞=2.579
		$\Delta p/q_\infty$	$\Delta p/q_\infty$	$\Delta p/q_\infty$
14.70	3.54	.034	.0394	.0595
13.40	3.28	.034	.0394	.0564
12.12	2.96	.034	.2743	.4546
10.83	2.65	.014	.0283	.0284
9.54	2.36	.012	.0195	.0284
4.60	2.84	.010	.0666	.0574
0.00	3.13	.006	.0109	.0158
7.00	5.06	.026	.1643	.0699

(c)

Figure 33.- Concluded.

[redacted]

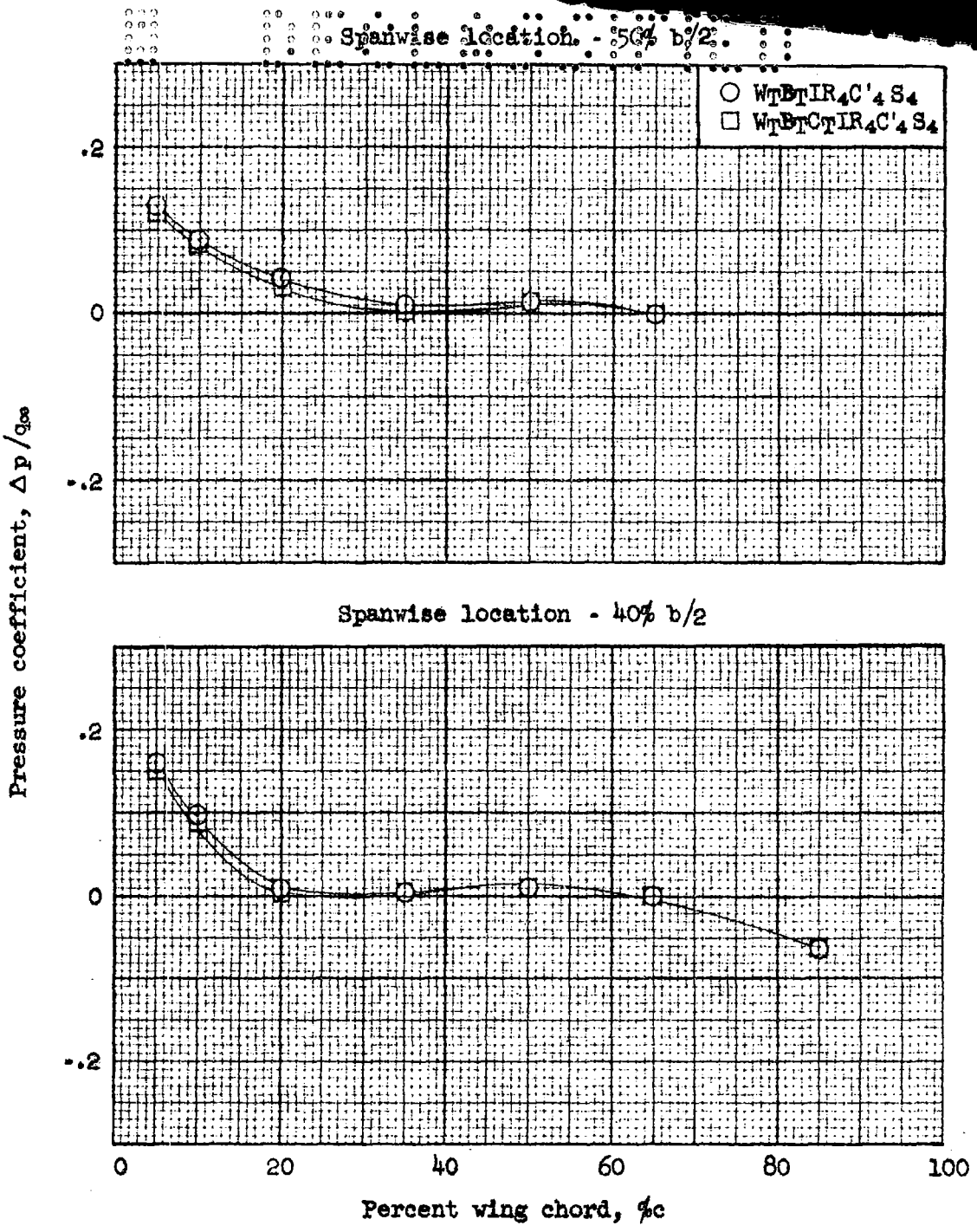

(a)

Figure 34.- Effect of canard on the lower surface pressure coefficients, of the Number 172 wing version, for optimum inlet pressure recovery at M_∞=2.955, α=2.2°, β=0°.

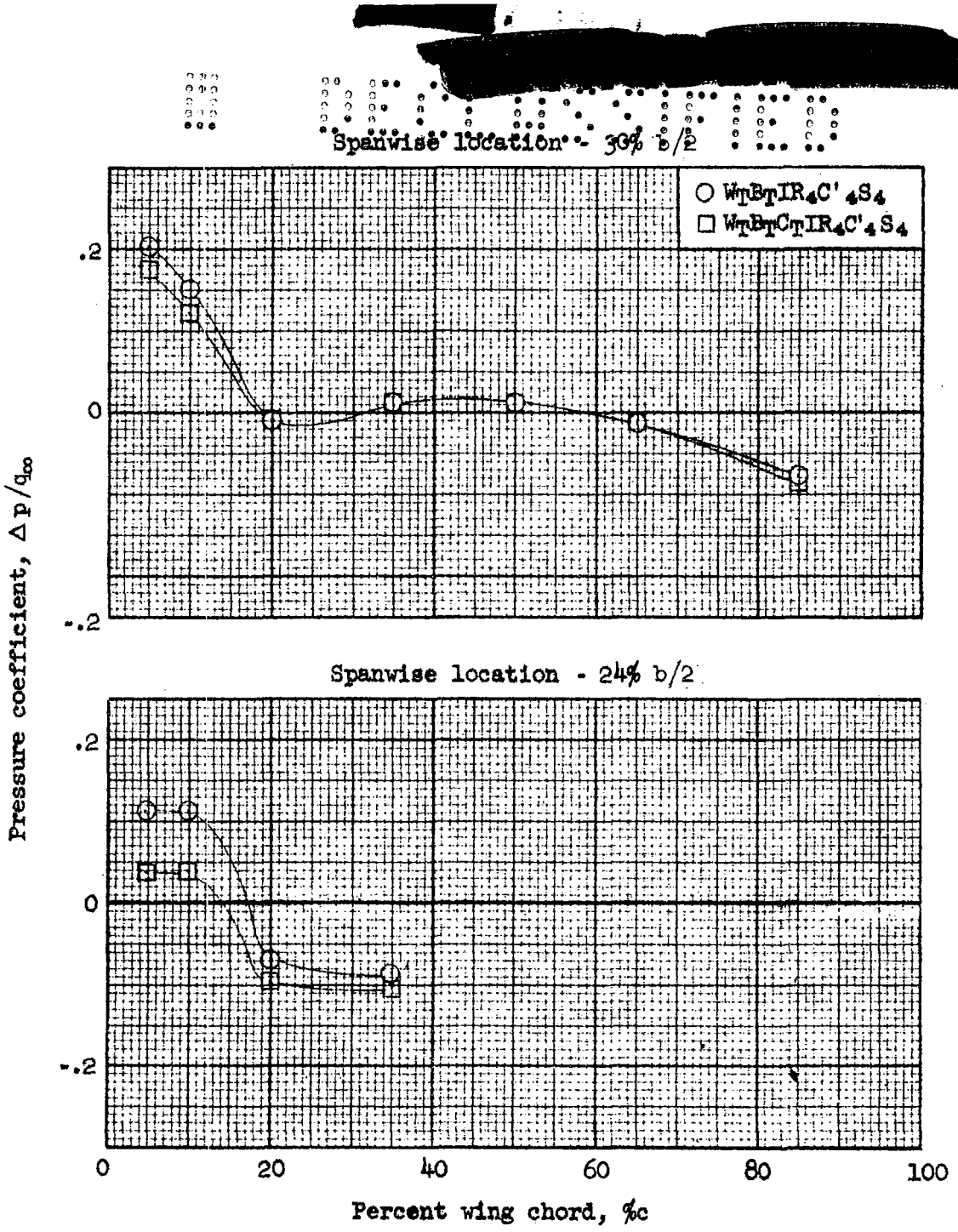

(b)

Figure 34.- Continued.

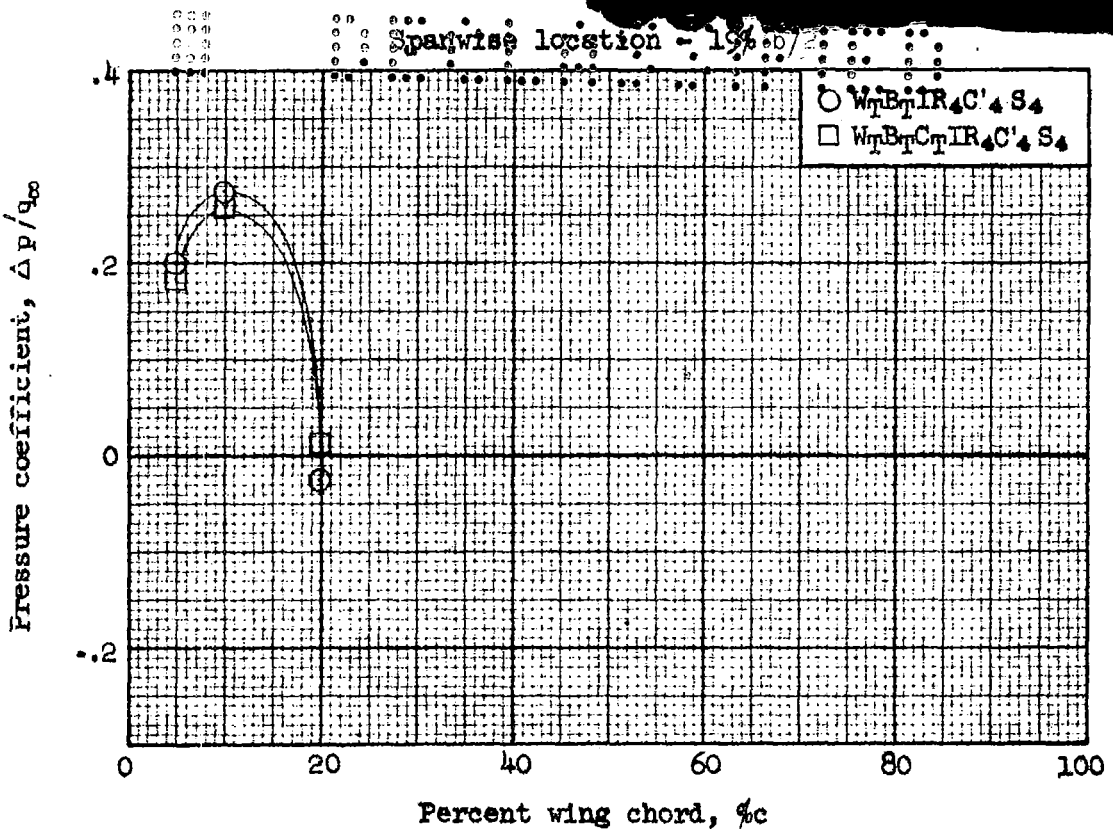

% b/2	%c	$\Delta p/q_\infty$	
		$W_T B_T C_T IR_4 C_4' S_4$	$W_T B_T IR_4 C_4' S_4$
14.70	3.54	.004	.160
13.40	3.28	.056	.062
12.12	2.96	.014	.062
10.83	2.65	.008	.012
9.54	2.36	.008	.008
7.00	5.06	.036	-.032
4.60	2.84	.008	-.056
0.00	3.13	.014	-.010

(c)

Figure 34.- Concluded.

[redacted]

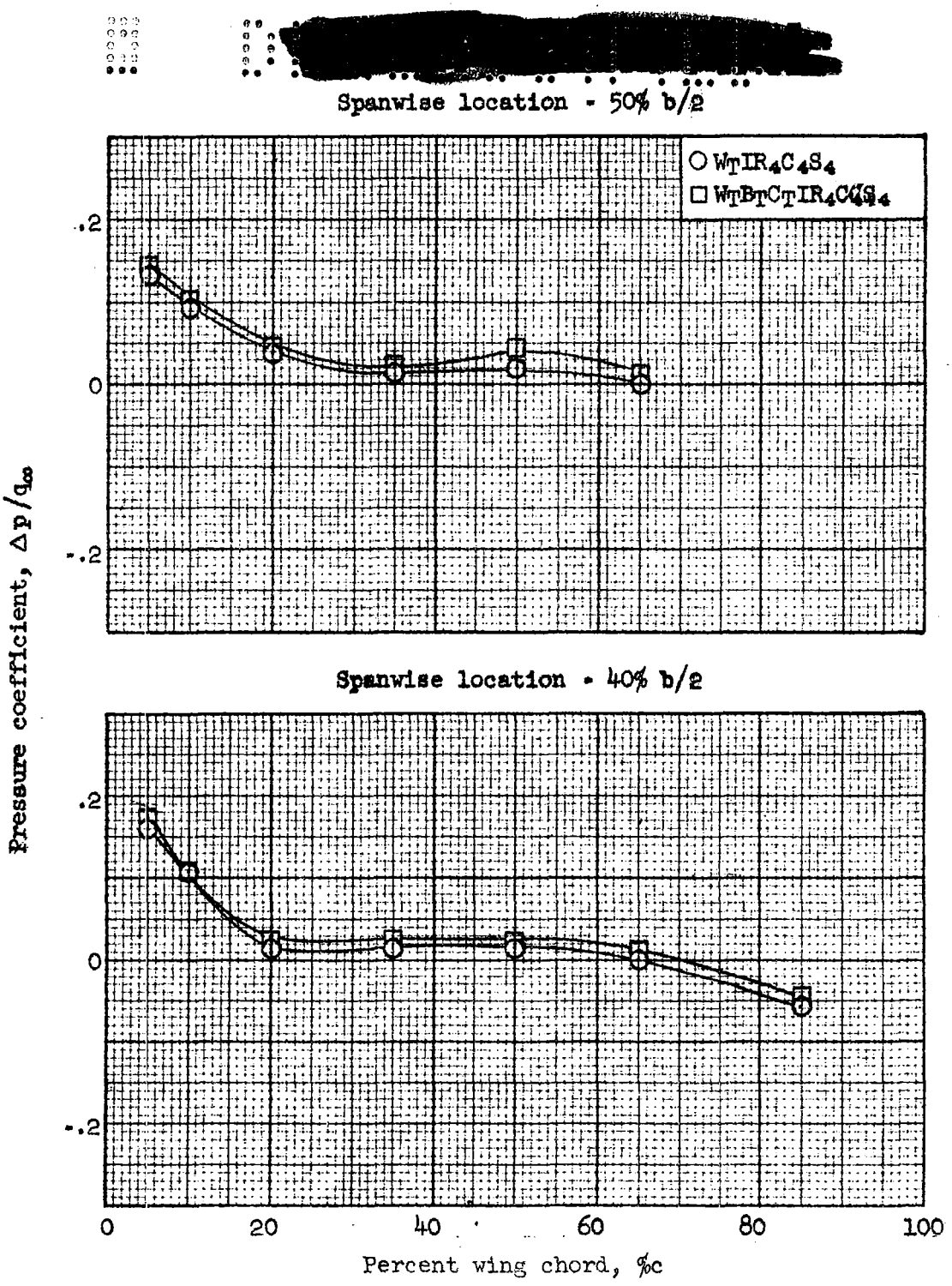

(a)

Figure 35.- Effect of forebody and canard on the lower surface coefficients of the Number 172 wing version for optimum inlet pressure recovery at M_∞=2.955, α=2.2°, β=0°.

[redacted]

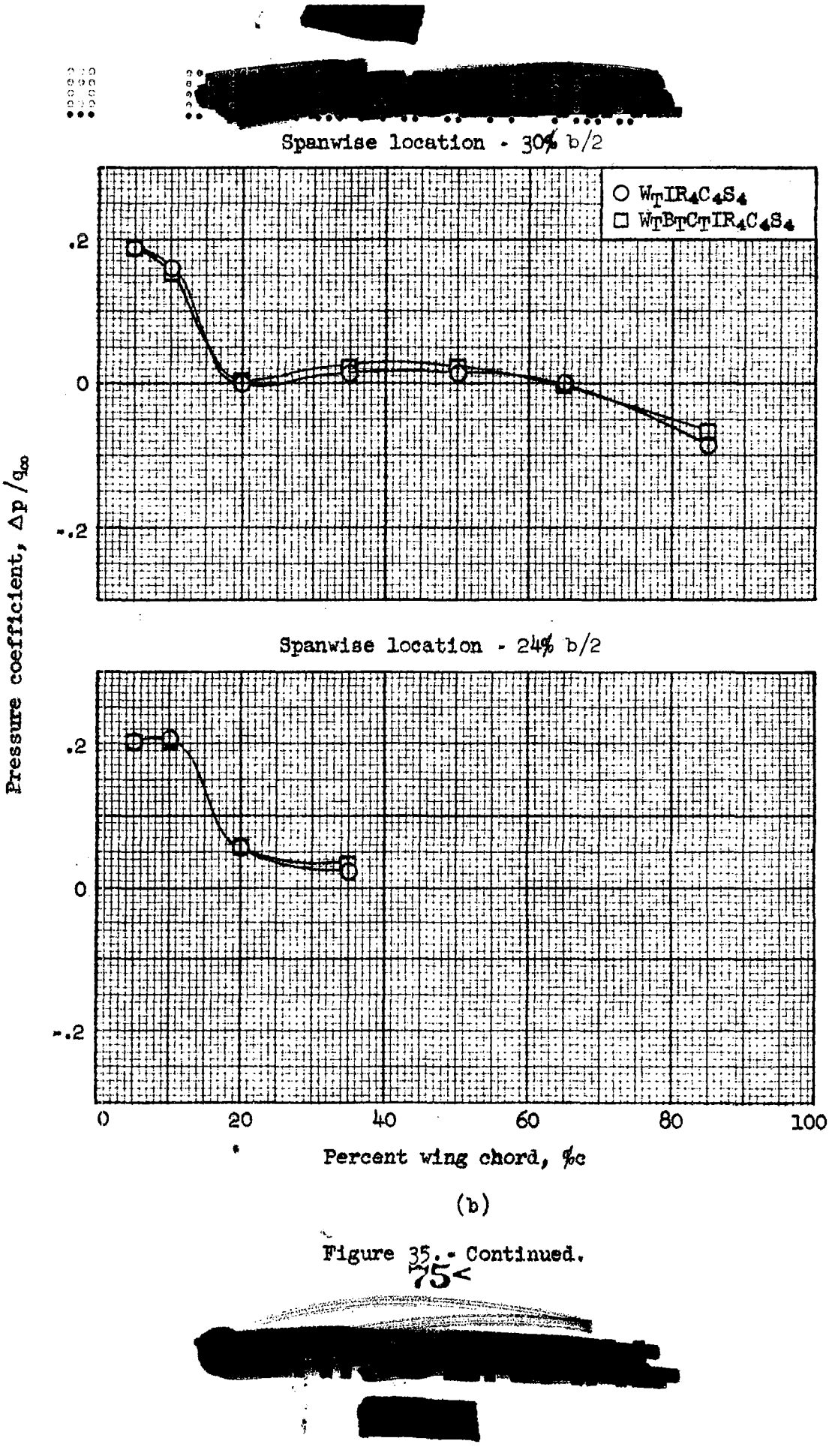

(b)

Figure 35.- Continued.

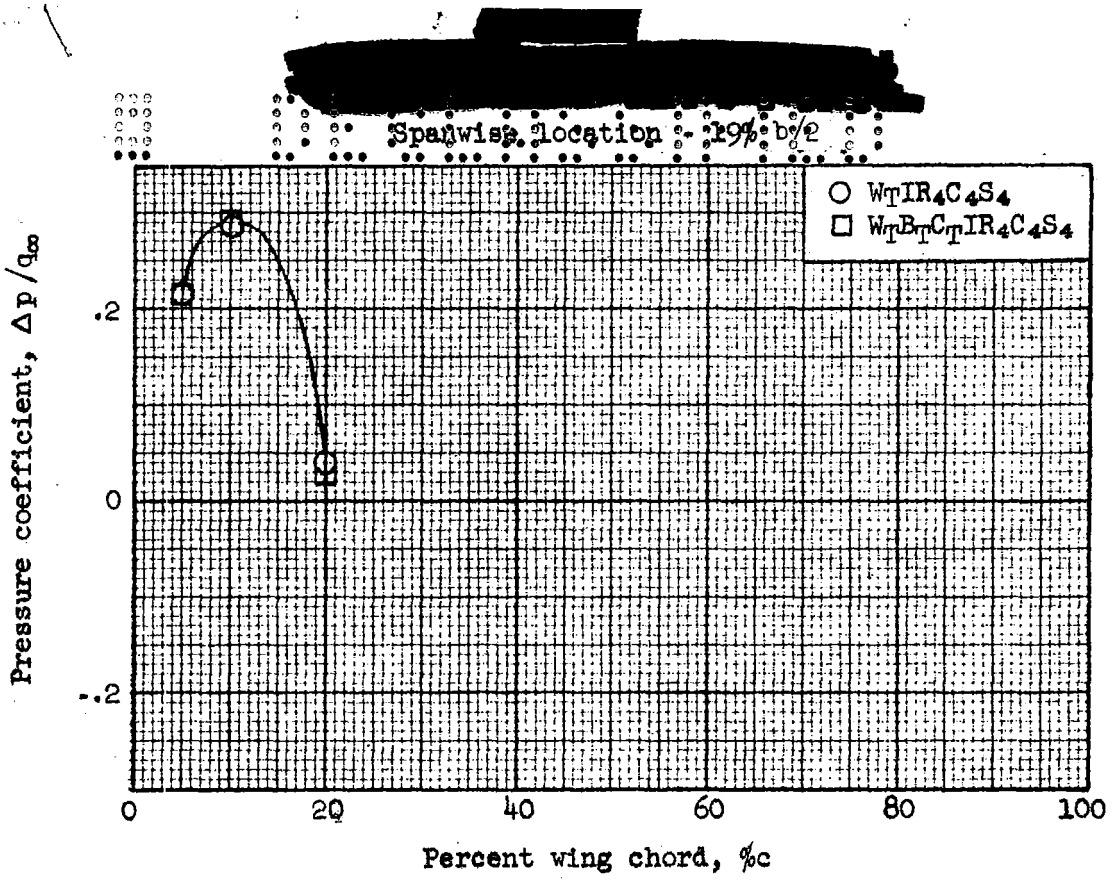

% b/2	%c	$\Delta p/q_\infty$	
		$W_TIR_4C_4S_4$	$W_TB_TC_TIR_4C_4S_4$
14.70	3.54	.034	.220
13.40	3.28	.034	.058
12.12	2.96	.034	.024
10.83	2.65	.014	.090
9.54	2.36	.012	.038
7.00	5.06	.026	.052
4.60	2.84	.010	.020
0.00	3.13	.006	.024

(c)

Figure 35.- Concluded.